

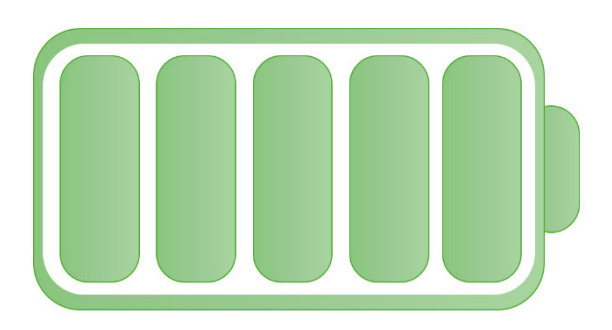


## Hochschule für Angewandte Wissenschaften Hamburg Fakultät Life Science

# Optimized Planning of Battery Storage Systems for Wind and Photovoltaic Power Plants in Germany by Development of a Simulation Program

**Master Thesis** 

in the study program Renewable Energy Systems



Submitted by: Lukas Tamschick

Enrollment number:

Submitted on: 28.03.2025

First reviewer: Prof. Dr. Timon Kampschulte (HAW Hamburg)

Second reviewer: Christoph Grote (CEE Operations GmbH)

#### Foreword

This master's thesis for the 'Renewable Energy Systems' program at HAW Hamburg is supported by the CEE Group.

The CEE Group is part of Brookfield Asset Management, a global leader in asset management. At its Hamburg office, the company manages solar and wind farms in Germany, France, the Netherlands, Sweden, Spain, and Denmark, with a total installed capacity of approximately 2.2 GW.

The combined wind and photovoltaic plant and analyzed in this thesis, is owned by the CEE Group. The CEE Group supports this research to enhance its expertise in battery energy storage systems. Furthermore, after the verification of the developed simulation program, its annual cash flow outputs are intended to serve as input parameters for a financial model.

I would like to thank my two supervisors, Prof. Dr. Timon Kampschulte from HAW Hamburg and Christoph Grote from the CEE Group, for their fast support regarding my work. Additionally, I extend my thanks to the proofreaders Manfred Schröder and Beatriz Bravo Hernandez of this thesis. Thanks to all colleagues involved for their support with subject-specific questions as well!

## Table of Content

Foreword	0
List of Abbreviations	A
Symbol Directory	C
Program Variable Directory	D
List of Figures	F
1 Introduction	1
2 Fundamentals	3
2.1 Total Plant Layout	3
2.2 Technical Setup Battery Energy Storage System	3
2.3 Modelling Technical Performance of Battery Storages	4
2.3.1 Technical Battery Parameters	4
2.3.2 Battery Efficiencies	6
2.3.3 Battery Degradation	8
2.4 Battery costs	10
2.4 Legal and Tax Regulations	13
2.5 Electricity Market: Requirements, Analysis and Marketing Strategies	15
2.6 Outages and Curtailments	19
3 Simulation Input Data	20
3.1 General Implementation Strategy	20
3.2 Battery Cost Implementation	23
3.3 System Round Trip Efficiencies Implementation	24
3.3 Legal and Tax Implementation	25
3.4 Electricity Market Implementation	27
3.4.1 Theoretical Forecasting Approach	27
3.4.2 Application of Forecasts	28
3.5 Implementation of Outages and Curtailments	31
4 Simulation Algorithm Development	34
4.1 Program Operation	34
4.2 Program Algorithms	36
4.2.1 Program Overview	36
4.2.2 Theoretical Plan Operation	37
4.2.3 Main Simulation Algorithm	45
4.2.4 Degradation Algorithm	54
4.2.5 Financial Figures	55
5 Application of the Simulation Tool	56
5.1 Baseline Simulation for	56

5.2 Parameter Optimization and Sensitivity Analysis	60
5.3 Main Simulation, Analysis and Validation	65
6 Summary and Outlook	70
References	73
Appendix	I
Affidavit and declaration of publication	XXXI

#### List of Abbreviations

AC = Alternating Current

CAPEX = Capital Expenditures = investment costs

CEE = Company name

BDEW = Bundesverband der Energie- und Wasserwirtschaft = association

BESS = Battery Energy Storage System

BMS = Battery Management System

BMWK = Bundesministerium für Wirtschaft und Klimaschutz der Bundesrepublik

Deutschland = federal ministry

BOL = Beginning of Life

BOS = Balance of System = costs for supporting components

DC = Direct Current

DM = Direct Marketer

DOD = Depth of Discharge = ratio of utilized capacity to nominal capacity

EnFG = Gesetz zu Finanzierung der Energiewende im Stromsektor durch Zahlungen

des Bundes und Erhebung von Umlagen = german law

EnWG = Gesetz über die Elektrizitäts- und Gasversorgung = german law

EOL = End of Life

EPC = Engineering-Procurement-Construction

GO = Grid Operator

IDE = Integrated Development Environment

INT = Intraday market

IRR = Internal Rate of Return

KAV = Verordnung über Konzessionsabgaben für Strom und Gas = german law

KWKG = Kraft-Wärme-Kopplungsgesetz = german law

LCOE = Levelized Costs of Energy

LCOS = Levelized Costs of Storage

LFP = Lithium-Iron-Phosphate = special type of lithium battery

LMO = Lithium Manganese Oxide

LTO = Lithium-Titanium-Oxide = special type of lithium battery

MV = Medium Voltage

NMC = Lithium-Nickel-Mangan-Cobalt-Oxide = special type of lithium battery

NPV = Net Present Value

OPEX = Operational Expenditures = operational costs

PCS = Power Conversion System

PPA = Power Purchase Agreement

PR = Primary Reserve = FCR = Frequency Containment Reserve

PV = Photovoltaic

RES = Renewable Energy Systems

RES+P = Discharging BESS to supply RES

RES-P = Charging BESS from RES

RTE = Round-Trip Efficiency

SOC = State of Charge = ratio of recent capacity to nominal capacity

SOH = State of Health

SR = Secondary Reserve = aFRR = automatic Frequency Restoration Reserve

SR+E = Positive SR energy

SR-E = Negative SR energy

SR+P = Positive SR power

SR±P = Simultaneous provision of positive and negative SR power

SR-P = Negative SR power

StromNEV = Verordnung über die Entgelte für den Zugang zu

Elektrizitätsversorgungsnetzen = german law

StromStG = Stromsteuergesetz = german law

TR = Tertiary Reserve = mFRR = manual Frequency Restoration Reserve

UstG = Umsatzsteuergesetz = german law

## **Symbol Directory**

C = Cash-flow

C-rate = Indicator for  $P_U$  = ratio of  $I_U$  to  $Q_N$ 

 $E_N$  = Rated energy

G(t) = Volatility of each timestamp

g = Scaling factor for volatility visualization

 $I_U$  = Operational current

k = Discount factor

 $N_p$  = Installed power-related grid fees

 $P_{loss}$  = Lost power

 $P_N$  = Rated power

 $P_U$  = Utilized power

 $Q_c$  = Charge capacity

 $Q_d$  = Discharge capacity

 $Q_E$  = Capacity at EOL

 $Q_{loss}$  = Lost capacity =  $Q(BOL) - Q(EOL) = Q_N - Q_U$ 

 $Q_N$  = Rated capacity

 $Q_U$  = Utilized capacity

 $\overline{SOC}$  = Average State of Charge

t = Time or timestamp

V =System voltage

 $V_p(t)$  = Recent value of time series

 $\overline{x(t)}$  = Mean value of time series

 $\Delta I$  = Deviation of current Intraday price interval from mean Intraday price interval

 $\delta$  = Capacity degradation battery

 $\delta_{idl}$  = Capacity degradation battery of idling

 $\delta_{cyc}$  = Capacity degradation battery of cycling

### **Program Variable Directory**

activation\_propability\_PR Probability of charging and discharging when

participating in the Primary Reserve market.

activation\_propability\_SR Probability of charging or discharging when

participating in the Secondary Reserve power markets.

activation\_propability\_SR\_minus\_P Probability of discharging when participating in the

negative Secondary Reserve power market.

activation\_propability\_SR\_plus\_P Probability of discharging when participating in the

positive Secondary Reserve power market.

annually.

annually.

annual\_timestamps\_SR\_plus\_P Number of timestamps, the BESS could participate at

the Secondary Reserve Markets annually.

capacity\_for\_charging Capacity that can be charged at the selected

timestamp.

capacity\_for\_discharging Capacity that can be discharged at the selected

timestamp.

calculation\_period Number of simulated years

*charge\_cycle* One complete sequence of charging

*curtailments\_GO* Curtailments of grid operator

cycle One complete sequence of charging and discharging

discharge\_cycle One complete sequence of discharging

end\_year End year of simulation. The end year itself is excluded

from simulation.

**future\_revenue** Indicator to compare different market scenarios.

losses\_pv Outages of PV plant

losses\_wind Outages of wind plant

lower\_bid\_for\_direct\_activation To assume 100 % activation, the bid on the secondary

energy reserve markets must be lower than the mean value. This variable sets how much lower. ( $\notin$  / MWh)

modified\_prediction\_horizon The prediction\_horizon is modified dependent on the

selected markets.

nominal\_price\_Intraday Converted Intraday price for comparison (€ / MW /

15-min / full active)

*nominal\_price\_PR* Converted Primary Reserve price for comparison (€ /

MW / 15-min / full active)

nominal\_price\_SR\_energy Converted Secondary Reserve energy price for

comparison (€ / MW / 15-min / full active)

nominal\_price\_SR\_power Converted Secondary Reserve power price for

comparison (€ / MW / 15-min / full active)

*number\_plans* Within the same *prediction\_horizon*, multiple plans

can be developed, depending on this factor.

*power\_factor* Usable capacity / usable power (MWh / MW)

*power\_pv* Power of PV plant (MW)

power\_wind Power of wind plant (MW)

*prediction\_horizon* Number of future timestamps investigated.

*price\_Intraday* Intraday market price in (€ / MWh)

*price\_PR* Primary Reserve market price (€ / MWh)

*price\_SR\_energy* Secondary Reserve energy market price (€ / MWh)

*price\_SR\_power* Secondary Reserve power market price (€ / MWh)

**RES\_production** Renewable production (MW)

self\_discharge\_factor Factor between 0 and 1, dependent on the self-

discharge rate of the BESS.

simulation\_power Usable power (MW)

system\_RTE System roundtrip efficiency

*system\_RTE\_factor* Factor > 1, dependent on system roundtrip efficiency.

year\_commissioning Start year of simulation

## List of Figures

Figure 1	Total Plant Layout of AC coupled renewable production, BESS and grid connection (own
	Figure, based on: (Lo Franco et al., 2021:13))
Figure 2	Technical Setup of a Commercially Utilized BESS (own Figure with Reference to
	(SMA Solar Technology AG, 2023:4) and (Crawford et al., 2022:15–18))
Figure 3 (	Capacity-Related Battery Parameters (own Figure)
Figure 4 I	PCS RTE dependent on SOC (Crawford et al., 2022:18)
Figure 5 I	DC- PCS- and System RTE dependent on P <sub>U</sub> (Crawford et al., 2022:24)
Figure 6	Idling Capacity Degradation in % per Day for NMC, LFP, LTO and LMO Dependent on
	Average SOC at 20 °C (own Figure, values from: (Fallahifar and Kalantar, 2023:4)) 9
Figure 7	Cycling Capacity Degradation in % per Day for NMC, LFP, LTO and LMO dependent on
	Average DOD for C-rates <= 1 at 20 °C (own Figure, values from:
	(Fallahifar and Kalantar, 2023:4))9
Figure 8	Learning Curve for Capacity-dependent CAPEX in \$ / kWh for Lithium-Ion Batteries
	(Mauler et al., 2021:4733)
Figure 9	Power-dependent CAPEX for 2020 and 2030 for 1 MW, 10 MW, and 100 MW (own Figure
	based on: Mongird et al., 2020:87.f)
Figure 10	Analysis of Capacity-dependent CAPEX in € / kWh of LFP and NMC in 2020 and
	2030 dependent on Installed Capacity and Power (own Figure based on: Mongird et al.,
	2020:87.ff)
Figure 11	Average Taxes and Duties of Electricity in ct / kWh for Industry Usage (BEDW, 2024) 14
Figure 12	Market Trading Time Slots and Requirements (Finhold et al., 2023:3)(50hertz et al.,
	2024c) (Graf von Luckner, Kiesel, 2019:9)(Tennet et al., 2022)
Figure 13	Hourly Dependency of Intraday Market Prices in € / MWh in Germany on June, 2024
	(Fraunhofer ISE, 2024)
Figure 14	PR Price Development in € / (MW * week) in Germany (Christian Schäfer, 2024)

Figure 15	Power-dependent CAPEX in € / kWh for Program Imports in the Form of an Excel File
	Dependent on Technology, Installed Power in MW, and Time (own Figure)
Figure 16	Calculated Learning Curves for Power-dependent CAPEX in € / kW for 1 MW, 10 MW and
	100 MW for Lithium-Technologies as Time-Dependent Functions (own Figure) 24
Figure 17	Forecast of Power Dependent Grid Fee in € / (kW * a) for MV Connection for BESS (own
	Figure, Assumptions based on Appendix 16)
Figure 18	Time-dependent Volatility Development of Tendered PR Power with g = 437 (own Figure)
Figure 19	Forecast Average Curtailed Energy in % per Produced Energy of Grid Operators in
	Germany (own Figure)
Figure 20	Example Slide of Simulation Program (own Figure)
Figure 21	Overview: Elements of the Simulation Program (own Figure)
Figure 22	Program Flow Chart 1: Development of Theoretical Plan Operation based on
	Comparable Market Prices (own Figure)
Figure 23	Optimum Price and Market Matrices of Charge, Discharge and Power Reserve Markets -
	Nominal Prices are Given in € / MW / full_active (own Figure)
Figure 24	Detail Program Flow Chart of Step 6 of Program Flow Chart 1. Distribution Process of
	Timestamps for Plan Operation (own Figure)
Figure 25	Example of Step 6 of Program Flowchart 1: Distribution Process of Timestamps for Plan
	Operation (own Figure)45
Figure 26	Example Comparison of future_revenue (own Figure)
Figure 27	Program Flow Chart 2: Development of Real Plan Operation based on Stack Prediction of
	Possible Cases of SOC and Market Requirements (own Figure)
Figure 28	Program Flow Chart 3: Development of Real Operation, SOC and Revenue Based on
	Real Plan Operation Considering Unexpected Events (own Figure)
Figure 29	Detailed Example of Main Simulation Program (own Figure)
Figure 30	Algorithm of Capacity Degradation (own Figure)

Figure 31 Re	epowering Project Combination Plant Wind + PV (internal Source) 56
Figure 32	Financial Parameters Costs, Revenue and Cashflow in M€ of BESS-Simulation with 357
	Cycles per Year, Usable Power = 1 MW and Usable Capacity = 2 MWh (own Figure) 60
Figure 33	Parameter Optimization of Capacity and Power of BESS for for 730 Target
	Cycles (own Figure)
Figure 34 .Pa	arameter Optimization of Cycles per Year for BESS of Power Factor 1 and 2 (own Figure)
Figure 35 IR	R Dependency on Prediction Horizon and Cycles per Year (own Figure)
Figure 36 IR	R Dependency on Replacement Period for Different Power Factors (own Figure) 63
Figure 37 Si	mulation Input Data for Main Simulation (own Figure)
Figure 38 Fir	nancial Result of Main Simulation (own Figure)
Figure 39 Ma	arket Utilization of Main Simulation Result (own Figure)
Figure 40 Ma	arket Revenue of Main Simulation Result (own Figure)

#### 1 Introduction

Germany's energy transition has led to a rapid expansion of photovoltaic (PV) and wind energy systems in recent years. By 2024, PV systems accounted for 14 % and wind energy systems for 33 % of Germany's net electricity generation (Fraunhofer ISE, 2025).

Since the feed-in power of renewable energy systems (RES) such as wind and PV fluctuates and can only be predicted approximately, the integration of RES poses a challenge to grid stability (Stroe et al., 2017:430). The curtailments of RES due to local grid overloads is expected to increase significantly in the coming years (Fraunhofer ISI et al., 2024:15).

The fluctuating RES generation also leads to increased volatility in market prices (Fraunhofer ISE, 2024). During summer, the high midday PV generation and the low levelized cost of electricity (LCOE) of photovoltaics result in minimum prices on the Intraday and Day-Ahead electricity markets (Fraunhofer ISE, 2024). In contrast, morning and evening peak demand, which is primarily covered by expensive conventional power plants, leads to price maxima (Fraunhofer ISE, 2024).

To enhance grid stability while simultaneously achieving economic benefits, short-term energy storage systems utilize market opportunities based on an arbitrage model: energy is purchased at the lowest prices and sold at the highest prices (Finhold et al., 2023:1). By reducing electricity price fluctuations, energy storage systems contribute to stabilizing electricity markets (Christian Schäfer, 2024).

Historically, storage capacity has primarily been provided by pumped storage power plants (Martinez-Bolanos et al., 2020:2). However, Germany lacks the geographical potential for additional pumped storage facilities (Connor Thelen et al., 2024:29).

Due to the exponential decline in lithium costs in recent years, lithium-ion battery electric storage systems (BESS) have become a viable economic alternative to pumped storage power plants. The installed power of battery storage systems in Germany increased by 41 % compared to the previous year to 12.1 GW in 2024, while total installed capacity rose by 39 % to 17.7 GWh (Fraunhofer ISE, 2025). Since 2024, the installed battery storage capacity in Germany has surpassed that of pumped storage power plants (Fraunhofer ISE, 2025).

For BESS to be deployed, they must be planned both technically and economically. From a technical perspective, key parameters such as storage capacity, power, degradation, and efficiency significantly influence the operation of BESS (Merten et al., 2020). From an economic perspective, the storage system must generate profit over its planned lifetime. This can be evaluated using financial metrics such as the Internal Rate of Return (IRR) and Net Present Value (NPV) (Buratynskyi et al., 2023:545). Given the many assumptions involved, a sensitivity analysis is also essential.

The highest profitability of a BESS can be achieved through cross-market optimization (Finhold et al., 2023:2). This means that a BESS is marketed across multiple electricity markets to maximize revenue. Additionally, decentralized storage systems are well suited for increasing grid stability (Stroe et al., 2017:430). A co-located battery storage system, as one installed near RES, can help balance fluctuating RES generation (Fan et al., 2021:1).

Several simulation programs for BESS planning are available on the market, such as HOMER Software (UL Solutions, 2024) and the System Advisor Model (NREL, 2024). However, a significant drawback of these tools is that they are based on assumptions, which are not always visible or customizable.

The objective of this study is to develop a custom simulation tool for lithium BESS incorporating cross-market optimization, specifically for co-located BESS installations near RES generation. To overcome the limitations of existing models, the tool will be designed to be transparent and customizable. All data will be accessible, allowing flexible adaptation. The tool will be applied to optimally size BESS for a case study involving wind and PV plants.

Following the introduction, this thesis is structured into the following sections:

Chapter 2 covers the technical design of BESS and their integration with co-located RES generation. This section also discusses technical key parameters such as efficiency and degradation, along with economic and regulatory aspects. The economic analysis differentiates between investment and operational costs and the revenue potential of BESS by applying the cross-market strategy.

Chapter 3 explains how forecasting data for the simulation is generated. It builds on the fundamentals and describes how data is converted into a format usable by the simulation program. Forecasting for example market data is based on literature, statistical analysis, and the impact of future battery storage installations on market prices. Other forecasts include levies, costs and production data from RES and BESS.

Chapter  $\underline{4}$  describes the development and functionalities of the simulation tool. The program consists of four main components:

- Market comparison, which determines the optimal market utilization each time step based on the predefined cycle limit of the BESS.
- The main algorithm, which ensures technical feasibility, accounts for unpredictable events such
  as curtailments, and calculates key outputs like the state of charge (SOC), operational strategy
  and the revenue for each simulation time step.
- Cost analysis, which evaluates investment and operational costs considering degradation effects.
- Output generation, where key economic indicators such as IRR and NPV are calculated, enabling subsequent optimizations based on economic performance.

Additionally, users will be able to access all intermediate results for detailed analysis.

Chapter <u>5</u> applies the simulation tool to a real project. After functionality validation of the simulation program, key parameters are identified and <u>optimized</u>. The optimal system sizing and operational strategy of a BESS for the wind and PV plant is calculated. The results are compared and discussed with literature findings.

Chapter 6 provides a summary of the methodology and key results. It also identifies opportunities for improving the simulation tool for applications in other renewable energy plants.

#### 2 Fundamentals

#### 2.1 Total Plant Layout

The layout of the overall plant considered in this study consists of RES generation, a BESS, and the grid connection point (Figure 1). Renewable generation may include wind energy, photovoltaics, or both. Electrical connections between the BESS, renewable generation, and the grid are represented by lines. The DC voltage from the renewable generation is converted to AC voltage by an inverter and then transformed to medium voltage by a transformer. The medium voltage is marked with red connections. In rare cases, a high-voltage transformation occurs before the grid connection.

RES and BESS are AC-coupled, as they are connected on the AC side. AC-coupling was chosen to economically separate the renewable generation from the BESS, which reduces the economic risk per plant. For large-scale plants, DC coupling would improve efficiency by only about 0.16 percentage points annually compared to AC coupling (Lo Franco et al., 2021:18).

All electrical cables are designed to support bidirectional flow. The connection from the BESS operates bidirectionally under the same load. Renewable generation also requires minimal power consumption for the communication interface. Therefore, the connection is used bidirectionally to a minimal extent of < 0.5 %. The consumed power of RES can be supplied by either the BESS or the grid.

Power meters are shown in green (Figure 1). It is essential to use three meters due to grid losses, which can reach up to 2 %. Accurate measurement of generated and consumed power is necessary for grid charges and tariffs.

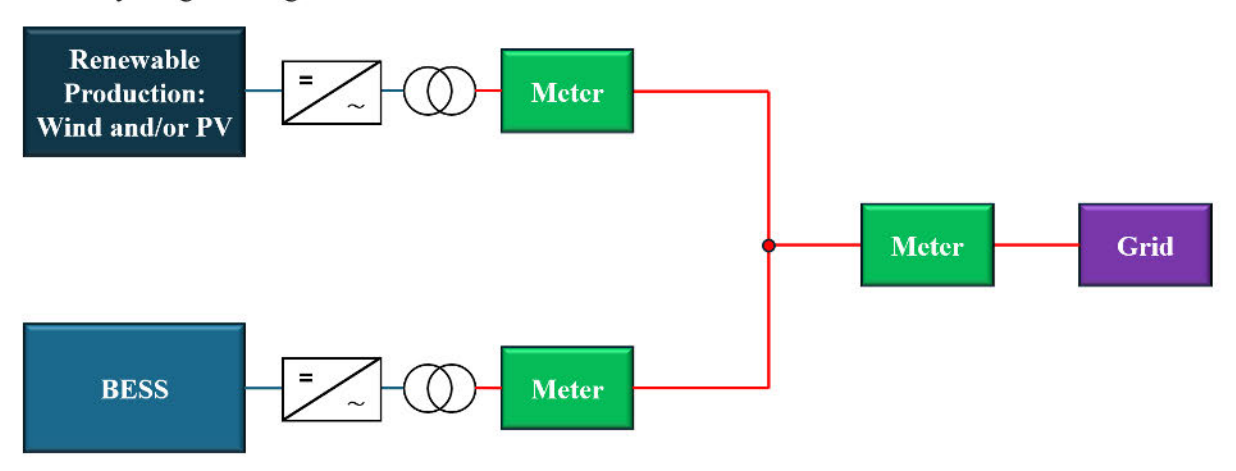


Figure 1 Total Plant Layout of AC coupled renewable production, BESS and grid connection (own Figure, based on: (Lo Franco et al., 2021:13))

#### 2.2 Technical Setup Battery Energy Storage System

The technical setup of a commercially utilized BESS is depicted in <u>Figure 2</u>. The battery system includes the Battery Bank, the Battery Management System (BMS), the Power Conversion System (PCS), and Auxiliary Units.

The Battery Bank contains battery cell stacks (Crawford et al., 2022:15). The BMS monitors the safety and efficiency of the Battery Bank and communicates with the control unit of the PCS (SMA Solar

Technology AG, 2023:4). The red connections in <u>Figure 2</u> symbolize the energy flow. When the batteries discharge, the bidirectional inverter converts the DC voltage of the Battery Bank into AC, and during charging, it converts it back to DC (SMA Solar Technology AG, 2023:4). The transformer increases the voltage during discharge to medium-voltage (MV) level and decreases it during charging (SMA Solar Technology AG, 2023:4). An MV switch can disconnect the facility from the grid (SMA Solar Technology AG, 2023:4). Auxiliary Units include temperature regulation, lighting system, and ventilation (Crawford et al., 2022:18). Auxiliary power is also needed by communication and control electronics and the fire protection for the BESS (Crawford et al., 2022:20). The meter is located at the grid connection point. It measures the system's power generation and consumption bidirectionally.

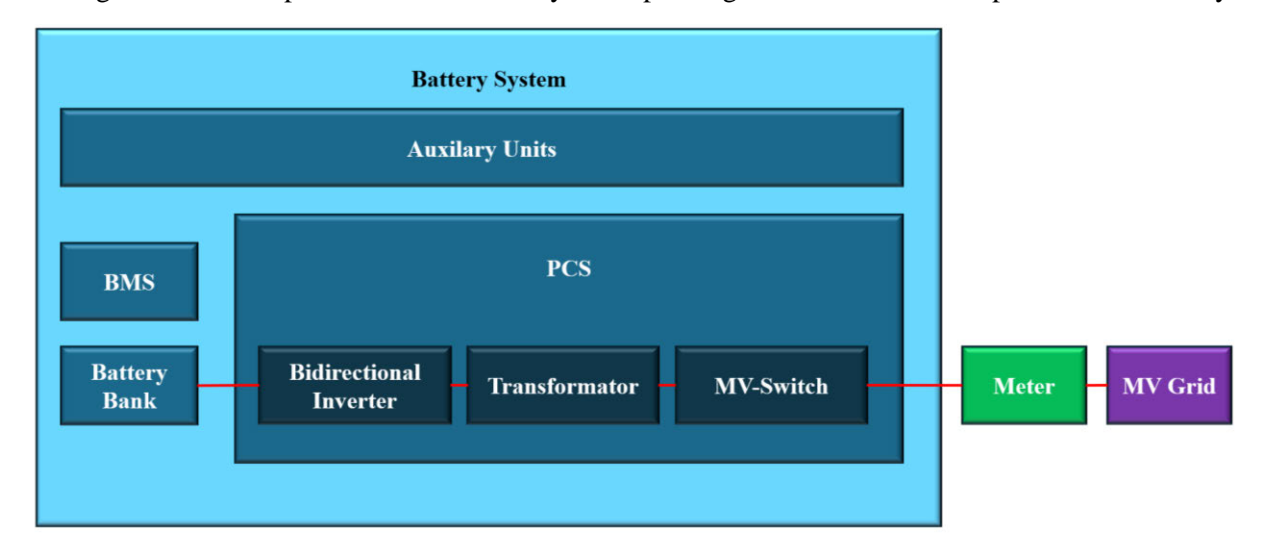


Figure 2 Technical Setup of a Commercially Utilized BESS (own Figure with Reference to (SMA Solar Technology AG, 2023:4) and (Crawford et al., 2022:15–18))

#### 2.3 Modelling Technical Performance of Battery Storages

#### 2.3.1 Technical Battery Parameters

The simulation program applies the following formulas for technical battery parameters in chapter  $\underline{3}$  and  $\underline{4}$ .

The technical modelling of BESS is complicated because of different definitions of important battery parameters (Sauer et al., 1999) and a lack of specifications in the literature sources. <u>Figure 3</u> graphically represents the key capacity-related battery parameters, which are explained in detail:

The rated capacity  $Q_N$  in Ah and the rated power of the battery  $P_N$  in kW are key parameters of the battery (Böttcher and Nagel, 2018:154.ff). The rated energy  $E_N$  in kWh is calculated from the product of the system voltage V in kV and  $Q_N$  (Böttcher and Nagel, 2018:154):

$$E_N (kWh) = Q_N (Ah) \cdot V (kV) \tag{1}$$

However, in literature, the term rated energy is often replaced by rated capacity (Martinez Bolanos et al., 2020:5), and thus the rated capacity is given in kWh. Since nominal capacity and power are rarely utilized in practice due to capacity and power losses during operation (R. Li et al., 2023:3075), utilized capacity  $Q_U$  and power  $P_U$  are also specified (IREA, 2012:8). In this work,  $Q_U$  and  $P_U$  are defined as constants over the runtime of the battery.  $Q_U$  and  $P_U$  are defined by the user

and describe the BESS which can be traded on the market. In contrast,  $P_N$  and  $Q_N$  are unknown and calculated by the program.

 $Q_E$  represents the capacity available at the end of operational life (EOL) (<u>Figure 3</u>). Since  $Q_U$  is assumed constant, the utilized capacity of the battery must be less than or equal to  $Q_E$ :

$$Q_U \le Q_E \tag{2}$$

The operational lifespan of a BESS depends on the time dependent battery capacity degradation  $\delta$  in % of  $Q_N$ . This degradation is categorized into idling degradation  $\delta_{idl}$  in % degradation of  $Q_N$  per day and cycling degradation  $\delta_{cyc}$  in % per cycle (Timur Sayfutdinov et al., 2020:3). Idling describes the degradation of the BESS during standby periods, while cycling refers to degradation during active operation (Timur Sayfutdinov et al., 2020:3). Total degradation is the sum of both idling and cycling effects (Timur Sayfutdinov et al., 2020:4):

$$\delta(t, cycles, \overline{SOC}, \overline{DOD})(\%) = \delta_{idl}(\overline{SOC}) \left(\frac{\%}{d}\right) \cdot t (d) + \delta_{cyc}(\overline{DOD}) \left(\frac{\%}{cycle}\right) \cdot cycles(t)(cycle)$$
(3)

 $\overline{SOC}$  describes the average State of Charge (7) and  $\overline{DOD}$  the average Depth of Discharge (6).

In <u>Figure 3</u>, capacity degradation is depicted by the red function. The absolute capacity losses  $Q_{loss}(t)$  are calculated as follows:

$$Q_{loss}(t) = \frac{\delta(t)(\%)}{100\,(\%)} \cdot Q_N \tag{4}$$

The remaining capacity, expressed as a percentage of  $Q_N$ , is referred to as State of Health (SOH) (Pregnolato, 2019:36):

$$SOH(t)(\%) = \left(\frac{Q_N - Q_{loss}(t)}{Q_N}\right) \cdot 100\% \tag{5}$$

In Figure 3, a distinction is made between the charged capacity  $Q_c$  and the discharged capacity  $Q_d$  of  $Q_U$  in a discharge cycle.

The DOD describes the ratio of discharged capacity to  $Q_N$  (Pregnolato, 2019:35.f):

$$DOD(t)(\%) = \frac{Q_d(t)}{Q_N} \cdot 100 \% \tag{6}$$

The SOC indicates the releasable capacity of the battery relative to  $Q_N$  (Pregnolato, 2019:36). The releasable capacity decreases with  $Q_{loss}$  and  $Q_d$ :

$$SOC(t)(\%) = \left(\frac{Q_N - Q_{loss}(t)}{Q_N} - \frac{Q_d(t)}{Q_N}\right) \cdot 100\% \tag{7}$$

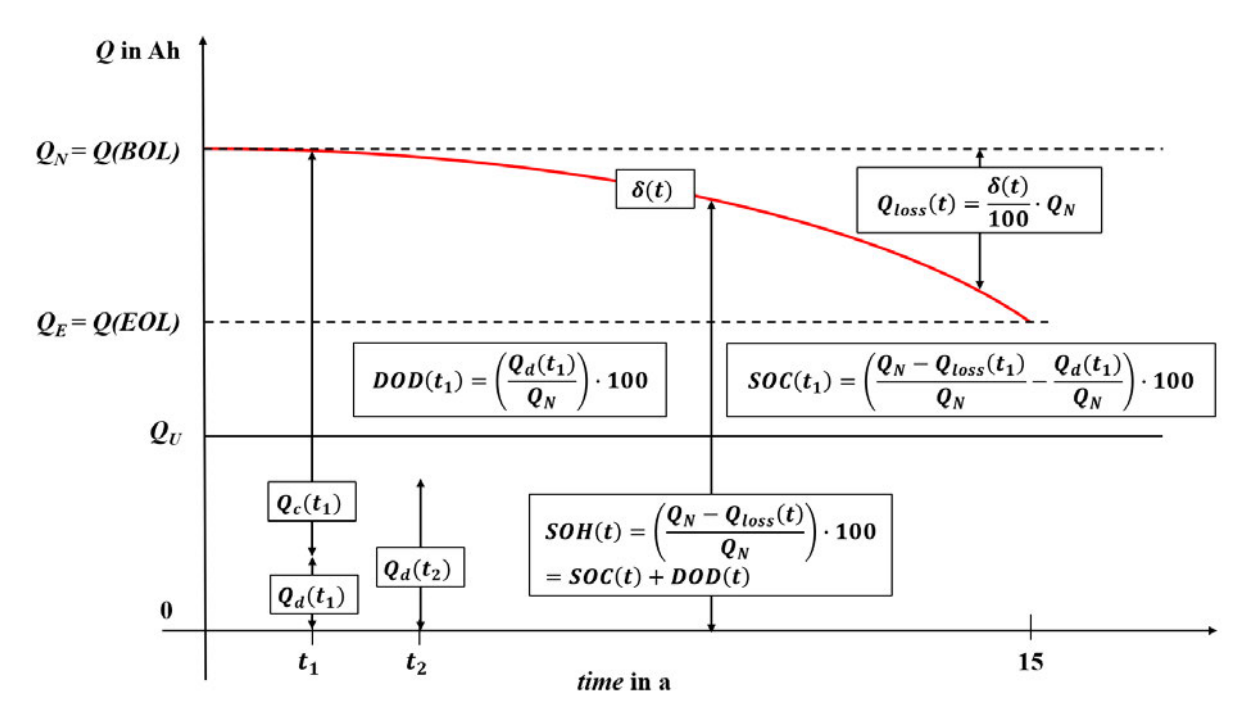


Figure 3 Capacity-Related Battery Parameters (own Figure)

Battery cycles are measured in full cycles or equivalent full cycles. A full cycle describes a complete charge and discharge relative to the nominal capacity (Tanim et al., 2021:663). An equivalent full cycle occurs with the same energy throughput as a full cycle (Tanim et al., 2021:663).

As  $P_U$ , the *C-rate* in  $\frac{1}{h}$  serves as an indicator of the operating power performance of the system (Böttcher and Nagel, 2018:141). The greater the currently used power of a battery, the greater the *C-rate*:

$$C-rate \left(\frac{1}{h}\right) = \frac{I_U(A)}{Q_N(Ah)} = \frac{P_U(kW)}{E_N(kWh)}$$
(8)

 $I_U$  represents the current intended for operation.

Batteries exhibit self-discharge, which is low for lithium batteries: self-discharge loss amounts to 2 to 3 % per month (Zheng et al., 2020:2). The self-discharge rate of lithium-ion batteries varies with technology: For Lithium-Nickel-Mangan-Cobalt-Oxide (NMC), 1 % per month, for Lithium-Titanium-Oxide (LTO) 2 % per month, for Lithium Manganese Oxide (LMO) 3 % per month and for Lithium-Iron-Phosphate (LFP) 4 % per month can be adopted (Timur Sayfutdinov et al., 2020:7). The learning rate of self-discharge is negligible in the near future (IREA, 2017:125).

The efficiency is divided into DC efficiency, PCS efficiency, and system efficiency (Crawford et al., 2022:24).

#### 2.3.2 Battery Efficiencies

Battery efficiencies or round-trip efficiencies (RTE) are generally calculated as the ratio of discharged energy to charged energy of the BESS (Mongird et al., 2020:6).

The DC RTE describes the efficiency of the battery unit. PCS RTE is represented by DC efficiency minus PCS losses. PCS losses are caused by the bidirectional inverter (Crawford et al., 2022:17) and the transformer which is partly contained in the same power station (SMA Solar Technology AG,

2023:4). Charging losses are a little larger than discharging losses: the efficiency of the bidirectional inverter is 96.6 % for rated charge and 98.7 % for rated discharge (Crawford et al., 2022:18).

The PCS RTE depends on SOC: if SOC falls below 20 % or exceeds 80 %, PCS RTE decreases significantly (<u>Figure 4</u>).

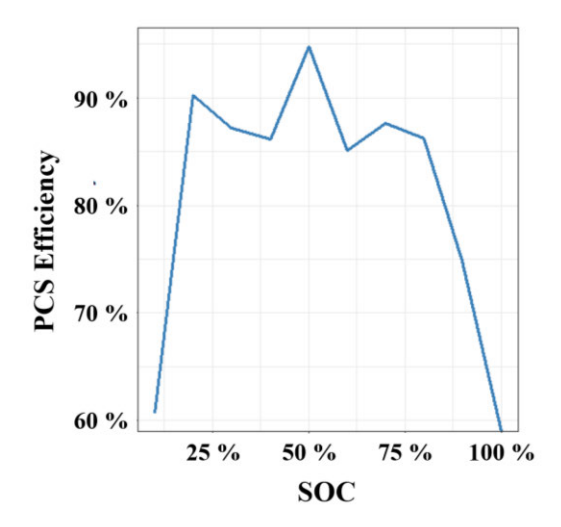


Figure 4 PCS RTE dependent on SOC (Crawford et al., 2022:18)

Auxiliary losses primarily arise from the thermal management system (Crawford et al., 2022:20). Considering all losses at the grid connection point results in system RTE. It includes also losses such as cable losses and losses from communication and control electronics (Crawford et al., 2022:18.ff).

<u>Figure 5</u> indicates a practical test of a LFP storage in 2022 with  $P_N = 1$  MW and  $Q_N = 5.5$  MWh. DC, PCS, and system RTE differ from each other. The losses of the battery unit are lower than the sum of losses from power conversion and auxiliary power. The system RTE ranges from 77 to 83 %, depending on  $P_U$ : the higher the utilized power, the lower the efficiency.

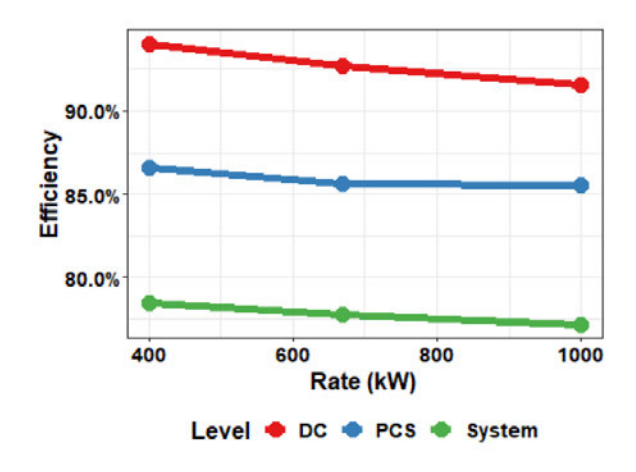


Figure 5 DC- PCS- and System RTE dependent on P<sub>U</sub> (Crawford et al., 2022:24)

In literature, RTE data is often opaque, as distinctions between DC-, PCS- and system RTE are not always clarified (Timur Sayfutdinov et al., 2020). Reported values vary considerably: for instance, system RTE values for 2017 range between 83 % and 87 %, as derived from practical tests (Mongird et al., 2020:13), whereas results from the practical test in <u>Figure 5</u> show significantly lower values.

System RTE is influenced not only by SOC (Figure 4) and  $P_U$  (Figure 5) but also by technology (Timur Sayfutdinov et al., 2020:7) and time (Mongird, 2020:87.ff). Temperature dependence can be disregarded due to the BMS, with NMC storage systems of the CEE operating at

The DC-RTE for four lithium technologies was measured in 2020. NMC, LMO, and LFP achieve the highest DC-RTE values, ranging from 97.5 % for LFP to 99 % for NMC, whereas LTO shows lower efficiency at 95 % (Timur Sayfutdinov et al., 2020:7).

A 2016 study estimates LFP RTE at 92 %, with other lithium technologies varying minimally between 95 % and 96 % RTE (IREA, 2017:125). However, as this study did not specify the RTE type, these values cannot be included in the analysis.

For all technologies, an improvement by 2 percentage points in efficiency is projected from 2016 to 2030 (IREA, 2017:125). For example, an increase in LFP from 92 % to 94 % (IREA, 2017:125). Another study forecasts an improvement in system RTE for NMC and LFP of 2 percentage points between 2020 and 2030 (Mongird et al., 2020:87.ff), with system efficiencies of NMC and LFP assumed at 86 % for 2020 in this study.

than 2 percentage points over a 10-year operational period, with minimal dependency on the *C-rate*. The 86 % NMC system RTE at BOL from the 2020 study has been verified as the most consistent by internal CEE sources.

#### 2.3.3 Battery Degradation

In addition to RTE degradation, both power and capacity of the battery degrade over time (Stroe et al., 2017:430). The capacity degradation  $\delta$  of a BESS is the sum of  $\delta_{cyc}$  and  $\delta_{idl}$  (chapter 2.3.1).  $\delta_{idl}$  depends on  $\overline{SOC}$ , temperature, technology, and time, while  $\delta_{cyc}$  also depends on  $\overline{SOC}$ , technology, and temperature (Timur Sayfutdinov et al., 2020:3). Additionally,  $\delta_{cyc}$  is influenced by the charge and discharge C- rate and DOD (Timur Sayfutdinov et al., 2020:3).

<u>Appendix 26</u> illustrates sharp degradation increases of lithium cells at temperatures above 25 °C. The BMS mitigates temperature effects by regulating it to approximately 23 °C (chapter <u>2.3.2</u>).

The effect of  $\overline{SOC}$  on auf  $\delta_{cyc}$  is minimal and can therefore be disregarded (Fallahifar and Kalantar, 2023:4). Appendix 12 presents the influence of the C-rate on  $\delta_{cyc}$ . The C-rate significantly impacts  $\delta_{cyc}$  for C-rates greater than 1, but since operations assume C-rates of  $\leq$  1, the effect of the C-rate on  $\delta_{cyc}$  is neglected.

These simplifications yield the following approximate equations for on  $\delta_{idl}$  and on  $\delta_{cyc}$  (Fallahifar and Kalantar, 2023:4):

$$\delta_{idl}(\overline{SOC})(\%) = (A \cdot (\overline{SOC})^2 + B \cdot \overline{SOC} + C) \cdot 100 \%$$
(9)

$$\delta_{cyc}(\overline{DOD})(\%) = (D \cdot (\overline{DOD})^2 + E \cdot \overline{DOD}) \cdot 100 \%$$
(10)

Factors A to E are curve-fitting parameters derived from measurement data (Fallahifar and Kalantar, 2023:4). Since the average SOC is explicitly described in (Fallahifar and Kalantar, 2023:4) it is assumed that the average DOD is also used due to the relationship between SOC and DOD (Figure 3).

Figure 6 and Figure 7 show the degradation behavior of various lithium battery technologies, calculated using formulas (9) and (10). The SOC dependency of idling degradation at 20 °C is approximately linear (Figure 6), while the DOD dependency is quadratic (Figure 7). Capacity degradation is shown on the y-axis as a percentage capacity loss of  $Q_N$  per day for  $\delta_{idl}$  (Figure 6) and per cycle for  $\delta_{cyc}$  (Figure 7).  $\delta_{cyc}$  exerts a much stronger degradation effect at higher DODs compared to  $\delta_{idl}$ . For LFP,  $\overline{DOD}$  would have to be less than 30 % so that degradation effects of idling and cycling are comparable. Furthermore, significant technological variations exist among lithium technologies: NMC and LFP degrade similarly, LMO has high degradation, and LTO exhibits low degradation. For BESS, minimal degradation is an important factor, making LTO an appealing option for costs reductions (Timur Sayfutdinov et al., 2020:10).

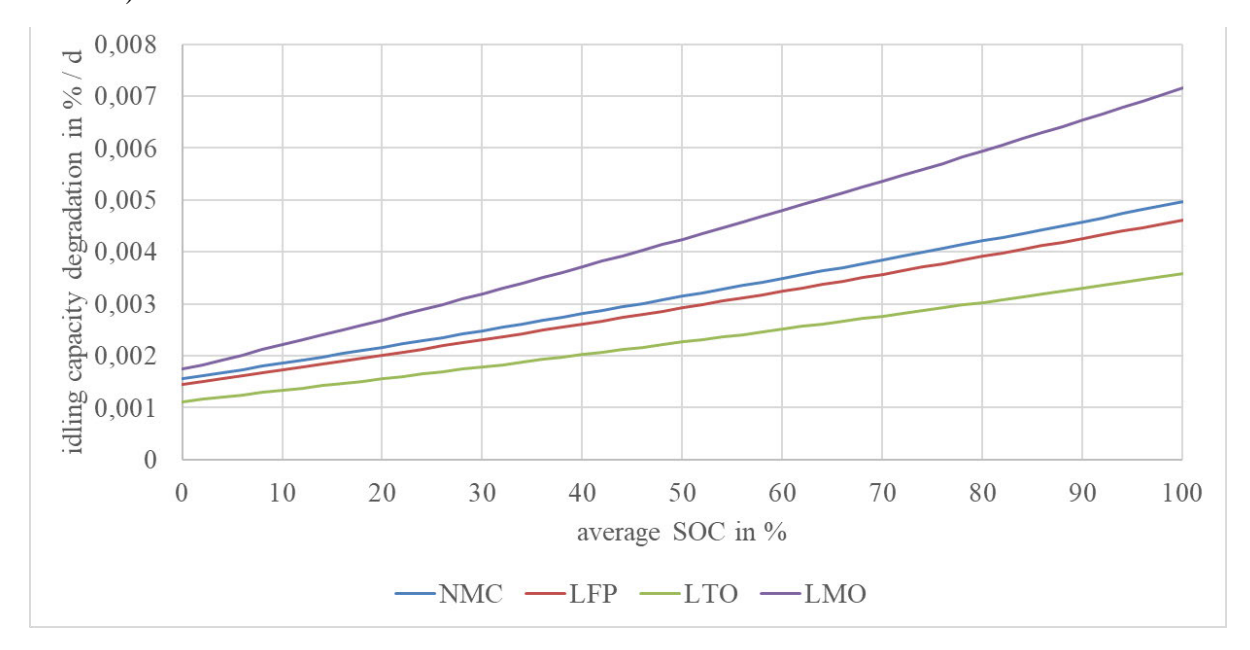


Figure 6 Idling Capacity Degradation in % per Day for NMC, LFP, LTO and LMO Dependent on Average SOC at 20 °C (own Figure, values from: (Fallahifar and Kalantar, 2023:4))

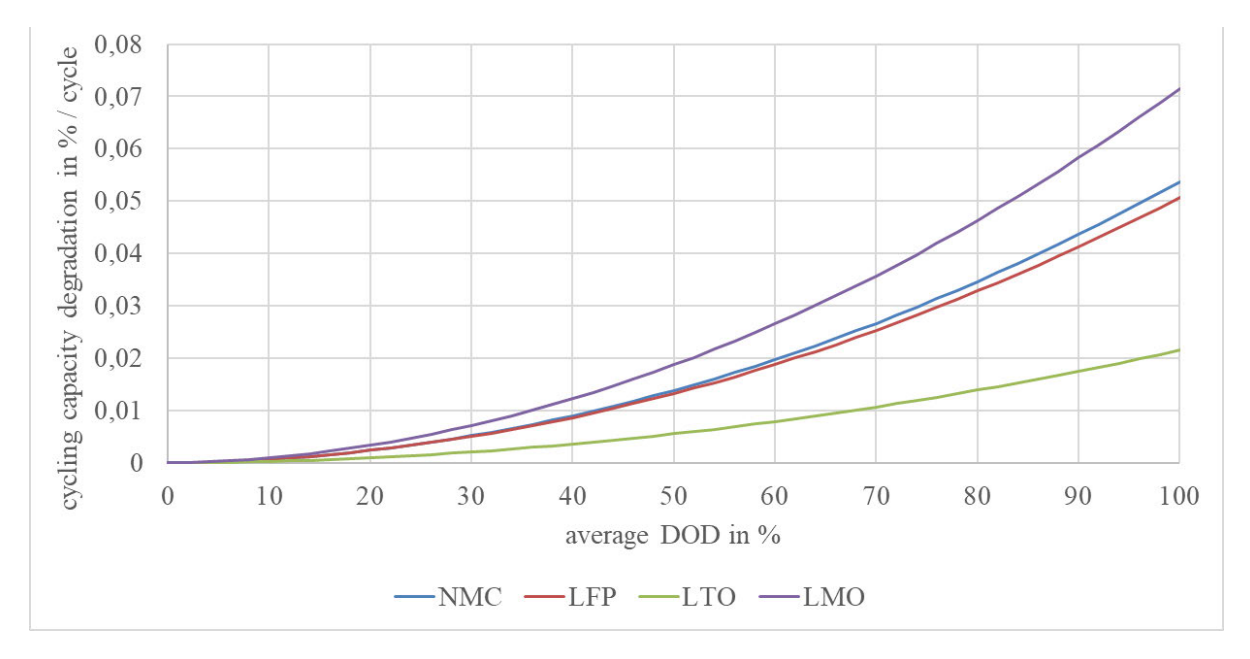


Figure 7 Cycling Capacity Degradation in % per Day for NMC, LFP, LTO and LMO dependent on Average DOD for C-rates <= 1 at 20 °C (own Figure, values from: (Fallahifar and Kalantar, 2023:4))

Power Degradation  $P_{loss}$  depends on the number of cycles and  $\overline{DOD}$  at 20 °C. The following formula for power degradation has been developed for LFP batteries (Swierczynski et al., 2015:3475):

$$P_{loss}(cycle, \overline{DOD})(\%) = \left(0.000036927 \cdot e^{0.08657 \cdot \frac{1}{\%} \cdot \overline{DOD}(\%)} \cdot cycle^{0.00434 \cdot 293 - 0.008 \cdot \frac{1}{\%} \cdot \overline{DOD}(\%) - 0.1504}\right) \%$$
(11)

Appendix 13 illustrates the power degradation of LFP as a function of  $\overline{DOD}$  and the number of cycles. As the DOD increases, power degradation rises exponentially, whereas the increase in power degradation with a rising number of cycles is approximately linear. Compared to capacity degradation, power degradation is significantly lower.

#### 2.4 Battery costs

The costs of the BESS have been analyzed, including capital expenditures (CAPEX), operational expenditures (OPEX) and the residual value.

CAPEX depend on storage capacity and storage power. In the literature, CAPEX values are not standardized (Mongird et al., 2020:87.f). In this work, cost components related to capacity and power are distinguished. The total CAPEX are then calculated as follows (Ekman and Jensen, 2010:1144):

$$total\ CAPEX\ (\textbf{@}) = capacity\ dependent\ CAPEX\ \left(\frac{\textbf{@}}{\textbf{kWh}}\right)\cdot\ Q_N(\textbf{kWh}) + \\ power\ dependent\ CAPEX\ \left(\frac{\textbf{@}}{\textbf{kW}}\right)\cdot P_N(\textbf{kW})$$

This separate consideration of capacity and power dependent costs is crucial, as both the optimal installed power and the optimal installed capacity need to be determined.

To compare the costs of different battery types, only capacity-dependent CAPEX are utilized. In addition to the storage unit, balance-of-system (BOS) costs, system integration costs, engineering, procurement, and construction (EPC) costs, as well as project development costs are included in the capacity-dependent CAPEX (Mongird et al., 2020:87.f).

Power-dependent costs consist of the costs of storage power electronics, controls and communication systems, and grid connection (Mongird et al., 2020:87.f).

Capacity-dependent CAPEX depend on the storage technology,  $Q_N$ , and  $P_N$  (Mongird et al., 2020:87.f). They also vary over time, since battery technology is still in the development phase (Mauler et al., 2021:4733). Power-dependent CAPEX depend on time and  $P_N$ . When comparing different lithium battery types, power-dependent CAPEX are not technology-dependent. However, if vanadium-flow or other non-lithium battery technologies are considered, power-dependent CAPEX also depend on the technology (Mongird et al., 2020:87.ff). For example, the costs for grid connection and project development differ for vanadium-flow batteries compared to lithium technologies.

Regardless of the development of raw material prices, continuously falling battery prices are expected (Mauler et al., 2021:4712). An analysis of numerous studies has yielded the following technology-independent learning curve for lithium-ion battery storage systems (Figure 8). It includes future projections from the literature and experts (Mauler et al., 2021:4733). The x-axis shows the development of capacity-dependent CAPEX in \$ / kWh over the years. Up to 2020, the red bars represent the actual development, while the examined forecast models are depicted with gray and white markers. The black curve describes the result in the form of a regression function through the data points. However,

deviations of more than 100 % exist between the different forecasted CAPEX values from the studies, so these should only be regarded as indicative figures (Mauler et al., 2021:4733).

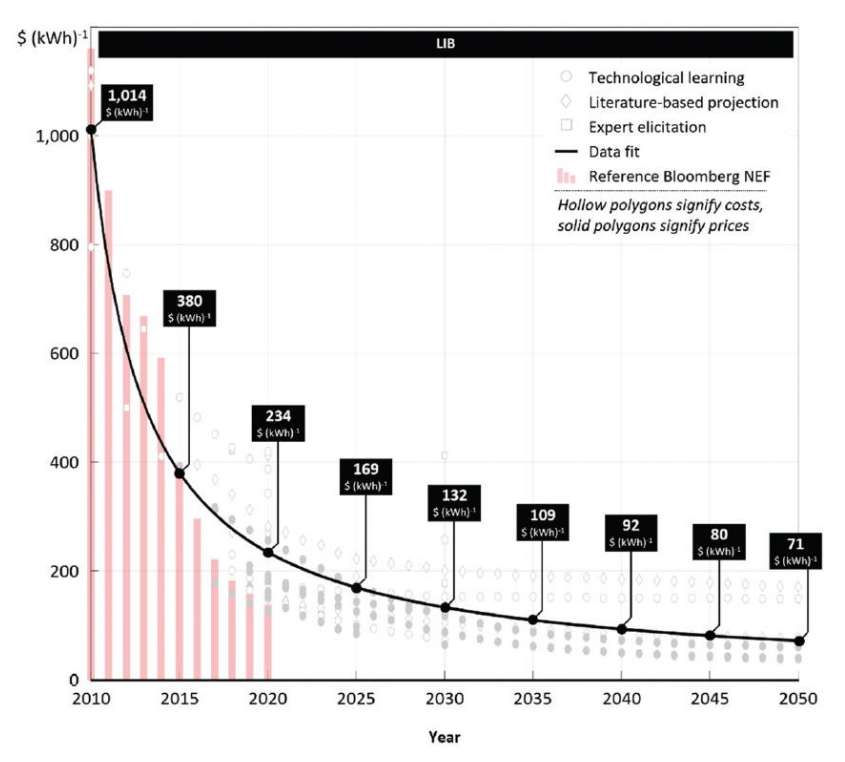


Figure 8 Learning Curve for Capacity-dependent CAPEX in \$ / kWh for Lithium-Ion Batteries (Mauler et al., 2021:4733)

Appendix 14 shows the power- and capacity-dependent components of the CAPEX for lithium BESS. Batteries with varying capacities and power levels are analyzed regarding their percentage contribution to total CAPEX. The costs of the storage block always account for the largest share. With increasing capacity or power installation for storage hours > 1, the proportion of power-related costs decreases.

The ratio of nominal capacity and power describes the storage hours:

storage hours (h) = 
$$\frac{Q_N \text{ (MWh)}}{P_N \text{ (MW)}}$$
 (13)

All costs given in US Dollar are converted to euros using the following formula, which corresponded to the conversion rate as of October 4, 2024 (tagesschau, 2024).

$$Euro = 0.91 \cdot USD \, Dollar \tag{14}$$

When comparing cost components of LFP with NMC, only the capacity-dependent CAPEX differ, with BOS are cheaper for LFP and battery block costs are cheaper for NMC (<u>Appendix 15</u>).

Figure 9 shows the power-dependent CAPEX, influenced by time and the scaling effects of  $P_N$ . The costs were converted to  $\frac{\epsilon}{kW}$  using Equation (14). In contrast to capacity-dependent CAPEX, the power dependent CAPEX are independent of  $Q_N$  (Mongird et al., 2020:87). The larger  $P_N$ , the lower the power-dependent costs. For a 100 MW BESS, the power-dependent CAPEX are reduced by almost half compared to a 1 MW BESS. The cost reduction effect due to the learning curve shows future potential.

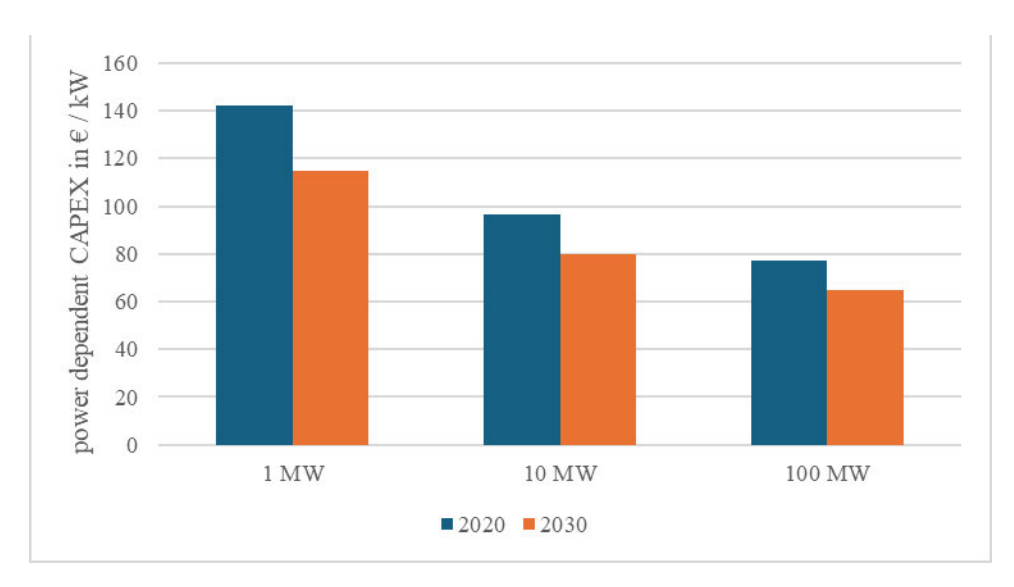


Figure 9 Power-dependent CAPEX for 2020 and 2030 for 1 MW, 10 MW, and 100 MW (own Figure based on: Mongird et al., 2020:87.f)

The capacity-dependent CAPEX in  $\frac{\varepsilon}{kWh}$  are shown on the y-axis in Figure 10, depending on installed capacity and power. The different colored bars represent LFP and NMC BESS for the years 2020 and 2030. Battery storage systems with varying capacities and power levels are plotted on the x-axis. Cost reductions due to economies of scale can be seen with increasing capacity as well as increasing power. A power increase from 1 to 100 MW leads to a price reduction of about 12.5 %. A capacity increase from 2 to 10 storage hours results in a comparable price reduction.

LFP and NMC differ only minimally in capacity-dependent CAPEX, with LFP being slightly cheaper than NMC. In the market, this difference fades due to the large price variability between offers, especially in forecasts (Mauler et al., 2021:4733). The temporal development shows significant cost reduction potential until 2030. The price reduction can be up to 30 % for 2030 compared to 2020.

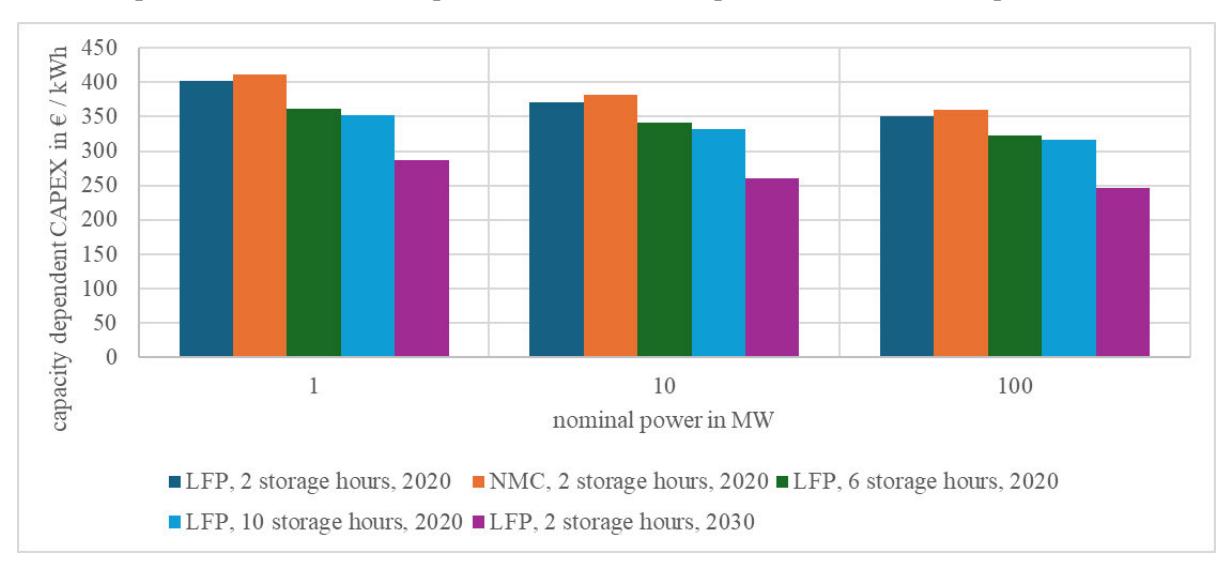


Figure 10 Analysis of Capacity-dependent CAPEX in  $\epsilon$  / kWh of LFP and NMC in 2020 and 2030 dependent on Installed Capacity and Power (own Figure based on: Mongird et al., 2020:87.ff)

The OPEX are divided into fixed and variable costs (Mongird et al., 2020:12.f). The fixed OPEX are specified in units of  $\frac{\epsilon}{kW \cdot a}$ , with the power rating referring to  $P_N$ . They depend on technology, time,

installed power and installed capacity (Mongird et al., 2020:87.ff). The dependency on installed capacity and time is minimal (Mongird et al., 2020:87.f). The cost difference between 2020 and 2030 for a 1 MW, 4 MWh LFP system amounts to  $0.7 \frac{\epsilon}{kW \cdot a}$ . The cost difference for a 10 MWh system with power ratings of 1 MW and 100 MW in 2030 is  $0.8 \frac{\epsilon}{kW \cdot a}$ .

Fixed OPEX can be assumed to increase linearly with installed capacity (Mongird et al., 2020:87.f). Their uncertainty can be up to 100 % (Mongird et al., 2019:46.f).

The variable OPEX, expressed in  $\frac{\epsilon}{\text{MWh}}$ , are dependent on the stored energy. In the literature, the definition of variable OPEX is inconsistent (Mongird et al., 2020:13). Generally, operational and maintenance costs increase with the degradation of the storage system due to usage: Less cycles per year result in lower maintenance costs than for heavily utilized systems (Mongird et al., 2020:13). For lithium BESS,  $0.273 \frac{\epsilon}{\text{MWh}}$  are estimated by comparison of different literature sources (Mongird et al., 2019:47).

The residual value of lithium batteries is only estimated imprecisely in literature: 2 to  $58 \frac{\epsilon}{\text{kWh}}$  is assumed in various studies (Mohammad Shahjalal et al., 2021:14).

#### 2.4 Legal and Tax Regulations

Due to the strong increase in the deployment of battery storages, the regulatory framework for electricity storage has also developed significantly in recent years (BMWK, 2023:10). The taxes and fees are generally paid by electricity consumers from the grid (EnFG, 2024, § 12) (StromStG, 2023, § 7).

The KWKG levy and offshore levy are charges consumers pay to support government subsidies for combined heat and power and the grid connection of offshore wind energy (EnFG, 2024, § 1). Consumers also pay the StromNEV levy to balance subsidies for grid fees (50hertz et al., 2024a). The concession fee is paid by consumers to municipalities to use public grid lines (KAV, 2006, § 1).

<u>Figure 11</u> provides an overview of the average taxes and duties on electricity for industrial consumption. Until mid-2022, the EEG levy represented the largest portion of industrial electricity charges but was then eliminated (BDEW, 2024). The electricity tax, which represented the second-largest portion of charges until 2023 and remained stable over the years, was almost eliminated in 2024. The largest charges in 2024 are the KWKG levy, StromNEV levy, and Offshore levy, which constitute 9 % of the total electricity price for industry on average (BEDW, 2024).

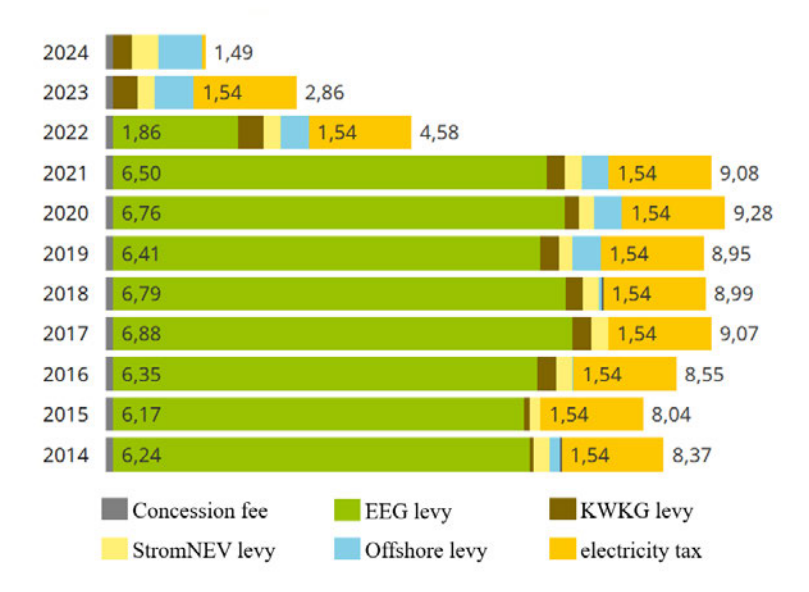


Figure 11 Average Taxes and Duties of Electricity in ct / kWh for Industry Usage (BDEW, 2024).

BESS benefit from additional tax and fee exemptions for electricity consumption from the grid.

The electricity tax is waived for BESS, both for electricity procurement from the grid and for self-consumption of electricity from RES (StromStG, 2023, § 9). The KWKG levy and Offshore levy are waived for BESS (EnFG, 2024, § 21). Efficiency losses are exempt from electricity tax (EnFG, 2024, § 21). The StromNEV levy does not apply (50hertz et al., 2024a).

Since the concession fee is to be paid by end consumers (KAV, 2006, § 1), it is assumed that a concession fee of  $0.11 \frac{\epsilon}{\text{kWh}}$  is levied on the system RTE, as these technically fall under end consumption. However, legal definitions may differ from technical interpretations and may change over time.

Sales tax is disregarded due to the possibility of input tax deduction (UStG, 2024, § 15).

BESS connected before August 4, 2029, are exempt from energy-related grid fees on electricity procurement for 20 years (EnWG, 2024, § 118). According to (StromNEV, 2023, § 19), installed power-related grid fees  $N_p$  for BESS are limited to efficiency losses. An individual grid fee is granted (StromNEV, 2023, § 19), which varies annually and depends on the connected voltage level and grid utilization (Westnetz GmbH, 2024b:16.). For PV and wind plants with nominal power of > 1 MW, the grid connection is often at MV level. Since the simulation only includes BESS located next to wind and PV plants, the MV connection is also likely for BESS. The maximum power-related grid fee for BESS with MV supply in 2024 is  $162.66 \frac{\epsilon}{kW \cdot a}$  (Westnetz GmbH, 2024b:16.). The individual grid fee may be as low as 20 % of the stated grid fee (StromNEV, 2023, § 19). As lithium BESS systems have system efficiency losses < 20 % (chapter 2.3.2), the expected grid fee for BESS with MV supply in 2025 can be calculated as:

$$N_p(year, storage\ technology, grid\ voltage) \cdot grid\ utilization\ (system\ RTE) \cdot P_N = \\ N_p(2025, \text{Lithium\ BESS}, \text{MV}) * grid\ utilization\ (>80\ \%) \cdot P_N = 162.66 \frac{\epsilon}{kW \cdot a} \cdot 0.2 \cdot P_N$$

<u>Appendix 16</u> shows the development of power-dependent grid fees for BESS with MV connection. Over the past 10 years, power-dependent grid fees have approximately doubled. Since 2019, there has been a strong increase in grid fees, attributed to grid expansion resulting from the grid integration of RES.

Regardless of the electricity purchase costs from the grid, the following additional regulations apply at BESS:

The parallel usage of capacity shares of storage systems across different markets is permitted (EnWG, 2024, § 11a). It is possible to utilize both the power and energy of a storage system simultaneously in balancing energy markets and wholesale markets, provided that the respective market conditions are met (Finhold et al., 2023:1).

If a reduction in the grid fee is claimed, the BESS may be controllable by the grid operator (EnWG, 2024, § 14a).

A reduction of the grid connection costs is possible (EnWG, 2024, § 14a).

Accelerated grid connections for all BESS are being planned (BMWK, 2023:15).

Incentives for decentralized storage at RES are intended (BMWK, 2023:14).

In summary, the operation of BESS incurs concession fees on system efficiency losses from grid electricity and reduced power-related grid fees. Further privileges for cost reduction and accelerated grid integration have already been created or are being planned. Although not all special cases of legal consideration of BESS could be covered by this information, the recent political goal is to remove barriers for the market ramp-up of BESS (BMWK, 2023:14).

#### 2.5 Electricity Market: Requirements, Analysis and Marketing Strategies

Electricity can be traded in various ways. Before electricity delivery, the following marketing opportunities exist:

The product market refers to the trade of electricity to meet supply and demand (Bundesnetzagentur, 2024a). The product market includes trading on and outside the stock exchange. Off-exchange transactions are called over-the-counter transactions (Liebau, 2012:40).

Exchange trading is divided into different sectors depending on the timing of the trade before electricity delivery. Up to 6 years before delivery, trading is possible on the futures market (Finhold et al., 2023:2). On the Day-Ahead Market, trading occurs one day before delivery. On the Intraday Market, trading is possible until 5 minutes before delivery (Finhold et al., 2023:2).

The balancing energy market ensures the electrical stability of the grid by minimizing frequency deviations from the target frequency of 50 Hz (50hertz et al., 2024c). There are three types of balancing energy, differing in the speed and duration of activation:

Primary Reserve (PR), also known as Frequency Containment Reserve (FCR), must be fully activated within 30 seconds and can be called for more than 15 minutes (50hertz et al., 2020a:1).

Secondary Reserve (SR), also known as Automatic Frequency Restoration Reserve (aFRR), must be available within 5 minutes and can be called for more than 10 minutes (50hertz et al., 2020b:1).

Tertiary Reserve (TR), also known as mFRR, must be available within 12.5 minutes (50hertz et al., 2024b) and can be called for more than 10 minutes (50hertz et al., 2020c:1).

A potential call for balancing energy to stabilize a frequency deviation is described in Appendix 1.

For the marketing of BESS, trading on the Day-Ahead and Intraday as well as PR and SR Markets is possible (<u>Appendix 2</u>). OTC trades are not considered because, unlike exchange trading, they are not publicly available.

The maximum profit of a BESS is achieved through a combination of different markets (<u>Appendix 2</u>). If only one market is traded, the profit of an energy storage system could be significantly reduced.

In the product trading markets, the BESS generates profits through the arbitrage model, by buying electricity at low prices and selling it at high prices (Finhold et al., 2023:1). The greater the volatility of the market, the higher the potential profit for the BESS.

Appendix 17 shows the Day-Ahead and Intraday market prices for April 2023. Although the average prices of the Day-Ahead and Intraday auctions are approaching each other, greater volatility is noticeable in Intraday trading (Christian Schäfer, 2024). If not just the traded average prices are considered, but the minima and maxima of the Intraday auction (Appendix 3), the potential of Intraday trading increases significantly. Since larger market volatilities are more advantageous for BESS, only the Intraday Market and not the Day-Ahead market is analyzed further.

The exact delivery times as well as market conditions for Intraday trading, PR, and SR are shown in Figure 12.

A direct marketer must decide by 08:00 on the previous day (t - 1 day) whether and which power of the BESS should be offered on the PR market for the time t of the following day and at which price. If the submission of a bid is chosen, the offered power will no longer be available for subsequent bids on the SR or Intraday markets. This applies regardless of whether the power is called upon or not. Energy activated in the PR market is not compensated separately.

The participation requirements of PR are a minimum power bid of 1 MW. In addition, the BESS must have capacity reserves for charging and discharging when providing positive and negative PR simultaneously. These are defined in Appendix 18. BESS with  $Q_N < 0.83$  MWh may not participate in the PR market (Tennet et al., 2022:67). Positive PR is equivalent to discharging and negative PR is equivalent to charging the BESS.

By 09:00 on the previous day, bids for power provisions and compensations on the SR market must be submitted. If a bid is accepted, the provider must also offer a price for the energy which could be activated on the SR-Energy Market. Trading SR energy is possible up to 25 minutes before the start of delivery. The SR market is divided into positive and negative balancing power as well as positive and negative balancing energy.

The minimum power bid in the SR market is 1 MW. For each MW of power bid, 1 MWh of capacity must be reserved (Tennet et al., 2022:41). If, for example, 2 MW are marketed positively and 1 MW negatively, the BESS requires  $Q_N >= 3$  MWh, whereby 2 MWh of discharge capacity and 1 MWh of charging capacity must be reserved. In case capacity losses are neglected and  $Q_N = 3$  MWh, it is only possible to participate in the market with SOC = 66.67 % for the example trades given (formular 7).

It is possible to participate only in the SR energy market, without trading on the SR power markets previously. In this case, only the SR energy price and not the power price would be remunerated in the event of activation. As the SR energy market is traded in 15-minute resolution and the minimum bid equals 1 MW, the minimum capacity is calculated as 0.25 MWh.

As positive and negative SR cannot be activated at the same time, bidding on the SR positive and SR negative power markets with the same power is also possible. Still, it must be ensured that each market

criteria of the capacity reserve is met. For example, a 1 MW / 2 MWh storage system can offer 1 MW on the positive SR and 1 MW on the negative SR power market only if SOC = 50 %.

The Intraday market is the last market in which trading can occur before delivery. On the Intraday market, 15-minute bids can be traded up to 5 minutes before the delivery start time. In contrast to the balancing power markets, on which available power is offered whose activation is unplanned, energy traded on the Intraday market is always fed into the grid. The minimum power is 0.1 MW and therefore the minimum capacity 0.025 MWh, as the bid length is 15 min.

Market	Market Closing	Min Length	Min Power	Min Capacity
PR	08:00 t - 1 d	4 h	1 MW	Appendix 18
SR power	09:00 t - 1 d	4 h	1 MW	1 MWh
SR energy	t – 25 min	15 min	1 MW	0.25 MWh
Intrady 15-min	t – 5 min	15 min	0.1 MW	0.025 MWh

Figure 12 Market Trading Time Slots and Requirements (Finhold et al., 2023:3)(50hertz et al., 2024c) (Graf von Luckner, Kiesel, 2019:9)(Tennet et al., 2022)

The various graphs of Figure 13 depict the development of Intraday market prices over 8 consecutive days in June 2024. The 15-minute average market price in  $\epsilon$  / MWh is shown as a function of the time of day. Around midday, the market price is low due to increased PV production and rises to local maxima in the morning and evening. At night, the price reaches a local minimum due to decreasing demand. The absolute height of these local extrema varies daily. Not only the average but also the volatility depends on the time of day (Appendix 5).

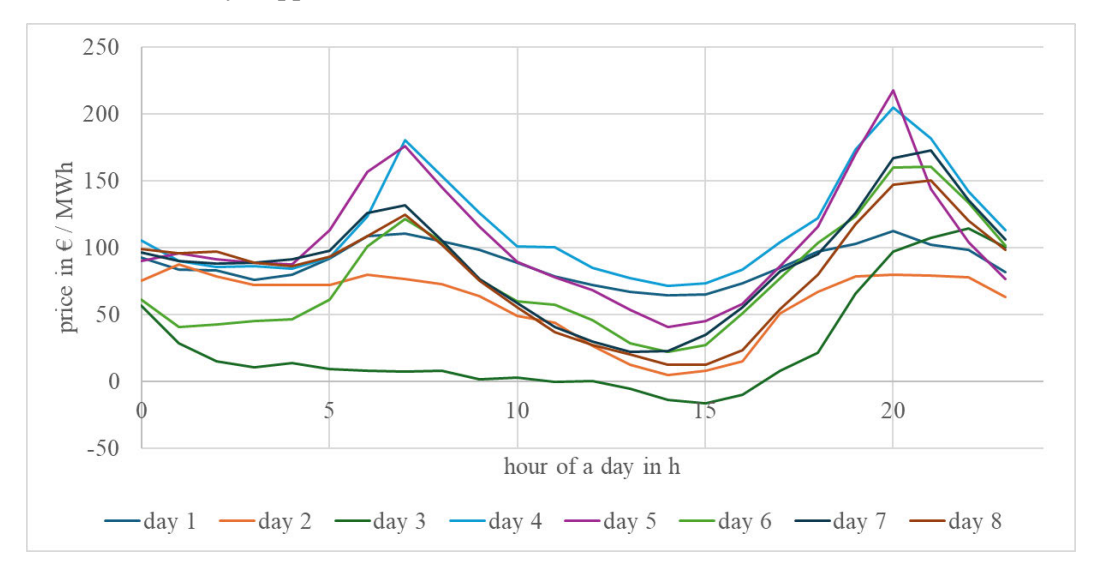


Figure 13 Hourly Dependency of Intraday Market Prices in  $\epsilon$  / MWh in Germany on June, 2024 (Fraunhofer ISE, 2024).

Additionally, market prices vary monthly (<u>Appendix 6</u>). From October 2021, both the average price and the volatility of the Intraday price have increased significantly. Although the average price in 2024 was around  $70 \frac{\epsilon}{\text{MWh}}$ , deviations of up to  $500 \frac{\epsilon}{\text{MWh}}$  from the average price in positive and negative directions are possible (<u>Appendix 7</u>). The energies traded on the Intraday Market have increased in recent years (European Energy Exchange AG, 2024).

Electricity prices can turn negative. The frequency of negative electricity price periods has increased significantly in recent years (Appendix 19). As long as conventional energy sources remain in the market, negative electricity prices may continue to occur more frequently. Turning off and on conventional power generation entails costs. Operators of conventional power plants seek to avoid them by submitting negative price bids (Philipp Götz et al., 2014:2). Additionally, the bidding design at the electricity exchange and the provision of power reserve services contribute to the amount of negative electricity prices (Philipp Götz et al., 2014:2).

The PR market shows an increase in tendered powers (Bundesnetzagentur, 2024b). Despite the rising tendered powers in recent years, the average activated powers have decreased (<u>Appendix 8</u>). The historical price development of the PR market is illustrated in <u>Figure 14</u>. The long-term average price is approximately  $2,500 \frac{\epsilon}{\text{MW} \cdot \text{week}}$ . Volatility increased following the opening of the European market in 2019 (Belmonte et al., 2023:916). The product length was reduced to the 4-hour period. A major influencing factor of rising electricity prices has been the rising gas prices due to the conflict with Russia, which started even before the war in the Ukraine (Belmonte et al., 2023:917).

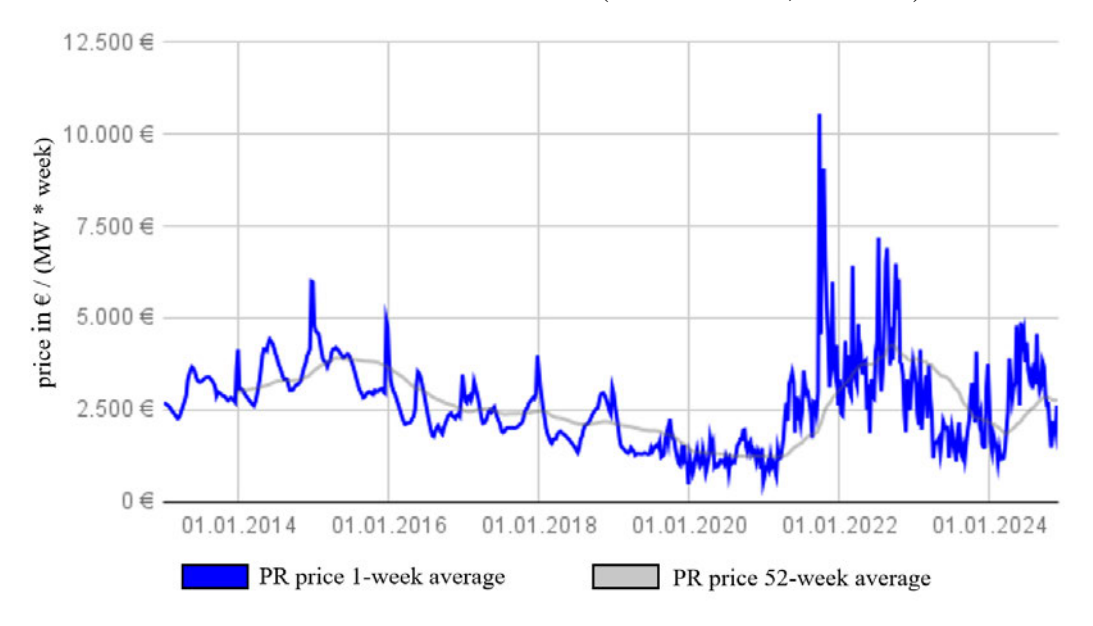


Figure 14 PR Price Development in € / (MW \* week) in Germany (Christian Schäfer, 2024)

The SR market exhibits similar behavior to the PR market. However, the tendered power on the SR market of approximately 2,000 MW is larger than the PR market power of about 600 MW. The amount of activated SR power has slightly decreased over the years (<u>Appendix 9</u>). The tendered power experienced a sudden increase in volatility following the opening of the European market in December 2022 (Belmonte et al., 2023:915).

Since 2021, there has been a significant rise in prices and increased volatility in both positive and negative SR energy and power prices. The average price in the years 2021 to 2022 for positive SR energy is  $296 \frac{\epsilon}{\text{MWh}}$ , while for negative SR energy it is  $62 \frac{\epsilon}{\text{MWh}}$  (Appendix 10). The average price of the SR energy markets is therefore significantly higher than on whole-sale markets. The power prices for positive and negative SR have followed a similar trend to those of PR and are comparable in value (Appendix 11).

The development of future BESS installations in Germany can be used as an indicator to assess the competition from other future market participants. The expected expansion of battery storage capacity is projected to increase linearly to 272 GW and 544 GWh by 2045 (Appendix 20). In contrast, the current capacity addition rate is growing exponentially (Tobias Reuther and Dr. Christoph Kost, 2024:26). In 2024, the installed battery storage capacity in Germany amounted to 12.1 GW, primarily consisting of residential storage systems (Fraunhofer ISE, 2025). Large-scale industrial storage systems with capacities exceeding 1 MWh account for 13 % of Germany's total storage capacity (Tobias Reuther and Dr. Christoph Kost, 2024:26). A significant increase in the installed capacity of large-scale industrial storage systems is predictable in the coming years (Fraunhofer ISE, 2025).

#### 2.6 Outages and Curtailments

At the start of a RES project, yield assessments are carried out. For simulating a BESS, hourly or quarter-hourly data is required to respond to highly fluctuating market prices. Simulation tools like PVsyst (PVsyst SA, 2024) or windPRO (EMD International A/S, 2024) can generate these hourly production data.

Simulation tools consider factors like solar irradiation or wind speeds and account for calculable system losses, such as inverter efficiency. Typically, these assessments are calculated assuming 100 % technical availability, meaning they exclude production outages.

Production outages can be categorized as shown in Appendix 42:

Technical outages in PV systems often involve inverter or string failures. Defective pitch or azimuth motors are examples of failures of wind turbines. Planned outages include inspections and maintenance. In the wind sector, additional planned losses may arise from bat protection. Other outages can be caused by environmental factors such as the snowfall on PV modules or ice formation on wind turbine blades.

Curtailments may be imposed by grid operators (GOs) to ensure grid stability. They are called Redispatch or Redispatch curtailments. Market-related curtailments, also called direct marketer (DM) curtailments, occur when energy cannot be sold or when market prices are negative. Curtailments in Germany are reimbursed, except for DM curtailments due to negative prices. Historically, such reimbursement has been subject to conditions outlined in (§ 51 EEG, 2024), which have evolved with successive updates. Starting in 2027, all plants for which the EEG 2023 is applied, will no longer receive compensation for negative spot market prices (§ 51 EEG, 2024). For newer plants often compensated via PPAs, such exclusions from compensation are also standard.

The outages marked black in <u>Appendix 42</u> are consistent over the years, whereas curtailments are not. <u>Appendix 21</u> illustrates the development of GO curtailments for different types of RES over the years. A significant increase is evident: over nine years, the curtailed energy volumes have increased approximately fivefold. While onshore wind energy GO curtailments have remained relatively stable over the past nine years, PV curtailments have shown a sharp increase in recent years.

Curtailments by GOs depend on the location of RES. The transmission lines of north-west and central Germany are the ones most affected by grid overloads in 2024 (Bundesnetzagentur, 2024c). In rare cases, some renewable plants may experience up to 50 % curtailment of annual yields.

Appendix 22 depicts the projected electricity production and usage in Germany during a week in July 2045. Large production peaks occur at midday on cloudless days, requiring renewable energy curtailments. BESS are used to shift peak production to the evening hours.

Not only RES, but also BESS can be controlled by the grid operator (EnWG, 2024, §13a). Unlike RES, which are used solely as generation units, the grid operator can charge (negative Redispatch) and discharge (positive Redispatch) BESS (Kyon Energy, 2024). Redispatch curtailments are prioritized to market behavior to prevent local grid overloads.

Redispatch forecasts from Germany's transmission grid operators indicate that equivalent energy volumes are curtailed in positive and negative Redispatch operations (50hertz et al., 2023:2). In 2024, an annual volume of 28.2 TWh each was expected for positive and negative Redispatch, increasing to 34.9 TWh annually by 2026 (50hertz et al., 2023:2).

Long-term forecasts predict GO curtailment volumes of 59 TWh annually in 2035, decreasing to 34 TWh by 2045 in a 100 % renewable energy system (<u>Appendix 23</u>). However, the study highlights that GO curtailments could reach up to 199 TWh annually by 2045 with accelerated PV expansion. (Fraunhofer ISI et al., 2024:32), corresponding to 14 % of Germany's total electricity production.

A seasonal analysis indicates that RES curtailments are more likely to occur from March to October (Fraunhofer ISI et al., 2024:16). This is attributed to high PV production on sunny days (<u>Appendix 22</u>). Due to the exponential rise in PV GO curtailments (<u>Appendix 21</u>), the proportion of PV curtailments relative to total curtailments is expected to increase from approximately 10 % in 2025 to about 45 % in 2030 and 50 % by 2045 (Fraunhofer ISI et al., 2024:17). For onshore and offshore wind combined, the share of curtailments decreases from 80 % in 2025 to 35 % in 2045 (Fraunhofer ISI et al., 2024:17).

Only part of the midday curtailments of <u>Appendix 22</u> can be attributed to local grid overloads. Market prices also drop with an oversupply of electricity, potentially resulting in negative prices. In such cases, the DM would typically curtail to avoid costs. DM curtailments are highly variable, ranging from 0 % to 28 % of injected energy for wind and PV plants in Germany during 2022 and 2023.

## 3 Simulation Input Data

#### 3.1 General Implementation Strategy

In the previous chapter, the theory of the BESS was described. The data of this theory will now be converted into the format required by the simulation program. The following list provides an overview of single input variables of the program. They are additionally described in detail in the related chapter:

- Technology of the storage system: The lithium technologies LFP or NMC can be selected.
   Additional technologies can easily be implemented, as an overview for lithium technologies LTO and LMO is given in chapter <u>2</u>.
- Year of commissioning: Time-dependent vectors, such as CAPEX for the BESS or market price forecasts, change over the years.
- Calculation period and replacement period: The calculation period defines the system's
  operational lifetime. Since BESS capacity degrades significantly, one or more capacity unit

- replacements before the end of the system's lifetime are recommended which is called replacement period.
- Activation and deactivation of markets: Generally, it is advisable to simulate BESS operation with all markets. However, if the potential of individual markets needs to be tested, markets can be excluded from the calculation.
- **Usable capacity and power**: The user can input the usable capacity and power, from which the program calculates the nominal values while considering operational degradation.
- **Grid limit**: Since RES and BESS are connected to the same grid connection point, the feed-in power at this point may be limited. This parameter only allows the feed-in limit to be reduced, not the consumption limit.
- **Power consumption of RES from BESS**: RES can be charged from the BESS. Technology-dependent charging power and prices, including taxes, can be defined. In periods when RES produces less than it consumes, the BESS can supply the power demand of RES.
- Fees: All fees incurred by the BESS for electricity consumption can be set as one fixed value.
- **Initial costs or revenue**: If additional costs or discounts that do not typically apply need to be considered at the beginning of a project, they can be recorded separately from CAPEX. For example, if a sufficiently powerful transformer is already available for connecting RES and BESS, the power-dependent CAPEX can be reduced.
- **Residual value**: At the end of each replacement period, the degraded capacity unit is sold at the indicated price.
- **Discount rate**: This rate converts future cashflows into present values.
- Energy-dependent OPEX: Some OPEX values depend on the energy throughput of the BESS.
- **DOD and reduced power usage**: Neither capacity nor power needs to be fully utilized. Partial power utilization increases efficiency (<u>Figure 5</u>), while partial capacity usage reduces capacity degradation (chapter 2.3.3). If the user-specified DOD is infeasible, the program recalculates the DOD based on capacity degradation. For example, 100 % DOD is not possible since capacity degrades. Then, the program assumes a constant usable capacity over the system's lifetime. If the degradation of a BESS with  $Q_U = 1$  MWh is 200 kWh,  $Q_N$  is calculated to 1.2 MWh.
- **Cycles per year**: The user determines the annual number of cycles, which affects both revenue and battery degradation.
- **Recovery time and activation**: A manufacturer-defined standby period for cooling the BESS after completing manufacturer-defined cycles should be applied to the simulation.
- **Self-discharge**: The self-discharge rate of the BESS depends on the storage technology and can reach up to 4 % per month for lithium technologies.
- Trading on SR energy markets for direct activation: It is possible to enforce the activation of SR energy since market participants with the lowest bid price are activated first. The program allows setting a user-defined bid below the auction average to approximate a 100 % activation probability. In praxis, however, such an approach does not guarantee activation, necessitating

alternative trading strategies. Nevertheless, this trading principle should be considered in the program.

- **Penalty**: If the BESS fails to deliver the traded energy due to outages, the shortfall is treated as a cost. The user can define how much higher penalty payments should be compared to the foregone revenues.
- **Prediction horizon**: The program calculates multiple possible future scenarios of different market participations and selects the one with the highest revenue. The number of generated scenarios can be adjusted.
- Storage duration for PR and SR: Figure 12 describes the storage duration, which can vary for PR depending on installed power and capacity. Additionally, users can define safety buffers.
- Safety factor charge capacity: A safety factor for the BESS charging allows for charging more energy than is required. The self-discharge and RES consumption are deducted from the additionally planned capacity. Moreover, increased charging capacity can help minimize penalty payments.
- Storage degradation costs: Since curtailments also compensate for BESS degradation, a forecast price for degradation can be specified. The forecast price can be estimated based on previous simulations.
- Loss due to non-optimal market behavior: The simulation program calculates optimal scenarios that may not be achievable in practice. A generalized loss can be defined to account for discrepancies between the real-world operation and the simulation results.
- **Multiple planning limitation**: If an optimal operation strategy has been planned, additional strategies can be incorporated as long as they do not compromise optimal operation. This is discussed further in chapter <u>4.2.3</u>.
- Additional dependencies on system RTE: The system RTE shows annual degradation effects and a dependency on the SOC, which can be taken into account.

Where single values are insufficient, vectors are used, which are imported into the program from Excel files. The following vectors are imported annually for the calculation period:

- Capacity and power-dependent CAPEX and power-dependent OPEX
- Power and energy-dependent grid charges
- System roundtrip efficiency

Vectors of 15-minute resolution are imported for the calculation period:

- Positive and negative curtailments by the grid operator
- Market prices
- Activation probabilities of PR and SR

For the following vectors, a 15-minute resolution for one year is sufficient. The program uses these values for all subsequent years. This concerns:

- RES production
- RES and BESS outages

The development of these vectors for the simulation program will be described in detail in the following chapters.

#### 3.2 Battery Cost Implementation

For the power-dependent CAPEX of the battery, dependencies on time and installed power were identified (Figure 9). Additionally, technological dependencies exist when non-lithium technologies are involved. In the simulation program, power-dependent CAPEX are therefore represented as a list in the form of an importable Excel file based on the above-mentioned dependencies (Figure 15). The values are manually adjustable, as forecasts can change rapidly due to fast developments in storage technologies. The current price assumptions are given in present prices. To take account of the time value of money, future prices are subsequently converted to the present value using the discount factor.

A	В	C	D	E	F	G	Н	1	J	K	L
technology_storage_syste	em total_power	2025	2026	2027	2028	2029	2030	2031	2032	2033	2034
Li-lon (LFP)	1	125	122	120	118	116	115	113	112	111	110
Li-lon (LFP)	10	86	85	83	82	81	80	79	78	78	77
Li-lon (LFP)	100	69	68	67	66	65	65	64	63	63	62
Li-lon (NMC)	1	125	122	120	118	116	115	113	112	111	110
Li-lon (NMC)	10	86	85	83	82	81	80	79	78	78	77
Li-lon (NMC)	100	69	68	67	66	65	65	64	63	63	62

Figure 15 Power-dependent CAPEX in  $\ell$  / kWh for Program Imports in the Form of an Excel File Dependent on Technology, Installed Power in MW, and Time (own Figure)

Linear interpolation is performed between different installed power levels. Each technology is listed individually. For the time t dependency, it is assumed that the learning curve for power-dependent CAPEX behaves similarly to that of capacity-dependent CAPEX. The time-dependent learning curve from Figure 8 is approximated by a regression function in the form of a fourth-degree polynomial r(t), and fitted to the literature values from Figure 9 using the following system of equations:

$$r(t_1) \cdot k + y = C_1$$

$$r(t_2) \cdot k + y = C_2$$
(16)

 $C_1$  describes the capacity-dependent CAPEX in 2020, and  $C_2$  the same for 2030. These are given by literature. The regression function r(t) is also known. The time stamps  $t_1$  and  $t_2$  correspond to the years 2020 and 2030. By solving the system of equations of the formulars (16), the parameters k and y are determined, ensuring the adjusted regression function for each storage technology and installed power matches the literature values. The values are converted to  $\frac{\epsilon}{kW}$  using equation (14). Figure 16 shows the power-dependent CAPEX over time for LFP and NMC for 1 MW, 10 MW, and 100 MW installed power. The larger the installed power, the lower the power-dependent CAPEX. However, the time-dependent cost reduction effects for less installed power are greater than for larger plants.

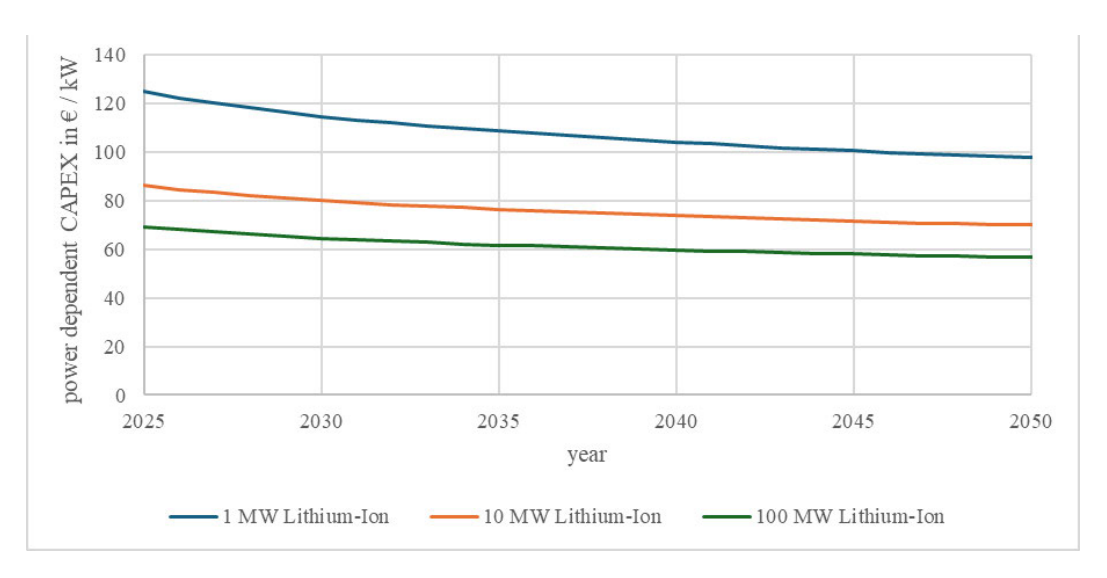


Figure 16 Calculated Learning Curves for Power-dependent CAPEX in  $\ell$  / kW for 1 MW, 10 MW and 100 MW for Lithium-Technologies as Time-Dependent Functions (own Figure)

The capacity-dependent CAPEX depend on time, installed power, installed capacity, and storage technology (<u>Figure 10</u>). As with the power-dependent CAPEX, the regression function from <u>Figure 8</u> is fitted to the given values from <u>Figure 10</u> using Equations (16). The results are again saved in the form of an Excel list and imported into the program.

Since variable OPEX are inconsistently documented in the literature and their impact on the total storage costs is expected to be minimal, a constant value of  $0.273 \frac{\epsilon}{\text{MWh}}$  can be assumed (chapter  $\underline{2.4}$ ). This variable can be adjusted by the user in the simulation program.

Given that fixed OPEX might have a significant impact on storage costs, all dependencies are taken into account: fixed OPEX depend on time, installed capacity, installed power, and storage technology (chapter 2.4). Since the learning curve of OPEX has a minimal effect on the overall result, a linear extrapolation is applied until 2030, with half the slope utilized for projections until 2050 (Appendix 34). When comparing different lithium technologies, fixed OPEX show little variation. Costs increase linearly with capacity growth. The cost reductions due to economies of scale with increasing capacity have significant influence on the OPEX (Appendix 34).

#### 3.3 System Round Trip Efficiencies Implementation

The RTE is influenced by SOC,  $P_U$ , battery technology, and time dependency (chapter <u>2.3.2</u>). Time dependency can be divided into learning rate and degradation effects (chapter <u>2.3.2</u>).

The SOC dependency is relevant only when SOC is below 20 % or above 80 % (<u>Figure 4</u>). This inefficiency below 20 % is minimized in the program by assuming a constant  $Q_U$ , whereas  $Q_N$  should be considerably greater due to degradation effects. The unused capacity, meaning the difference between  $Q_U$  and  $Q_N$  is considered charged to minimize cycling degradation (<u>Figure 7</u>). This is why the SOC rarely falls into the < 20 % range. Whenever SOC exceeds 80 %, the efficiency is assumed to be reduced linearly until maximal 26 percentage points system RTE reduction is reached at SOC = 100 % (<u>Figure 4</u>). The RTE reduction rate is adjustable by the user as well.

A BESS operated at 50 % of  $P_N$  is approximately 1.17 percentage points more efficient than when operated at  $P_N$  (Figure 5). The dependency of system RTE on  $P_U$  can be considered linear (Figure 5).

The learning rate has a slightly larger influence on system RTE than  $P_U$ : for lithium technologies, efficiency improvements of approximately 0.2 percentage points per year can be expected until 2030 (chapter 2.3.2). Due to the anticipated ramp-up phase for battery storage after 2030 (Bürklin et al., 2022:7), improvements are projected to be around 0.1 percentage points per year from 2030 to 2050, remaining constant thereafter.

Degradation rates of the RTE are estimated at 0.2 percentage points per year across lithium technologies, with minimal dependency on  $P_U$ , which is thus neglected (chapter <u>2.3.2</u>).

Battery technology has the greatest influence on system RTE, with a difference of up to 4 percentage points observed between lithium battery types (chapter <u>2.3.2</u>). This effect is more pronounced when comparing lithium batteries to other battery types (Martinez-Bolanos et al., 2020:6).

Since an RTE of 86 % was most consistently verified for NMC technology at beginning-of-life (BOL) with  $P_U = P_N$  in 2020, this value is set as the reference. LFP is rated 1.5 percentage points lower than NMC, with a 2016 study estimating this difference at 4 percentage points (chapter <u>2.3.2</u>). For this work, the RTE of LFP is assumed to be 3 percentage points lower than NMC:

system RTE(LFP, 2020, BOL, 
$$P_N$$
)(%) =  $(0.86 - 0.03) \cdot 100 = 83$  % (17)

In the Excel sheet, dependencies of  $P_U$ , technology, and learning rate are recorded. RTE degradation and SOC-dependency are calculated within the program and can be adjusted as fixed parameters in the simulation program.

Appendix 43 displays examples of calculated system RTEs based on technology, learning rate, degradation, and  $P_U$  in comparison.

#### 3.3 Legal and Tax Implementation

Since currently only the concession fee for BESS is applied to grid-consumed electricity, a user input field with a default value of  $0.11 \frac{\epsilon}{\text{kWh}}$  is provided (chapter <u>2.4</u>). The input contains the sum of all fees which may change in future.

For grid fees dependent on installed power, a time series in annual resolution is included. A grid utilization factor of 0.2 is assumed for the calculation (chapter 2.4), and the historical development shown in Appendix 16 is analyzed. As grid fees have nearly exclusively increased over recent years, a continued upward trend is expected. This is driven by the necessary grid expansion, which, according to current trends, will require further investments funded through grid fees. However, the specific impact of this increase on power-dependent grid fees for MV supply is uncertain. Therefore, historical development is linearly extrapolated up to 2035, with grid fees held constant until 2045 (Figure 17). After 2045, grid fees are expected to fall more sharply than they have risen before. By 2045, a complete grid expansion for RES integration is expected, likely leading to a significant reduction in costs. Nonetheless, residual grid optimizations are anticipated beyond 2045. In Figure 17, historical developments are depicted in light blue and projections in dark blue dots.

The projected power-dependent grid fees for BESS shown in <u>Figure 17</u> are stored as an annual time-dependent vector in an Excel file. Given that power-dependent grid fees behave similarly across higher voltage levels (<u>Appendix 16</u>), no distinction is made between different voltage levels.

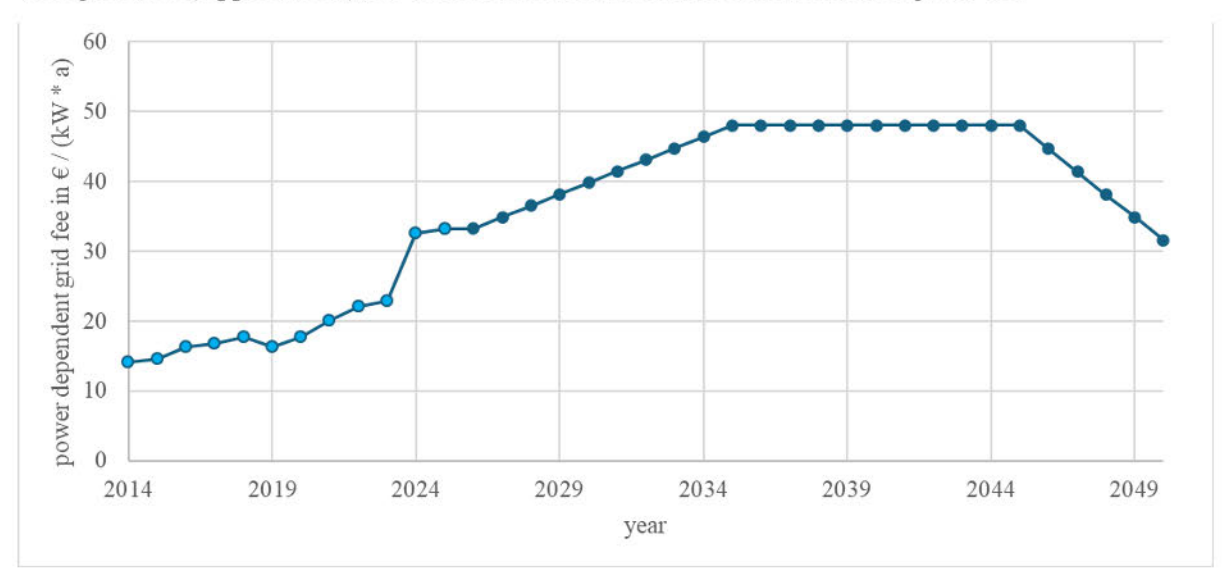


Figure 17 Forecast of Power Dependent Grid Fee in  $\epsilon$  / (kW \* a) for MV Connection for BESS (own Figure, Assumptions based on <u>Appendix 16</u>)

Energy-dependent grid fees are waived until August 4, 2029, for a period of 20 years (chapter <u>2.4</u>). Whether this waiver or a reduction of energy-dependent grid fees will continue post-2029 remains uncertain. Consequently, for installations commencing in 2030 or later, energy charges for the upper annual utilization hours for MV supply by Westnetz GmbH are projected based on historical trends (Westnetz GmbH, 2024a). This approach mirrors that of the power-dependent grid fee projection (Appendix <u>24</u>).

If the electricity consumption of RES is to be provided by the BESS, costs related to energy prices, grid fees, and levies can be saved. For the calculation, it is assumed that the BESS is compensated for these costs, which would otherwise have to be paid by RES to represent the benefit of a BESS installation. In practice, BESS would not receive any taxes and levies from RES. Instead, the profit of saved costs might be shared between RES and BESS.

Power-dependent charges for the grid connection remain in place to ensure that RES can still be supplied with electricity in case of a BESS failure. For this purpose, the electricity tariffs are analyzed as follows:  $1.041 \frac{\text{ct}}{\text{kWh}}$  are attributed to levies,  $7.61 \frac{\text{ct}}{\text{kWh}}$  to grid fees and  $14.84 \frac{\text{ct}}{\text{kWh}}$  to the energy price.

In the program, energy prices for the RES are stored as constants, as the utilized power of approximately 60 kW (chapter 5.1) represents only a minimal share of the BESS, which operates in the MW range. Therefore, the cost savings relative to the overall project profits are low. Since energy-dependent grid fees for BESS are expected to increase in the coming years (Appendix 24), grid fees are forecasted at  $9 \frac{ct}{kWh}$ . As energy prices are currently higher than normal due to gas shortages, future energy prices are assumed to be lower:  $11 \frac{ct}{kWh}$ . Consequently, the default cost for RES electricity consumption is set at  $21.04 \frac{ct}{kWh}$  in the program.

# 3.4 Electricity Market Implementation

## 3.4.1 Theoretical Forecasting Approach

For the commercialization of the BESS, the markets Intraday, PR, and SR are considered (<u>Figure 12</u>). Additionally, trading with RES is regarded as a separate market, whose prices equal the Intraday market but without taxes and levies. The maximum revenue can be achieved through the cross-market strategy (Appendix 2).

In practice, trading on the Day-Ahead market should also take place. However, due to the similarity of its prices to those of the Intraday market and the slightly higher volatility of the Intraday market (chapter <u>2.5</u>), the simulation omits an implementation of the Day-Ahead market.

For forecasting market prices and activation probabilities of the respective markets, historical data are statistically analyzed based on mean and volatility. The data is subsequently extrapolated for forecasts. However, historical data do not account for the impact of future BESS competition on market price developments. With the increasing expansion of BESS (<u>Appendix 20</u>), a rising supply in the markets is expected. This increased supply will likely lead to reduced price volatility, as BESS operate based on the arbitrage model.

The methodology for forecasting volatility time series is first presented theoretically and then visualized for the analyzed markets using diagrams.

Each historical time series of market prices or activation probabilities is divided into two parts: Part 1 and Part 2. Part 1 represents an older time frame compared to Part 2. The Volatility of both parts are analyzed separately.

The volatility G(t) is determined for each timestamp t using the squared deviations of the current value  $V_p(t)$  from the mean value  $\overline{x(t)}$  of the time series, scaled by the factor g for better visualization in the diagrams:

$$G(t) = \frac{\left(\overline{x(t)} - V_p(t)\right)^2}{g} \tag{18}$$

The time series G(t) is evaluated using a histogram. A total of 23 discrete intervals for G are defined, to which all values G(t) are assigned. For instance, the first part of a time series contains one million values, with squared deviations falling within the interval [1, 230]. Under linear scaling, the first discrete interval would range from 1 to 10, the second from 11 to 20, and so on, up to the last interval from 221 to 230. In an example evaluation, 200,000 values fall into Interval 1, 500,000 values into Interval 2, and 100,000 values into the last interval of G.

Next, the number of values per interval is converted into probabilities. In the case of one million values from Part 1 of the time series, the probability of a sample falling into Interval 1 is 20%, for Interval 2 it is 50%, and for the last interval 10%.

The probabilities for both parts of the time series are then compared for each interval. The probabilities for Part 1 have already been determined as 20 % for Interval 1, 50 % for Interval 2, and 10 % for the last interval. For Part 2, the following probabilities are assumed: 18 % for Interval 1, 48 % for Interval 2, and 20 % for the last interval.

The changes in probabilities are linearly extrapolated for the future and subsequently normalized to sum to 100 %. However, this probability change can only serve as an indicator for future G(t) values and cannot be directly computed via extrapolation.

For example, the following assumption would be incorrect: One year separates Part 1 and Part 2 of the time series. The probability of G(t) falling into the last interval has increased by 10 % over this period. Then in nine years, the probability of values being in the last interval would be:

$$10\% + 10\% \cdot 9 = 100\% \tag{19}$$

This statement is false because the sample period is too short to make reliable long-term projections.

Instead, a more accurate statement would be: The historical analysis indicates a significant increase in the probability of large volatilities and a slight reduction in small volatilities. Therefore, it can be assumed that the mean volatility of the time series will increase in the future. Additionally, the change rate of larger volatilities is expected to be positive and exert a greater influence than the negative change rate of smaller volatilities. The limited availability of data reduces the accuracy of such forecasts.

To estimate the impact of increasing BESS market competition in the future, all volatilities in intervals where G > 10 are manually reduced, with larger volatilities being reduced by a greater factor than smaller ones.

Finally, the forecasted probabilities of volatilities are converted into volatility values using a randomization function. This determines a random number between 0 and 10000 for each timestamp. If the probability for the first interval is 10 %, all random numbers between 0 and 999 are assigned to the volatility of the first interval. If the probability for the second interval is 30 %, all random numbers between 1000 and 3999 are assigned to the second interval and so on.

By rearranging formular (18) for  $V_p(t)$ , and incorporating the predicted mean value or the updated mean function, the forecasted time series can be generated.

#### 3.4.2 Application of Forecasts

BESS are particularly well suited for participation in the PR market, as they meet the requirements for rapid activation. Due to the activation probability of approximately 10 % for both positive and negative PR, exhibit low cycle utilization on the battery.

For forecasting PR time series in the simulation program, historical evaluations from chapter <u>2.5</u> are used as a reference. The required inputs include a price time series and a time series of activation probabilities.

The time series of activation probabilities is expressed as a percentage of the BESS nominal power. Only the following values are permitted: 0 %, 100 %, or -100 %. Positive values indicate charging of the BESS, while negative values represent discharging.

The activation probability  $p_A$  at each time step can be calculated from the historical tendered power  $P_V$  and activated power  $P_A$  using the following formula:

$$p_A(\%) = \frac{P_A}{P_V} \cdot 100 \% \tag{20}$$

However, since tendered power data is only available until September 2022, while activation power data is only available from July 2022 onward, the short data availability period does not allow for a

meaningful forecast. Instead, tendered and activated power are forecasted separately and subsequently converted into a time series of predicted activation probabilities using formula (20).

The historical tendered power exhibits a slightly increasing mean value (Bundesnetzagentur, 2024b). This trend is linearly extrapolated until 2040 and assumed to remain constant thereafter. The rationale behind this assumption is the extensive integration of renewable energies up to 2040 (<u>Appendix 23</u>). As the generation of renewable energies can only be predicted with limited accuracy, the demand for balancing energy is likely to increase with increased installed RES power.

For the volatility analysis of tendered power, two sample periods are considered: the first covering the years 2019 and 2020, and the second covering 2021 and 2022. Histograms of both time series are generated and compared. In <u>Figure 18</u>, the histogram for 2019/2020 is marked in dark blue, while that for 2021/2022 is shown in orange. The factor g in formula (18) is 437. The probability changes are linearly extrapolated until 2040. To account for the observed trend, it is assumed that the probabilities change every five years by the deviation determined between the two sample periods for each interval.

For example, the deviation in probability for G(1) = [0,1) between the 2019/2020 and 2021/2022 samples is 7.8 percentage points. Although this probability changed by 7.8 percentage points over two years, for long-term forecasting, the rate of change is reduced due to the limited sample period. It is assumed that the probability for G(1) = [0,1) increases by 7.8 percentage points every five years.

Subsequently, the data is normalized to 100 %, which reduces the effect for G(1). Instead of reaching 37.25 % in 2030, normalization reduces the value to 33.40 %, as visualized in <u>Figure 18</u> by the light blue column at G(1).

Since some values of G fall outside the scale, the last interval G(23) is extended to  $G(23) = (22, \infty]$ . The weighted average G of the last interval is shown in the diagram, in this case G = 38. If more values show volatility outside the scale, this is indicated by an increase of the red marked G shown in the diagram (Figure 18).

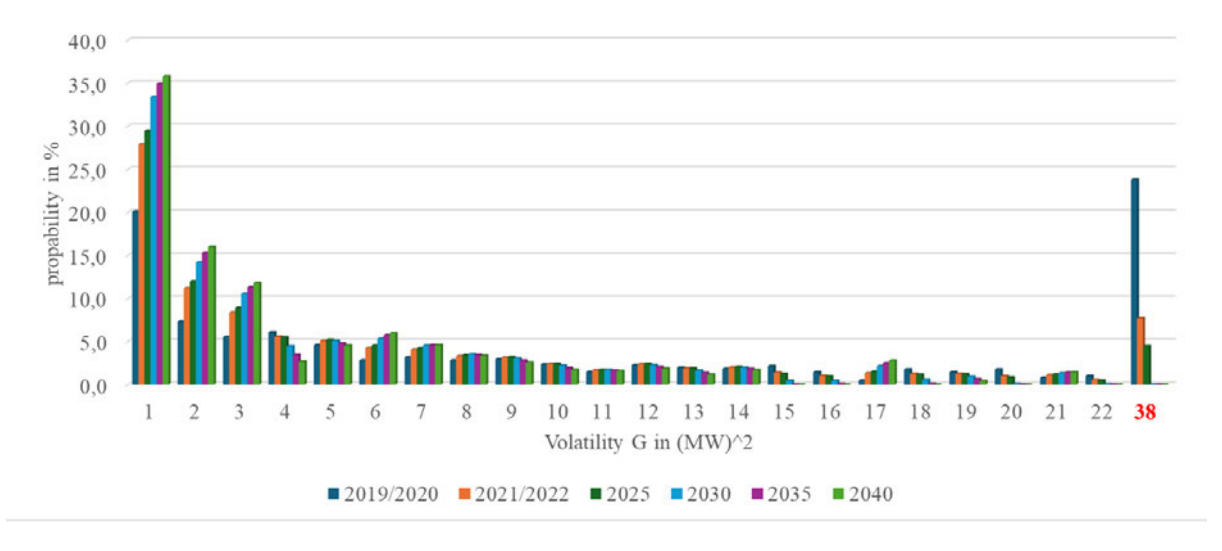


Figure 18 Time-dependent Volatility Development of Tendered PR Power with g = 437 (own Figure)

Considering the histogram from (<u>Figure 18</u>) and assuming the mean value trend, a time series of tendered volumes is forecasted. The probabilities of G are recalculated every five years using a stochastic algorithm until 2040 and are assumed to be constant thereafter until 2050. By rearranging formula (18) for  $V_p(t)$ , the forecasted auction volumes  $V_p(t)$  can be back-calculated using the predicted  $\overline{x(t)}$  and G(t).

Appendix 33 provides an example of tendered power in April data for different years for the period 2025 to 2050, with a 15-minute resolution. In the future, increasing fluctuations in RES generation and electricity consumption are expected to lead to growing forecast uncertainty in wholesale markets. Since the use of balancing power is driven by deviations between generation and consumption (50hertz et al., 2024c), rising forecast uncertainty will, in the long term, result in an increased demand for PR. This confirms the forecast presented in Appendix 33.

In the case of increased forecast uncertainty due to RES expansion, it is expected that the activated reserve power will also increase. However, the activated reserve power and its volatility in the PR market have slightly decreased overall in recent years (<u>Appendix 8</u>). This could be attributed to improved forecasting models or the analytical uncertainty of a short sample period.

As a compromise between the theoretically expected and actual developments, it is assumed that the historical average of activated power over recent years can be used unchanged for future projections.

Since the volatility of positive and negative activated PR power differs only slightly, and the sample size is limited to two years, the volatility trends for both are assumed to be the same. The volatility forecasts are determined using the same approach as the volatility forecast of tendered power in Figure 18. The activated power has remained relatively stable over the study period (Appendix 35). Cases in which particularly high PR power was activated have decreased. This results in an overall reduction of the standard deviation of activated power.

According to formula (20), the activation probability of PR at each timestamp can be calculated based on the forecasted tendered and activated power. Assuming a constant average activated power, an increase in tendered power leads to a decline in activation probability (formula 20).

A random algorithm determines whether an activation occurs based on the calculated activation probabilities. Activations of positive and negative PR are distributed with equal probability. Since the activation duration of PR is approximately 15 minutes (<u>Appendix 1</u>), the case of activation is recalculated for each timestamp.

This probability is approximately 4 % on average for each positive and negative PR between 2025 and 2050. This implies that a BESS participating exclusively in the PR market undergoes charge and discharge cycles for about 8 % of the year on average.

The forecasts for the individual markets Primary Reserve, Secondary Reserve, and Intraday market are described in more detail in <u>Appendix 44</u>. These forecasts were developed following the same principle as the forecast for PR activation probability. The mean and volatility were predicted separately based on historical analysis.

Volatility is estimated using histogram evaluation as in <u>Figure 18</u>. However, due to the rapid expansion of BESS, an increasing number of arbitrage participants can be expected in the future. These participants will bid at peak prices and shift to other markets when prices are too low. Since this future assumption is not reflected in historical data, extreme volatilities of G > 10 are manually adjusted downward.

The mean analysis accounts for market-specific dependencies. For instance, the Intraday market fluctuates depending on the time of day (<u>Appendix 5</u>) and varies monthly (<u>Appendix 6</u>).

All market forecasts were developed independently of each other. However, in praxis, there is a dependency between them: if Intraday market prices are high at time t, it is highly likely that reserve market prices will also be high at the same time. Nevertheless, deviations between the markets can still occur.

Considering market coupling is crucial for data forecasting because dependent data reduces the possible number of BESS cycles. According to <u>Figure 13</u>, the Intraday market experiences only two peak and two low prices per day, meaning there are only two buying and two selling periods for the BESS. In contrast, with independent data, there would be multiple peaks and lows, allowing for more frequent market trading. Since the number of cycles directly affects the IRR, the financial outcome would be significantly higher without market coupling than in reality.

All prices should be linked to the Intraday market, as this market accounts for most dependencies. To achieve this, Intraday market prices are divided into 200 intervals, like the previous volatility analysis. The interval corresponding to the mean value is identified, for example at interval 96.

For each timestamp t, the deviation  $\Delta I$  of the current Intraday price interval from the mean interval is determined. Suppose at time t, the prices are slightly lower than the mean, resulting in interval 80. The deviation between recent and mean interval is therefore  $\Delta I = -16$ , with the negative sign indicating values lower than the mean.

All other markets are also divided into 200 intervals, with interval step sizes varying by market, as they depend on the respective market prices.

The market-coupled prices are calculated as follows:

$$coupled\_price(t, market) = price(t, market) + \Delta I(t) \cdot step\_size(market)$$
 (21)

For the PR market price of  $6 \frac{\epsilon}{\text{MW} \cdot 0.25 \text{ h}}$ , with a market-dependent step size of  $0.05 \frac{\epsilon}{\text{MW} \cdot 0.25 \text{ h}}$  per interval, the coupled price at time t is calculated as follows:

$$coupled\_price(t, PR) = 6 \frac{\epsilon}{MW \cdot 0.25 \text{ h}} - 16 \cdot 0.05 \frac{\epsilon}{MW \cdot 0.25 \text{ h}} = 5.2 \frac{\epsilon}{MW \cdot 0.25 \text{ h}}$$
(22)

Additionally, SR+E and SR-E prices are limited to a maximum permissible deviation of  $100 \frac{\epsilon}{MWh}$  from the Intraday price at each timestamp.

## 3.5 Implementation of Outages and Curtailments

The production data from wind and/or PV are provided to the BESS simulation in the form of yield simulation data without grid consumption. Simulation data is more accurate as it better reflects the state-of-the-art compared to historical data. For PV plants, this includes aspects such as optimizing row spacing. In wind plants, advancements in blade design and drivetrain components have improved efficiency over time.

The production data resolution is 15 minutes, which aligns with the standard for Intraday market bids. Hourly time series from simulation tools like Wind Pro or PVSyst must be converted into the target format.

In addition to production, the following must be considered as well: production outages excluding curtailments, GO curtailments, DM curtailments at positive and negative market prices and electricity consumption of RES. All production data is limited to one year in the simulation program.

The planned yield from the yield report, excluding production outages from Appendix 42, is used for the BESS simulation. If yield simulations incorporate production outages, either these must be subtracted from the production time series, or the loss time series must be adjusted accordingly.

Production outages excluding curtailments are specific to each installation and vary seasonally (Appendix 29). Wind plants typically experience higher losses (5 %) than PV plants (4 %) annually. Degradation effects of RES are neglected.

An annual time series for production outages as a percentage of total production, based on <u>Appendix 29</u> is used for the simulation. Technical losses are assumed to decrease by 25 % compared to the historical analysis due to technological advances. This is an estimate because of missing long-term data for newer plants. Planned and other outages are assumed to remain unchanged.

Technical losses typically affect only parts of a plant, for example, inverter failures in PV plants or outages in individual wind turbines. Planned shutdowns and other outages may impact the entire plant, such as during grid maintenance or icing of wind turbine blades in winter.

Planned outages can affect either the entire plant or only specific components. For example, when inverters in a PV plant are serviced, individual inverters are sequentially shut down while the remaining inverters continue feeding power into the grid. In contrast, curtailment tests typically require shutting down the entire plant. In wind plants, planned outages for the maintenance of individual wind turbines generally impact only one turbine at once whereas planned outages due to bat protection affect the entire plant.

Other outages generally assume a complete plant outage: This includes grid-related work or failures, as well as ice formation on wind turbine blades during winter.

During grid work and grid outages, it would theoretically be possible to charge the BESS from the RES, as the grid would not be used. However, for safety reasons, the grid would then have to be switched off at the grid connection point and the inverters would also have to be able to operate in stand-alone mode, which is currently not the case.

The downtime of the BESS was assumed to be 5 % (Mongird et al., 2020:87-90). Only total outages are assumed for BESS.

Based on this analysis, the outages of RES and BESS are distributed across the months using a random generator, while ensuring that outages within a category are largely clustered, as this often reflects real-world conditions (Appendix 30). This time series is consistently applied across all years of the simulation.

Since the contractual structure of the RES regarding compensation during negative prices differs (chapter 2.6), the DM curtailments are not deducted from the RES yield simulation. Instead of curtailments, it is possible to store the energy from RES in the BESS, provided that the SOC is below 100 % and the market prices are not so negative that grid power consumption would be more economical for the BESS. Information about negative prices is contained in the market price series.

When the grid operator curtails RES, it represents a negative Redispatch measure aimed at reducing local grid power. Since BESS and RES are connected at the same grid connection point, Redispatch measures theoretically apply to both systems. This is also the simplified assumption in the simulation.

In practice, it could happen that only one of the two systems is affected because Redispatch measures reduce only a partial load of the local grid. Which plants are curtailed is at the discretion of the grid operator. If the BESS were charged during the negative Redispatch measure, the charging process would be compensated by the GO. If RES would sell energy to the BESS instead of a Redispatch measure, RES would not receive any Redispatch remuneration, as the principle of Redispatch states that no financial advantage may arise (EnWG, 2024, §13a)

For the simulation, the annual development of GO curtailments of <u>Figure 19</u> is assumed based on a combined studies analysis of chapter <u>2.6</u>. The average energy losses due to curtailments are expressed as a percentage of total production. The three graphs illustrate a forecast of production outages in general and individually for wind and PV plants. The green graph can be applied to both the negative and positive curtailments of BESS. Starting in 2045, the overall curtailed energy approximates the levels observed in 2025, though the curtailed energy shifts from wind to PV plants due to increased PV expansion.

With the more substantial PV expansion, the total curtailed energy of RES is expected to peak at  $96 \frac{\text{TWh}}{\text{a}}$  by 2035 and then to decrease until 2045 due to slower growth rates in RES expansion and progress in grid development. As no forecasts are available beyond 2045, curtailment energy for subsequent years is assumed to remain constant.

Projections of curtailments from wind and PV reveal differing trends. While wind on- and offshore curtailments currently account for 80 % of all curtailments, offshore wind curtailments constitute the largest share according to <u>Appendix 21</u>. Onshore wind curtailments, given their peak production in winter, are expected to be minimally impacted by curtailment developments. In contrast, PV plants are expected to be significantly affected due to their midday peak production and highest production from spring to late summer.

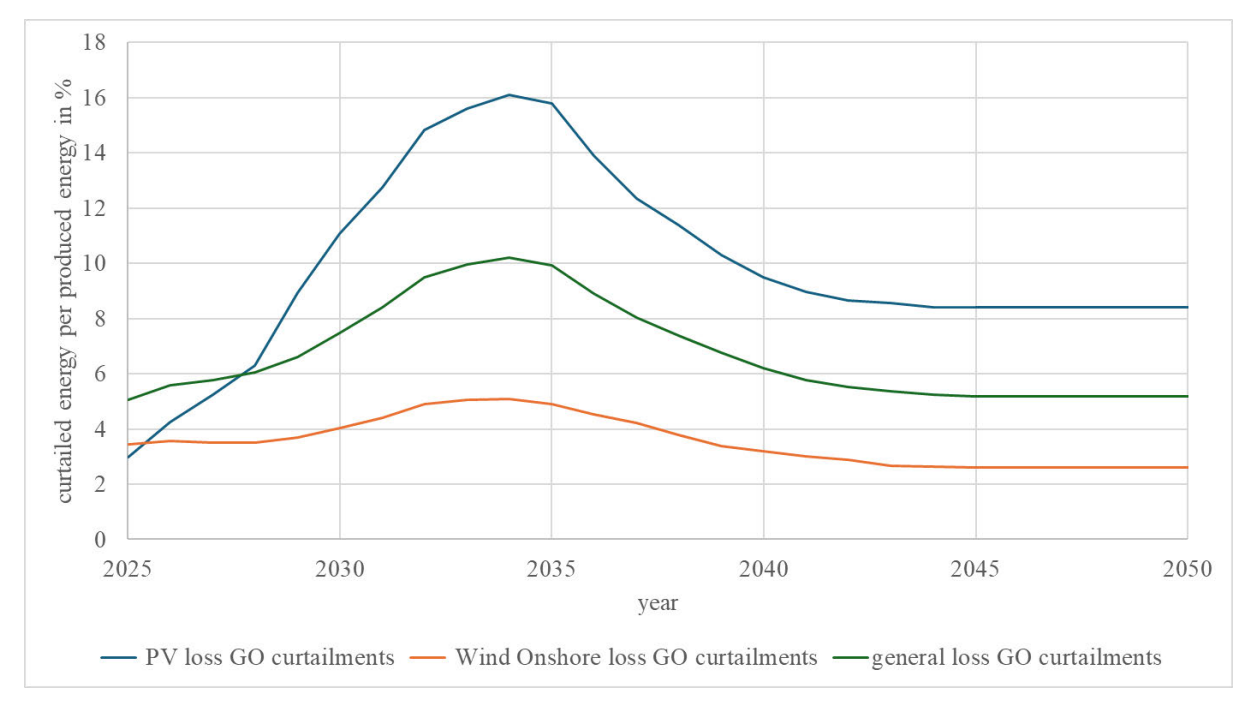


Figure 19 Forecast Average Curtailed Energy in % per Produced Energy of Grid Operators in Germany (own Figure)

<u>Appendix 31</u> shows the forecast of monthly distribution of GO curtailments. The forecasted distribution is assumed to be constant for all years of the simulation. An additional parameter determines the likelihood of daytime curtailments, enabling the differentiation of curtailments between wind and PV of Figure 19.

Based on monthly and annual distribution, the forecast of the GO curtailment time series from 2025 to 2050 in 15-minute resolution is developed by a randomize-algorithm.

Simplified assumptions are made that all GO curtailments occur at 100 %, which is often the case. Additionally, one-hour curtailments are assumed, even though curtailment durations vary in practice.

The average GO curtailments in Germany must be adjusted based on the location of grid connection, as grid bottlenecks vary significantly by region (<u>Appendix 32</u>). To achieve this, it is necessary to determine the factors by which local grid constraints of positive and negative curtailments are higher or lower than the average. If measurements from existing installations at the grid connection point are available, these can serve as a data source. Alternatively, <u>Appendix 32</u> can be used as an indicator for congestion areas, though it only reflects curtailments requested by transmission system operators and not those by distribution grid operators. For detailed planning of the BESS, inquiries should be made with the grid operator. Appendix 32 also shows local differences between positive and negative Redispatch.

For instance, if positive and negative expected curtailments are half the average, a random algorithm can be used to remove half of the values from the average GO curtailment dataset. Conversely, if positive and negative curtailments are expected to be twice as frequent as the average, a random algorithm can double the existing curtailment periods. It is crucial that this is not done entirely randomly so that PV curtailments can be weighted more than wind curtailments (Figure 19).

# 4 Simulation Algorithm Development

#### 4.1 Program Operation

The primary function of the simulation program is the dimensioning of capacity and power for a BESS that is connected to the same grid connection point as RES and planning its optimal operation. The dimensioning is performed through a cross-market optimization, meaning that the simulation algorithm trades the BESS across multiple markets to maximize profit. The simulation result with the maximum IRR is the final output.

In addition to the primary functionality, the program automatically generates a revenue time series for the financial model of a BESS. Since the revenue of a BESS is influenced by numerous variables, sensitivity analyses can be conducted to determine the impact of different parameters on the battery storage's profitability. Users can access and change every input parameter and time series to test their impact on the IRR. The program also enables the simulation of already-dimensioned BESS to verify financial key figures. By setting the RES production vector to 0, the BESS can be simulated independently of RES.

Chapter <u>3</u> described the development of all default input parameters for the simulations within this master's thesis. For application-specific simulations, all assumptions should be reviewed considering the guidelines provided, as parameters such as market price forecasts may change over the years. Some parameters, such as GO curtailments, depend on the installation location of the system.

In the application example in chapter  $\underline{5}$ , many application possibilities will be exemplarily tested, analyzed, and verified.

All functions of the program can be carried out via a graphical user interface. For faster program usage, such as sensitivity analysis, direct stack simulation in the code is recommended. This means that the simulation is run multiple times sequentially, with one or more input variables changing linearly.

To use the program via the graphical interface, the program can be executed by the 'Simulation.exe' file. Otherwise, Python must be installed. Additionally, installing an integrated development environment (IDE) is recommended. The program was developed using Visual Studio Code. The provided program ZIP file must be extracted, and the file 'main.py' must be executed after following the installation instructions which are described in the file 'READ\_ME.txt'. The graphical version of the program is activated by default. The program consists of multiple slides where input parameters can be entered. Once all slides are completed, the simulation can be started. If the simulation is completed successfully, a notification will be displayed in a pop-up window.

An example slide of the program is shown in <u>Figure 20</u>. It consists of a title (red) describing the current topic of the variables to be entered. Below, a description text (light orange) provides information about the variables to be entered. Excel files (green) store vectors, matrices, and lists for the simulation. All input Excel files are located in the 'data' folder and can be modified by the user according to the provided comments. Individual parameters can directly be entered by the user (blue). By clicking a button (purple), the inputs are validated and saved, proceeding to the next slide. If validation fails, the button turns red, and an error message is displayed in the terminal of the IDE.

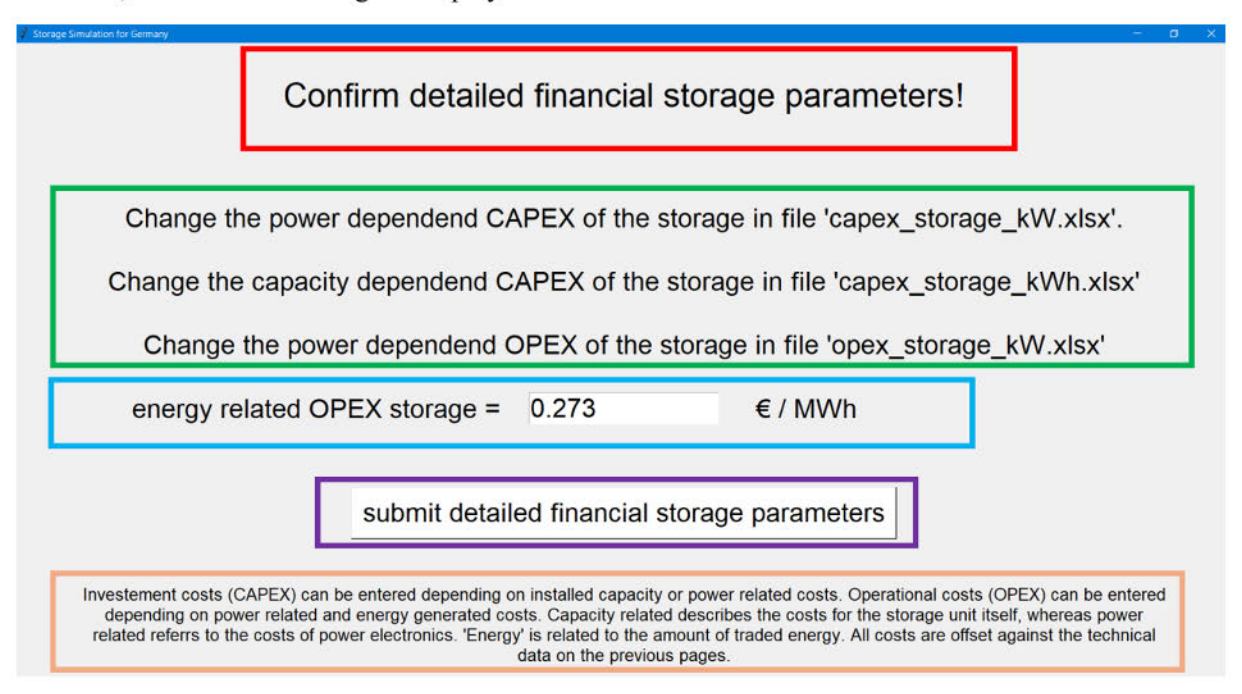


Figure 20 Example Slide of Simulation Program (own Figure)

How to start the program as a developer, for example, for sensitivity analysis, is described in Appendix 37.

The simulation results are provided in the 'output' folder in Excel format. The file 'main\_output\_vectors.xlsx' contains the key output vectors, including SOC, operational behavior, for example market participation, and revenue in a 15-minute resolution. The IRR and NPV are displayed in file 'main financial output.xlsx.'

# 4.2 Program Algorithms

### 4.2.1 Program Overview

After entering the input parameters, which can be provided either through the graphical interface or directly in the programming environment (chapter 4.1), the program executes the following steps, as illustrated in Figure 21.

Once all data has been loaded into the program, it is standardized into a uniform format, as the vectors partially differ in length. All data is trimmed to the simulation period.

Since cross-market optimization is employed, the prices of all selected markets are first converted into a comparable format and sorted by the most favorable prices. Depending on the number of cycles per year of the BESS specified by the user, the markets with the most advantageous prices are saved as a theoretical operational plan. In this process, charging and discharging cycles are alternately distributed. According to the arbitrage model, it is crucial to sell electricity at high prices and purchase it at low prices.

The theoretical planning of market participation based on the most favorable prices and number of cycles cannot be fully realized in practice because SOC and market conditions are not considered yet. For example, in reserve power markets, a minimum capacity must be charged or discharged to enable participation. This aspect is subsequently addressed by generating multiple operational forecasts under real conditions, starting from the current timestamp. These forecasts depend on the prediction horizon and the *power\_factor* of the BESS.

The prediction horizon defines the number of future timestamps the program can use to plan for the current timestamp. The *power factor* describes the ratio between usable power and capacity, similar to the concept of storage hours. The forecasts generated each represent a practically feasible operation of the BESS. A comparison price is calculated for each forecast to select the operation with the most advantageous price. This step is referred to as 'New Plan Operation' in **Step 4** of <u>Figure 21</u>.

With the BESS operation now optimally planned, trading would take place on the markets defined in the 'New Plan Operation'. However, once delivery occurs, further unforeseeable events such as curtailments or failures can arise. These are addressed in **Step 5**. If trading has already occurred and the BESS is unable to meet delivery obligations, for example due to an outage, the BESS must pay compensation.

The output of the main simulation includes a time series of the SOC, operations and revenue. The user specifies consistently usable power and capacity over the simulation period. Using degradation calculations, the nominal power and capacity of the BESS can be determined. Changes in capacity units are also accounted for. Financial metrics, such as IRR and NPV, are calculated.

The simulation program can perform multiple iterations with varying input parameters. The scenario with the highest IRR is identified as the result.

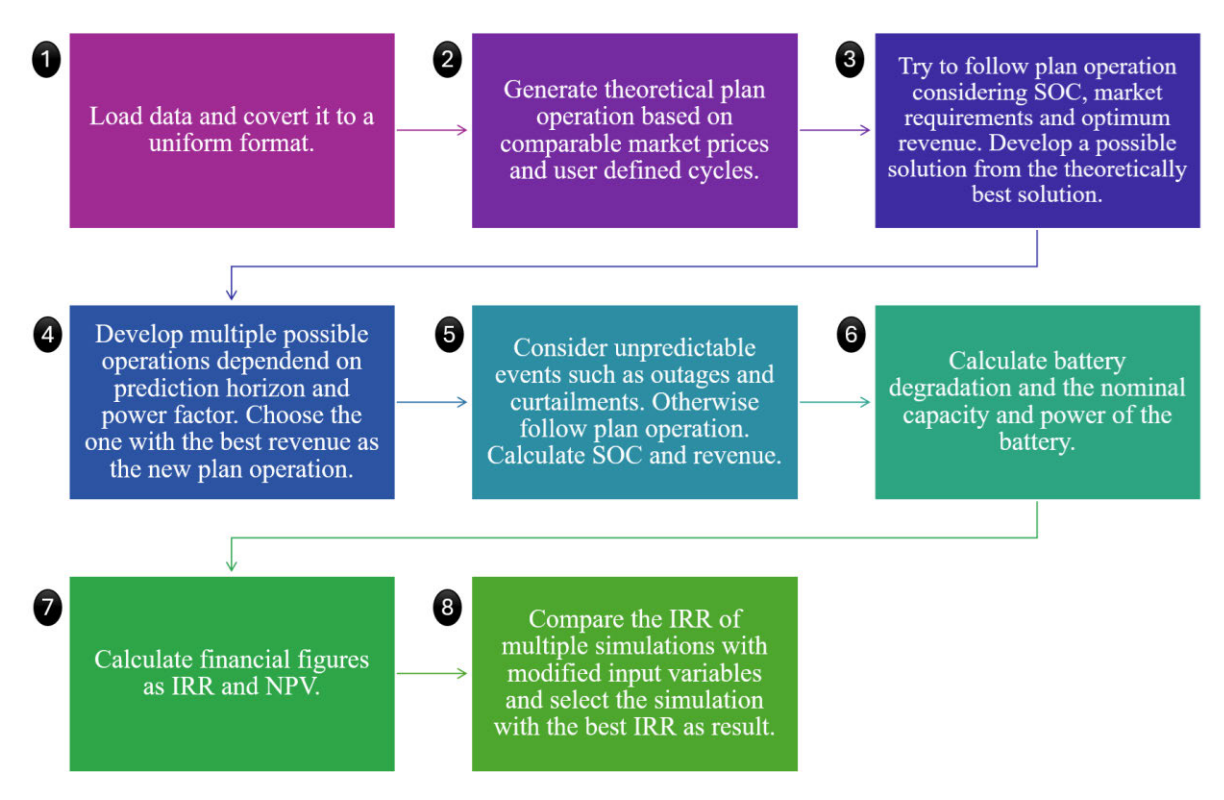


Figure 21 Overview: Elements of the Simulation Program (own Figure)

#### 4.2.2 Theoretical Plan Operation

The first part of the program is shown in <u>Figure 22</u> as an abstract program flow chart. This comprises **Steps 1 and 2** in <u>Figure 21</u>. The description comes afterwards.

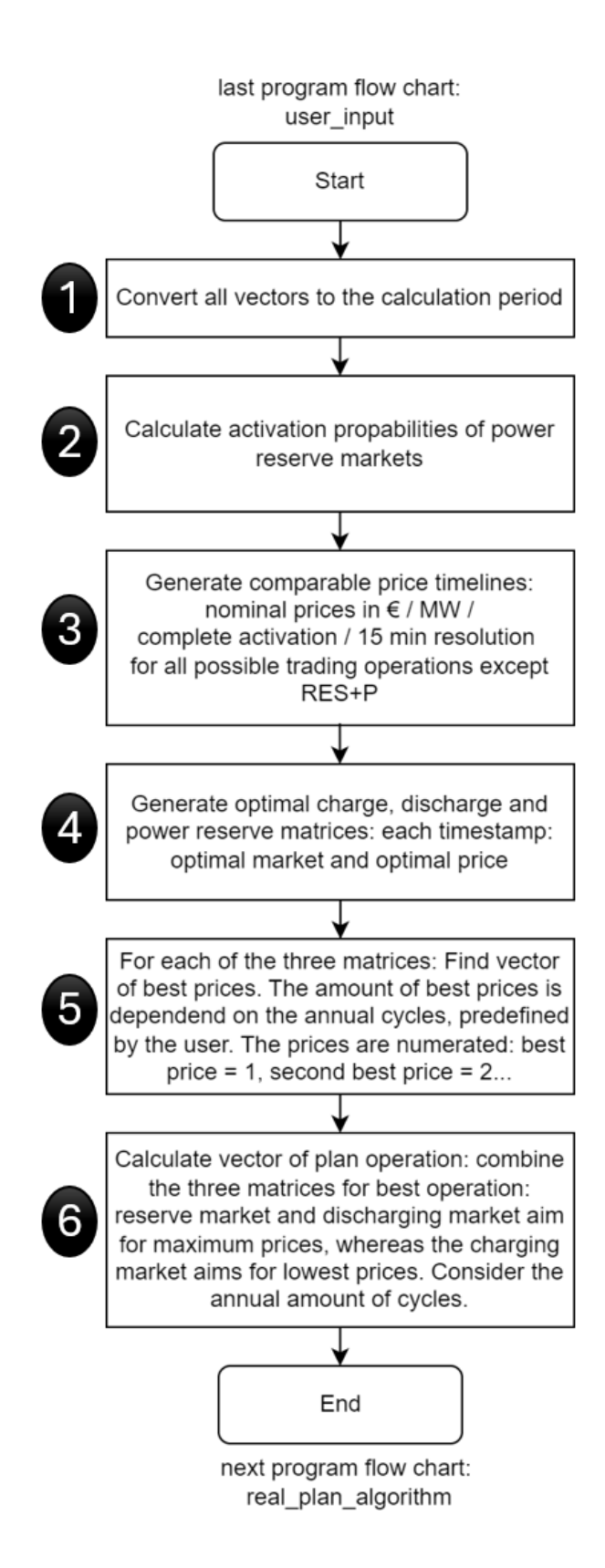


Figure 22 Program Flow Chart 1: Development of Theoretical Plan Operation based on Comparable Market Prices (own Figure)

The variables entered by the user are directly stored in the structure *input\_data.py*. In contrast, the data from the Excel files is imported using various methods. The objective is to convert the data into a unified format and shorten it to match the calculation period.

If the data consists of values that change annually, it is already truncated to the calculation period during the import process, which is defined by the *year\_commissioning* and the *end\_year*. The *year\_commissioning* is included in the calculation, while the *end\_year* is excluded, fulfilling the following formula:

$$year\_commissioning + calculation\_period = end\_year$$
 (23)

The *calculation\_period* specifies the number of full years included in the simulation.

The data for wind and PV power, as well as their outage periods, is imported annually without accounting for leap years, that means 35040 values. From this, renewable production *RES\_production* is calculated using the following formula:

$$RES\_production (MW) = (power\_pv (MW) \cdot losses\_pv + power\_wind (MW) \cdot losses\_wind) \cdot curtailments\_GO$$
(24)

The PV production *power\_pv* and wind production *power\_wind* are given in MW. The losses for PV and wind *losses\_pv* and *losses\_wind* are expressed as percentage factors between 0 and 1 and represent the downtime rates of the respective technologies. The grid operator's curtailments *curtailments\_GO* are also expressed as a percentage factor, where a factor of 1 indicates no losses and 0 indicates a complete outage.

For the simulation, it is assumed that the same Redispatch measures apply to RES and the BESS (chapter <u>2.6</u>). Therefore, in the simulation program, the RES production is reduced by the Redispatch measure in formula (24).

In the program, units are converted accordingly within the formula. Additionally, the program allows deactivating PV or wind production. In such cases, the corresponding power in formula (24) is set to 0.

All 15-minute resolution vectors must be compatible for calculations. Since the vectors cover different time periods and treat leap years differently, a unified format must be established.

Market data, GO Curtailments, BESS outages, and reserve power activations are provided in 15-minute intervals over 25 years, including leap years. This results in 876576 values. The program uses nominal years, where one nominal year consists of 35063 values. Consequently, all data with 876576 values is reduced by one value and the data with 35040 values is adjusted to nominal years by padding the remaining values with zeros and repeating the sequence 25 times.

All vectors with 15-minute resolution now consist of 876575 values, representing 25 nominal years.

This completes **Step 1** of <u>Figure 22</u>.

The objective is to calculate a comparative price between the various markets in which the BESS can participate. Charging the BESS should occur during low-price periods, while discharging should take place during peak-price periods. However, the Intraday, SR Power, PR Power, and SR Energy markets have different structures:

In the Intraday and SR Energy markets, the bid length is 15 minutes, whereas bids in the reserve power markets span 4 hours (Figure 12). Reserve power is provided, but the corresponding energy is not always activated. Consequently, energy prices are only remunerated when energy is supplied, whereas the reserved capacity is always compensated. Additionally, different marketing strategies undergo varying cycles of the BESS: trading on the Intraday market ensures that energy is supplied, whereas activation in the reserve power and reserve energy markets are infrequent.

To calculate comparative prices, the ratio between profit and expenditure must be maximized. Profit refers to the income generated by the BESS through market participation. Expenditure is defined as the BESS cycles, as they primarily contribute to degradation (Figure 7).

For comparability, all prices are converted into nominal prices with the unit  $\frac{\epsilon}{\text{MW} \cdot 15 \, \text{min} \cdot \text{full activation}}$ . The cycle equivalent is expressed through full activation and refers to the case where usable power *simulation\_power* is injected.

Markets are categorized into charging markets, discharging markets, and reserve power markets. Charging markets include charging from the Intraday market (INT-P), from renewable generation (RES-P), and from the negative secondary reserve energy market (SR-E). Discharging is possible in the Intraday market (INT+P) and the positive secondary reserve energy market (SR+E). Reserve power markets include Primary Reserve (PR), positive Secondary Reserve (SR+P), negative Secondary Reserve (SR-P), and the simultaneous provision of positive and negative Secondary Reserve (SR±P).

A nominal price can be determined for each category.

The following formula is used to convert the original Intraday price *price\_Intraday* into the nominal price *nominal\_price\_Intraday*, considering 15-min resolution:

$$nominal\_price\_intraday \left(\frac{\epsilon}{MW}\right) = \frac{price\_intraday \left(\frac{\epsilon}{MWh}\right)}{4 \left(\frac{1}{h}\right)}$$
 (25)

If energy must be bought or sold short term, for example, to adjust the SOC for the next planned trade, trading can occur on the SR energy market without prior trading on the SR power market. In this case, only the energy price is remunerated for the 15-min period, while the power price is not. Unlike the Intraday market, the SR energy markets do not guarantee 100 % activation, as the activation probability is around 1-2 %. The lowest energy price bidder is always activated. This means that offering lower than the program's stored average energy price increases the likelihood of activation. The variable *lower\_bid\_for\_direct\_activation*, defined by the user, determines how much lower the offer must be to assume a 100 % activation probability in the program:

$$nominal\_price\_SR\_energy \left(\frac{\epsilon}{MW}\right) = \frac{(price\_SR\_energy - lower\_bid\_for\_direct\_activation) \left(\frac{\epsilon}{MWh}\right)}{4 \left(\frac{1}{L}\right)}$$
(26)

This allows SR energy markets to be utilized as both charging and discharging markets. Since this assumption cannot be relied upon in reality, an alternative market should be considered for charging or discharging in case activation does not occur despite the lower bid. Nonetheless, the potential of SR energy markets without utilizing the associated power markets should not be disregarded. Therefore, activation is simplified by assuming lower bids than the auction mean price.

The PR and SR power markets, which have a bid length of 4 hours, have already been converted to a 15-minute resolution. For a 4-hour bid, the sum of the specified power prices from the 15-minute time series is used. For reserve power markets, activation cannot be predicted. Instead, activation probabilities should be used to determine the nominal price. The activation time series for positive and negative PR and SR, stored in the Excel files, are converted into activation probabilities.

**Step 2** of Figure 22 is thus completed.

Even though activation time series are stored in the program, they are unknown at the time of planning and therefore cannot be directly considered. For PR participation the activation cannot be forced. The normalized price for the PR market is calculated as follows:

$$nominal\_price\_PR\ \left(\frac{\epsilon}{MW}\right) = \frac{price\_PR\left(\frac{\epsilon}{MW}\right)}{activation\_propability\_PR}$$
(27)

The activation probability is a percentage factor between 0 and 1. The lower the activation probability, the higher the normalized PR price, as the system operator receives payment for a service that is rarely required. Energy prices are not included in this case, as they are not additionally remunerated. The PR market also does not differentiate between positive and negative PR.

For all SR power markets, the following formula applies:

$$nominal\_price\_SR\_power\left(\frac{\notin}{MW}\right)$$

$$= \frac{price\_SR\_power\left(\frac{\notin}{MW}\right) + \frac{price\_SR\_energy\left(\frac{\notin}{MWh}\right)}{4\left(\frac{1}{h}\right)} \cdot activation\_propability\_SR}}{activation\_propability\_SR}$$
(28)

The power price is divided by the activation probability in green to account for full activation. Additionally, the price for activated energy is obtained, but only if activation occurs. Therefore, another multiplication by the blue activation probability is necessary. The blue activation probability separates the remuneration ratio of SR power and energy by making energy remuneration less likely, while the green activation probability accounts for reduced cycle impact. In contrast to formular (26), the auction mean value is assumed. The activation probability varies depending on the selected SR Power market  $SR\pm P$ , SR+P or SR-P.

Another remuneration series describes electricity trading between RES and BESS. Since it is assumed that RES is also marketed on the Intraday or Day-Ahead market, the Intraday market time series of positive prices is used for the BESS charging process. This results in the following advantages when purchasing RES electricity compared to Intraday electricity:

If purchasing occurs during RES production and positive market prices, RES electricity is prioritized for storage because avoided grid usage reduces grid and concession fees for the BESS (chapter <u>2.4</u>).

If RES production exceeds a grid limit, it is assumed that the BESS can purchase the excess amount at a price of 0.

RES can purchase electricity from the BESS at a fixed price set by the user since electricity consumption is not traded on the market (RES+P). This fixed price includes the taxes that RES would otherwise have to pay to account for the additional profit of the BESS. Additionally, the fees that the BESS would incur when feeding power into the grid are deducted.

**Step 3** of Figure 22 is now completed.

Some of the eight different markets compete. An optimum is determined for each set of competing markets. The categorization is as follows: power marketing, BESS charging at low energy prices, and BESS discharging at high energy prices.

For power marketing, the competing markets are PR, SR+P, SR-P and SR±P. The charging markets are INT-P, RES-P and SR-E, while discharging is possible in the markets INT+P and SR+E.

The case of RES+P is considered separately because the exchanged power is minimal compared to the *simulation\_power*.

Matrices are created for the three described categories, each with two columns and t rows, where t represents the number of simulation timestamps. The first column contains the optimal price, and the second column specifies the market acronym where the optimal price can be achieved.

**Step 4** of <u>Figure 22</u> is now completed.

The example output of the three matrices is shown in <u>Figure 23</u>. The three different market types of charging, discharging and reserve markets are shown in different colors. The prices are given in nominal prices. The optimum market for each market type is formed for each time stamp. In cell C5, for example, the RES-P market was the optimal charging market at 01.01.2025 01:15 AM. The SR-E market was optimal at 01:30 AM.

	А	В	С	D	E	F	G
1		Price charge	Market charge	Price discharge	Market discharge	Price power reserve	Market power reserve
2	01.01.2025 00:15	-10,825	SR-E	50,375	SR+E	759,308	SR+P
3	01.01.2025 00:30	-8,075	SR-E	50,375	SR+E	759,308	SR+P
4	01.01.2025 00:45	-28,750	SR-E	45,375	SR+E	754,308	SR+P
5	01.01.2025 01:00	12,825	RES-P	37,150	SR+E	746,083	SR+P
6	01.01.2025 01:15	-3,750	SR-E	44,250	SR+E	753,183	SR+P
7	01.01.2025 01:30	-3,750	SR-E	25,375	SR+E	734,308	SR+P
8	01.01.2025 01:45	-3,750	SR-E	25,375	SR+E	734,308	SR+P
9	01.01.2025 02:00	-3,750	SR-E	55,375	SR+E	764,308	SR+P
10	01.01.2025 02:15	-28,750	SR-E	64,950	SR+E	773,883	SR+P
11	01.01.2025 02:30	-3,750	SR-E	46,825	SR+E	755,758	SR+P
12	01.01.2025 02:45	-28,750	SR-E	42,450	SR+E	751,383	SR+P
13	01.01.2025 03:00	14,225	RES-P	75,375	SR+E	784,308	SR+P
14	01.01.2025 03:15	11,350	RES-P	60,375	SR+E	769,308	SR+P
15	01.01.2025 03:30	-8,750	SR-E	50,375	SR+E	759,308	SR+P
16	01.01.2025 03:45	2,875	SR-E	75,375	SR+E	784,308	SR+P
17	01.01.2025 04:00	1,850	SR-E	46,825	SR+E	755,758	SR+P
18	01.01.2025 04:15	2,875	SR-E	41,700	SR+E	501,635	SR+P

Figure 23 Optimum Price and Market Matrices of Charge, Discharge and Power Reserve Markets - Nominal Prices are Given in  $\ell$  /MW / full\_active (own Figure).

The goal is to find out which prices are best for each matrix. The number of best prices depends on the number of cycles per year defined by the user. A cycle consists of a charge- and a discharge cycle:

$$cycle = charge\_cycle + discharge\_cycle$$
 (29)

The number of best price timestamps is influenced not only by the cycles, but also by the power factor, system efficiency, self-discharge, and the activation probabilities of the reserve power markets.

The number of annual affected discharge timestamps is calculated as follows:

$$annual\_discharge\_timestamps = cycles \cdot power\_factor\left(\frac{MWh}{MW}\right) \cdot 4\left(\frac{MW}{MWh}\right)$$
(30)

The annual user-defined number of cycles are multiplied by 4 because the storage system requires four timestamps to charge 1 MWh at 1 MW. The *power\_factor* indicates the ratio of usable capacity to power. If, for example, the capacity doubles, twice as many timestamps would be required at constant power to complete one cycle.

The number of charge cycles is greater than that of discharge cycles due to system RTE losses and self-discharge. Therefore, formula (30) is adjusted accordingly to convert the number of charge cycles into the number of affected timestamps:

$$annual\_charge\_timestamps = annual\_discharge\_timestamps \cdot system\_RTE\_factor \cdot \\ self\_discharge\_factor$$
 (31)

The factors for self-discharge *self\_discharge\_factor* and for the system RTE *system\_RTE\_factor* also access user inputs. They are > 1, which is why the number of annual charging time stamps is greater than the discharging time stamps.

For reserve power markets, the number of usable timestamps is based on the activation probabilities for each year.

Since SR+P has a low probability of discharge, the usable timestamps are calculated as follows:

$$annual\_timestamps\_SR\_plus\_P = \frac{annual\_discharge\_timestamps}{activation\_propability\_SR\_plus\_P} \tag{32}$$

Since SR-P has a low probability of charging, the usable timestamps are determined as follows:

$$annual\_timestamps\_SR\_minus\_P = \frac{annual\_charge\_timestamps}{activation\_propability\_SR\_minus\_P} \tag{33}$$

For PR and SR±P, the average of charge and discharge timestamps and each activation probability is considered. Since the activation probability << 1, the number of tradable timestamps in the reserve power markets is significantly higher than in the charge or discharge matrices.

Due to the low activation probabilities of the SR power reserve markets of around 1 %, it is possible that more time stamps are calculated than available. Depending on the stored input data, this limit could already be exceeded from 87 cycles per year for a power factor of 1. Therefore, if this limit is exceeded, the number of examined time stamps is set to the maximum available for simplification.

The three matrices for charging, discharging, and power reserve nominal prices & markets are sorted according to the best possible nominal prices while considering the calculated number of timestamps according to formulars (30) to (33).

For example, in the charging matrix (<u>Figure 23</u>), the lowest price is assigned to number 1, and the second-lowest price is assigned to number 2. At the same time, the number of used timestamps is increased according to formulars (30) to (33).

**Step 5** of <u>Figure 22</u> is now completed.

The scheduled operations determined for each of the three matrices shall be merged into a single scheduled plan operation. The plan operation corresponds to **Step 6** of <u>Figure 22</u>, which is depicted as a detailed program flowchart in <u>Figure 24</u> and explained using the example of <u>Figure 25</u>.

The algorithm distributes optimal charging, discharging, and power reserve market participation within the plan operation, based on the three nominal price matrices. The distribution terminates when the user-defined target cycles are met. Since both selling electricity at high prices and purchasing it at low prices are essential, charging and discharging timestamps should be alternately assigned. If a power reserve timestamp is allocated, the sequence between charging and discharging timestamps should remain unchanged. As a simplification, each timestamp is traded on only one optimal market.

For each of the three matrices, the optimal price and its corresponding index are determined. If a charging timestamp is to be assigned, the charging market is inserted at the corresponding index in the plan operation. Otherwise, the algorithm selects the optimal market based on the nominal discharging

and power reserve prices and assigns it accordingly. This process is repeated for all charging and discharging timestamps within a year and iterated in an outer loop for all years. Power reserve market participation is counted proportionately toward charge and discharge timestamps based on its respective activation probability.

Due to the typically low activation probability of power reserve markets, it is possible that all timestamps are assigned without achieving the target number of charging and discharging timestamps. In such cases, the assigned power reserve timestamps are overwritten with optimal charging and discharging timestamps, thereby increasing the total number of distributed timestamps until the target is met.

The **Final Step** of <u>Figure 22</u> is completed.

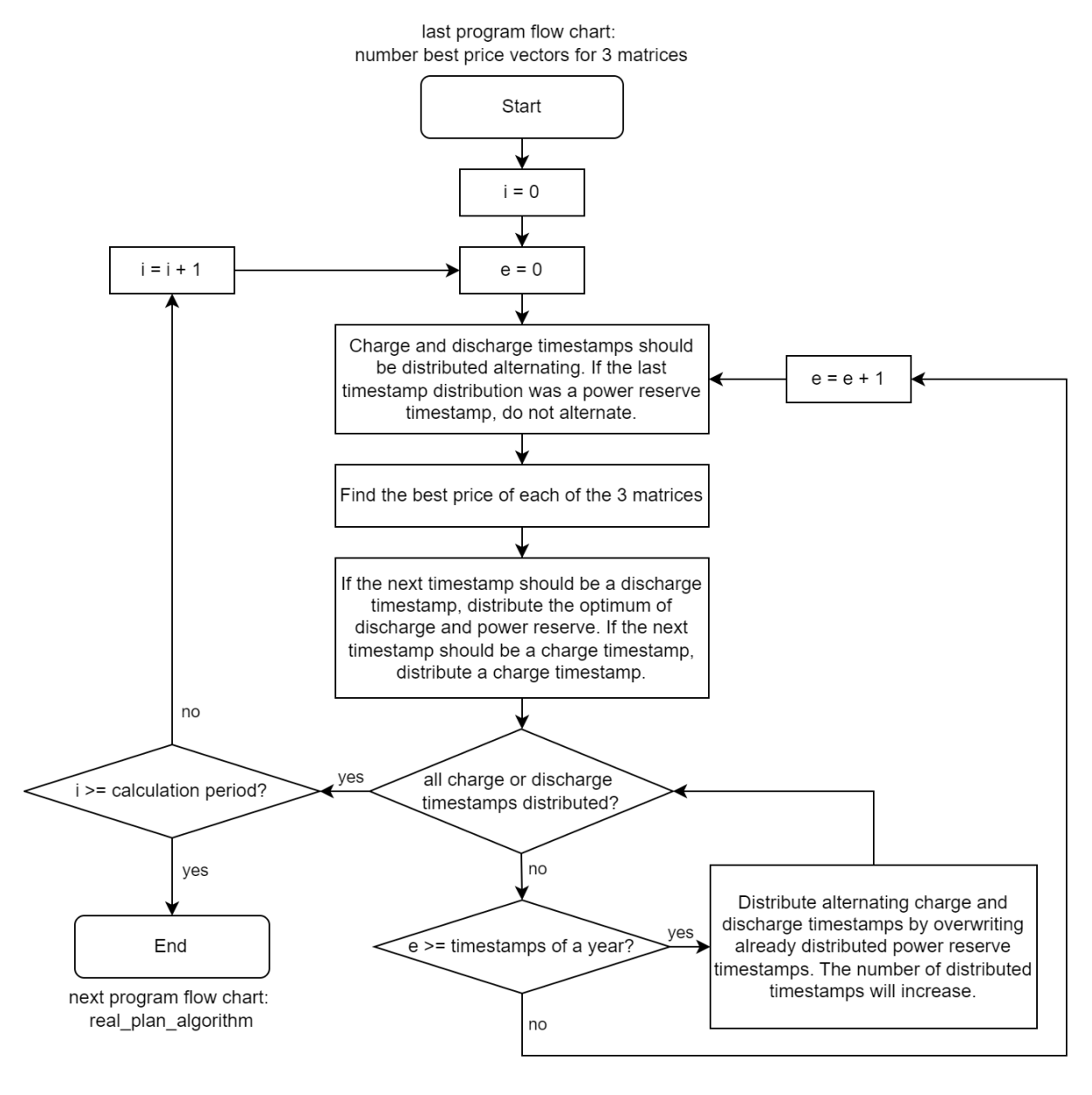


Figure 24 Detail Program Flow Chart of Step 6 of Program Flow Chart 1. Distribution Process of Timestamps for Plan Operation (own Figure)

<u>Figure 25</u> illustrates the functionality of the algorithm from <u>Figure 24</u> as an example. Columns F to K display an excerpt of the three matrices representing the charging, discharging, and reserve power

markets. Values highlighted in purple indicate those transferred to the planned operation in column B. Column A depicts the planned operation without the overwriting of power reserve timestamps. In both columns A and B, the highlighted values indicate changes due to the overwriting process.

Columns C to E show the price numbering of the three matrices from **Step 5** in <u>Figure 22</u>. A heatmap is applied to these columns to visually distinguish the values. Since the reserve market yields significantly higher nominal prices (column J) over the entire period compared to the discharge market (column H), the planned operation without correction exclusively follows the reserve market.

The user-defined number of cycles cannot be fulfilled by exclusive participation in the theoretically optimal reserve markets. Therefore, reserve time stamps are exchanged with charge and discharge time stamps until the user-defined number of cycles can be achieved. This can be observed in the marked rows in columns A and B: Row 5 has been replaced by the optimal charging market, and row 11 by the optimal discharging market. This is also reflected in the numbering of columns D and E, where the lowest values were used (marked red). A cross-check with columns F and I confirms this statement.

				-	-	-	-				14
	A plan operation without	plan operation	reserve power	charge operation	1000	charge price	charge market	H discharge price in €/MW	discharge market	reserve price in €/MW	reserve market
1	correction		operation								
2	SR+P	SR+P	31463	99999	99999	1,425	SR-E	57,475	INT+P	332,22	SR+P
3	SR+P	SR+P	29335	99999	99999	-3,75	SR-E	58,65	SR+E	369,69	SR+P
4	SR+P	SR+P	29897	99999	99999	-1,15	SR-E	50,85	INT+P	358,09	SR+P
5	SR+P	SR-E	29642	2203	99999	-29,65	SR-E	62,5	INT+P	361,77	SR+P
6	SR+P	SR+P	29898	99999	99999	-3,75	SR-E	73,15	INT+P	358,09	SR+P
7	SR+P	SR+P	29899	99999	99999	-3,75	SR-E	53,75	INT+P	358,09	SR+P
8	SR+P	SR+P	29643	99999	99999	-13,775	SR-E	53,45	INT+P	361,77	SR+P
9	SR+P	SR+P	31130	99999	99999	3,1	SR-E	64,05	INT+P	346,52	SR+P
10	SR+P	SR+P	29900	99999	2094	22,15	SR-E	74,75	INT+P	358,09	SR+P
11	SR+P	INT+P	29901	99999	1348	-3,75	SR-E	76,95	INT+P	358,09	SR+P
12	SR+P	SR+P	29410	99999	99999	-10,1	SR-E	60,8	INT+P	367,07	SR+P
13	SR+P	SR+P	31464	99999	99999	-3,75	SR-E	57,525	INT+P	332,19	SR+P
14	SR-P	SR-P	5205	2213	99999	-29,65	SR-E	46,775	INT+P	751,20	SR-P
15	SR-P	SR-P	7496	99999	99999	0,725	SR-E	60,425	INT+P	720,83	SR-P
16	SR-P	SR-P	7009	99999	99999	-3,75	SR-E	49,95	INT+P	725,30	SR-P
17	SR-P	SR-P	7010	99999	99999	-3,75	SR-E	58,65	SR+E	725,30	SR-P
18	SR-P	SR-P	9187	99999	99999	22,15	SR-E	42,875	INT+P	699,40	
19	SR-P	SR-P	7011	99999	99999	-3,75	SR-E	54,3	INT+P	725,30	SR-P
20	SR-P	SR-P	5206	2220	99999	-29,65	SR-E	50,725	SR+E	751,20	SR-P
21	SR-P	SR-P	7259	99999	99999	-1,15	SR-E	43,625	INT+P	722,70	SR-P

Figure 25 Example of Step 6 of Program Flowchart 1: Distribution Process of Timestamps for Plan Operation (own Figure)

#### 4.2.3 Main Simulation Algorithm

The main program algorithm includes **Steps 3 to 5** in <u>Figure 21</u>. Due to its high complexity, the algorithm is described using two interacting flowcharts. The first part is shown in <u>Figure 27</u> and covers **Steps 3 and 4** of <u>Figure 21</u>. The second part is shown in <u>Figure 28</u> and corresponds to **Step 5** of <u>Figure 21</u>.

For the simulation of a time segment within the *prediction\_horizon*, whose length can be adjusted by the user, both main simulation parts are executed once. The variable i represents the currently analyzed timestamp. All elements from i to  $i + prediction_horizon - 1$  are examined to find the best markets for operation. As i itself is included, and the prediction horizon defines the number of values to be analyzed. This means that the last known timestamp is i - 1.

In <u>Figure 28</u>, the variable i is incremented by a *modified\_prediction\_horizon*, ensuring that the next iteration in <u>Figure 27</u> starts not with i = i + 1 but with  $i = i + modified_prediction_horizon$ .

In addition to the main loop that increments by i, Figure 27 includes two additional loops nested within the main loop:

The innermost loop, which iterates with index e, defines the number of all forecasts of a comparable revenue within the **prediction\_horizon**. It determines the necessary conditions to achieve planned operation at time e. For example, if discharging is required at time e = 3 and SOC = 0, charging must occur within the interval e = [0, 2] to meet the discharge requirements.

The number of revised plans *number\_plans* represents the multiple integration of several planning time stamps within the same planning process. For instance, if discharging is scheduled at e = 5 according to Plan 1, charging may occur at e = 0 and e = 4 to meet the discharge requirement.

Additionally, another Plan 2 can be implemented, overlapping with Plan 1's operation times. For example, if charging occurs at e = 1 to fulfill a discharge plan at e = 12, e = 1 falls within the timeframe of the first plan. Since e = 0, e = 1, and e = 4 are charging operations and they precede the discharge operations at e = 5 and e = 12, both plans can theoretically coexist despite overlapping timeframes.

Using *number\_plans*, the advantage of batteries with a higher *power\_factor* is assessed because with increasing *power\_factor*, the battery can theoretically implement a higher *number\_plans*.

After initializing the variables i, e, and  $number\_plans$ , Step 4 of Figure 27 verifies whether achieving planned operation at time e is feasible. For example, if e = 0 and discharging is required, this is impossible if SOC = 0 because no timestamp can be planned for charging before e = 0.

To ensure planned operation, the system always attempts to provide the maximum available power. If the usable storage power is 4 MW, then 4 MW is also the discharging requirement in the simulation program. However, in praxis, offering lower power on the market would also be possible.

An exception is the grid feed-in limits, which are considered by the program: If RES and BESS feed into the grid simultaneously and exceed the grid limit, the BESS power is reduced accordingly. Grid limits for power consumption are not included in the program.

If RES is selected as the charging source and provides less power than BESS *simulation\_power*, the *simulation\_power* is adjusted accordingly.

Discharging is assumed to occur without losses, meaning the discharge capacity, *capacity for discharging*, equals the stored capacity in the BESS.

$$capacity_for\_discharging (MWh) = 0.25 (h) \cdot simulation\_power (MW)$$
 (34)

For BESS charging capacity, *capacity\_for\_charging*, charging and discharging losses are deducted using the *system\_RTE*:

$$capacity\_for\_charging (MWh) = capacity\_for\_discharging (MWh) \cdot \frac{system\_RTE (\%)}{100}$$
(35)

Due to the consideration of system RTE, in the case of charging at positive Intraday market prices, the BESS must pay the price for *capacity\_for\_discharging* even though only *capacity\_for\_charging* is

stored in the BESS. If Intraday market prices are negative, the BESS is compensated more for charged energy than the energy stored.

The product length of the reserve power markets in <u>Figure 12</u> is considered by allowing the utilization of reserve power markets only every four hours. To correctly compare four-hour reserve power market prices with competing prices of other markets, the user must specify a constant price for each four-hour period in the respective input Excel files.

If planned operation is feasible at *e*, the program determines whether charging or discharging must occur before reaching *e* and what capacity must be charged or discharged. If planned operation at *e* is impossible, the case is discarded by setting the comparable revenue *future\_revenue* for time stamp *e* to the highest value, 999999. The lowest values of *future\_revenue* are defined as optimal.

**Step 5** of <u>Figure 27</u> describes the planning of charging and discharging timestamps to achieve the planned operation at time *e*. This planning is conducted by selecting the best prices from the charging and discharging matrix. Values are selected iteratively until the respective charging or discharging condition is met.

If discharging is required, it is likely that two charging values will be chosen since, according to Equations (34) and (35), the charging capacity is lower than the discharging capacity. If possible, the maximum capacity from Equations (34) and (35) is used for each timestamp. However, this assumption may lead to market or SOC limits being exceeded or undershot. For example, given a storage system with  $Q_U = 1$  MWh,  $P_U = 1$  MW and SOC = 50 % and a charging power of 1 MW to enable subsequent discharging of 1 MW, the SOC would exceed 100 % after charging. In the case of such an exceedance, a verification function limits the usable power.

**Step 6** of <u>Figure 27</u> describes the conversion of the market vector into a comparative *future\_revenue* to enable different forecasts to be evaluated. In contrast to the approach of <u>Figure 24</u>, all charging, discharging and power reserve markets must now be comparable.

The nominal prices of equations (25) to (28) cannot be used directly for this comparison because charging markets should be utilized at the lowest price, while discharging markets should be utilized at the highest price. Furthermore, a direct comparison between nominal discharging and reserve markets could lead to a local optimum:

The nominal prices of reserve markets are significantly higher than those of discharging markets due to lower activation probabilities. If reserve markets were preferentially selected, this would significantly reduce the user-defined target cycle amount because reserve markets are activated less probably. The program might identify a local optimum for reserve markets that does not necessarily correspond to the global optimum, as OPEX and idle degradation costs of storage are not included in nominal price formation.

Therefore, sorting of the three matrices, as indicated in **Step 5** of <u>Figure 22</u>, is applied. All values of the time series are included in the sorting. For each selected market, the number of sorting is saved. That would be number 1 for the lowest price for example. For each prediction, the mean value of all saved sorting numbers is calculated, called *future\_revenue*. The lowest *future\_revenue* of all predictions within the prediction horizon determines the optimum.

<u>Figure 26</u> illustrates this problem: The prices for each charging, discharging, and reserve market are sorted by their best possible values in columns G, J, and M. The developed operation Plan 1, already validated for feasibility, aims to reach the planned operation with market SR-E in row 4. This requires one discharging time stamp. Discharging aligns with the lowest indices in column J, representing the lowest discharging prices. Possible discharging timestamps are only rows 2 and 3, as discharging must occur before reaching the planned operation. SR+E in row 2 is selected for discharging, and the corresponding index 1 is assigned. The mean value of the two active markets in Plan 1 is (1+1)/2 = 1 (highlighted orange in Figure 26).

A second plan involves participation in discharging market SR+P in row 5. Achieving this requires two charging time stamps. The lowest charging values are 1 and 2 in rows 2 and 4, both assigned to market SR-E. The mean value calculation is (1 + 1 + 2) / 3 = 1.3333 (highlighted orange in Figure 26).

The mean values of the assigned indices of both plans correspond to the *future\_revenue*. Since Plan 1 has a lower *future\_revenue* than Plan 2, Plan 1 is preferred, and Plan 2 is discarded.

	А	В	C	D	E	F	G	Н	1	J	K	L	M
		real plan 1		real plan 2	charge price	charge	number	discharge	discharge	number	reserve	reserve	number
1	real plan 1	future_revenu	real plan 2	future_revenu	55 555	market	charge	price	market	discharge	power price	power	reserve
2	SR+E	1	SR-E	2	-10,825	SR-E	2	50,375	SR+E	1	746,083	SR+P	3
3	INACTIVE	-	INACTIVE	-	-8,075	SR-E	3	50,375	SR+E	2	754,308	SR+P	2
4	SR-E	1	SR-E	1	-28,75	SR-E	1	45,375	SR+E	3	746,083	SR+P	4
5			SR+P	1	12,825	SR-E	4	37,15	SR+E	4	759,308	SR+P	1
6													
7		1		1,3333									

Figure 26 Example Comparison of future\_revenue (own Figure)

The steps described are repeated in the loop indexed by *e* for as long as the user-defined *prediction\_horizon* specifies. The default assumption are 10 values. The results of each iteration are stored in the *future\_revenue* vector and subsequently compared as shown in <u>Figure 26</u>. As the best values have an index 1, the minimum value of *future\_revenue* is selected. The corresponding real operation plan vector of the markets (as in column A of <u>Figure 26</u>) and the vector of utilized charging or discharging capacity are stored.

The loop indexed by *number\_plans* runs depending on the *power\_factor*: The larger the BESS *simulation\_capacity* is compared to its *simulation\_power*, the more iterations can be performed because the SOC limits are reached less frequent. The existing plan from **Step 8** is stored and cannot be discarded. However, additional plans can be added, even if they overlap, as long as all plans remain feasible. A detailed example is provided in <u>Figure 29</u>.

If additional plans are possible, *future\_revenue* should remain similar. The allowable tolerance between *future\_revenue* of the previous and current plans can be user-defined. A default setting allows for a value up to 50 % higher than the previously stored value. If no higher value than the last stored one would be permitted, the program calculates the revenue of the best possible simulation within the prediction horizon. However, to achieve the highest possible revenue for BESS with a larger *power\_factor*, it may be necessary to combine the second- or third-best with the best possible value to maximize revenue. This presents another potential local optimum into which the simulation may be directed. Allowing all values would make the simulation program follow the real planned operation more closely but also accept less favorable prices.

The result of the simulation in <u>Figure 27</u> is a feasible operational plan that maximizes profit while covering multiple and overlapping operational values. The output includes the operational vector and

the vector of utilized capacities, which are passed to the second simulation part in <u>Figure 28</u>. The identified markets would already be actively traded in real-time.

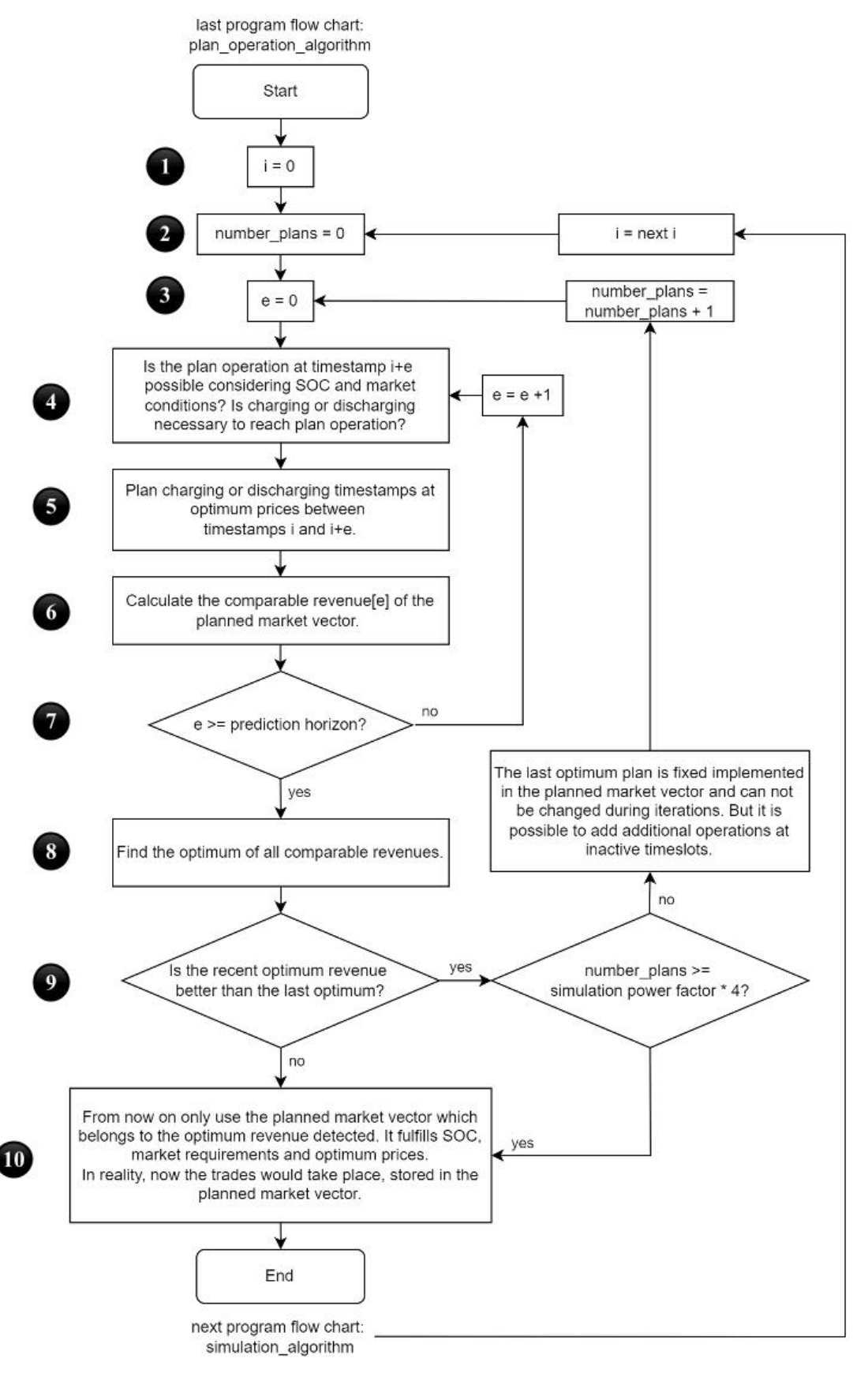


Figure 27 Program Flow Chart 2: Development of Real Plan Operation based on Stack Prediction of Possible Cases of SOC and Market Requirements (own Figure)

The simulation results from <u>Figure 27</u> are passed on to the second program section, which is executed within the same iteration *i*. However, the number of timestamps to be examined is adjusted for the second part: If a reserve power market is selected in real operational planning, the period is extended by 15 additional values to ensure that the four-hour period of reserve power markets is maintained. Otherwise, the analysis period is shortened to the last planned value (**Step 2** of Figure 28).

For example, if a charge and discharge cycle is scheduled within the period between timestamp 3 and 8, and no further planning occurs beyond timestamp 8, only the period between timestamp 0 and 8 is considered for the subsequent simulation section instead of the period: 0 to *prediction\_horizon* -1.

If the BESS has been continuously operating for a manufacturer defined number of part- or full cycles, a safety cooling process must take place. Since the activation of unplanned reserve power can also cause excessive heating of the storage system, the safety shutdown due to overheating is considered in the second program part. The cooling duration is defined by the manufacturer as well (**Step 4** of <u>Figure 28</u>).

Unexpected outages may also occur. These can be modified for each timestamp in the input data of the Excel file. The program only considers total outages, as only a single operating state is evaluated per timestamp (**Step 5** of <u>Figure 28</u>).

Redispatch measures cannot be accounted for in the planning process either. The activation of positive and negative Redispatch measures is only carried out if SOC conditions permit activation, the BESS is not participating in reserve power markets, and the BESS is not planned to operate with the same result as the Redispatch measure. This means that if the storage system is scheduled to discharge at time t, and the Redispatch measure also requires discharging at time t, the Redispatch measure is not executed because it does not improve grid stability. In the program, as well as in practice, a BESS participating in the reserve power market is generally not affected by Redispatch. However, exceptions may apply voluntarily (Bundesnetzagentur, 2024d:5) (**Step 6** of <u>Figure 28</u>).

The compensation of Redispatch measures follows the principle of economic neutrality concerning the impact of the measure on the BESS's revenue: neither profit nor loss should be generated (EnWG, 2024: §13a). Compensation is provided for the lost revenue from planned operation, the degradation of the BESS, and the costs of the measure (EnWG, 2024: §13a). If the BESS saves costs due to the measure, these savings must be refunded to the grid operator (EnWG, 2024: §13a). This means that negative compensation for the measure is also possible.

In the simulation program, the BESS costs are determined in the case of planned operation. If the BESS generates revenue, this amount is credited. If there are expenses, these must be paid.

The measure itself is remunerated based on the Intraday market prices. If the BESS would have to pay for the measure in the optimal charge and discharge market, the loss is set to zero, as the BESS would typically not execute such a measure. For example, if the BESS is forced to discharge at an optimal Intraday market price of -500  $\frac{\epsilon}{\text{MWh}}$ , a massive loss would result from the discharge process, disregarding the principle of cost neutrality. Additionally, the cycle degradation is credited as profit. The degradation per cycle is user-defined and can also be estimated by the simulation program.

In practice, the legal framework for compensating Redispatch measures for BESS has not yet been finalized. Currently, it is still possible to generate profit from Redispatch measures, which contradicts the principle of cost neutrality (Kyon Energy, 2024). However, the simulation program does not exploit legal loopholes.

After a Redispatch measure, in practice, time would be available to restore the SOC for future planned operation. Alternatively, the Redispatch measure would need to compensate for the resulting financial losses of trading that cannot be fulfilled by the BESS because of the SOC change. In the simulation program, after a Redispatch measure, further plan execution is stopped, and new planning begins from the Redispatch measure onwards.

If the storage system experiences an outage, a safety shutdown, or is otherwise unable to follow the planned operation, a penalty payment is recorded (**Step 7** of <u>Figure 28</u>). Redispatch measures are excluded from penalty payments.

If no penalty payment is recorded, the BESS follows the planned operation (**Step 8** of <u>Figure 28</u>). The target variables usable SOC, operating state, and revenue are stored as vectors with a length corresponding to the simulation period. The usable SOC is defined by the SOC relative to usable capacity.

Additionally, self-discharge is considered, as well as electricity procurement from RES, if required and feasible (**Step 9 and 10** of <u>Figure 28</u>). Thus, RES+P can occur in inactive operational periods only. A safety factor during the charging process of the BESS ensures that slightly more energy is stored than required for the respective planned market.

With increment k, the process is repeated for all planned operations within the same prediction horizon.

The next element i for the subsequent planned operations is described by i = i + k + 1.

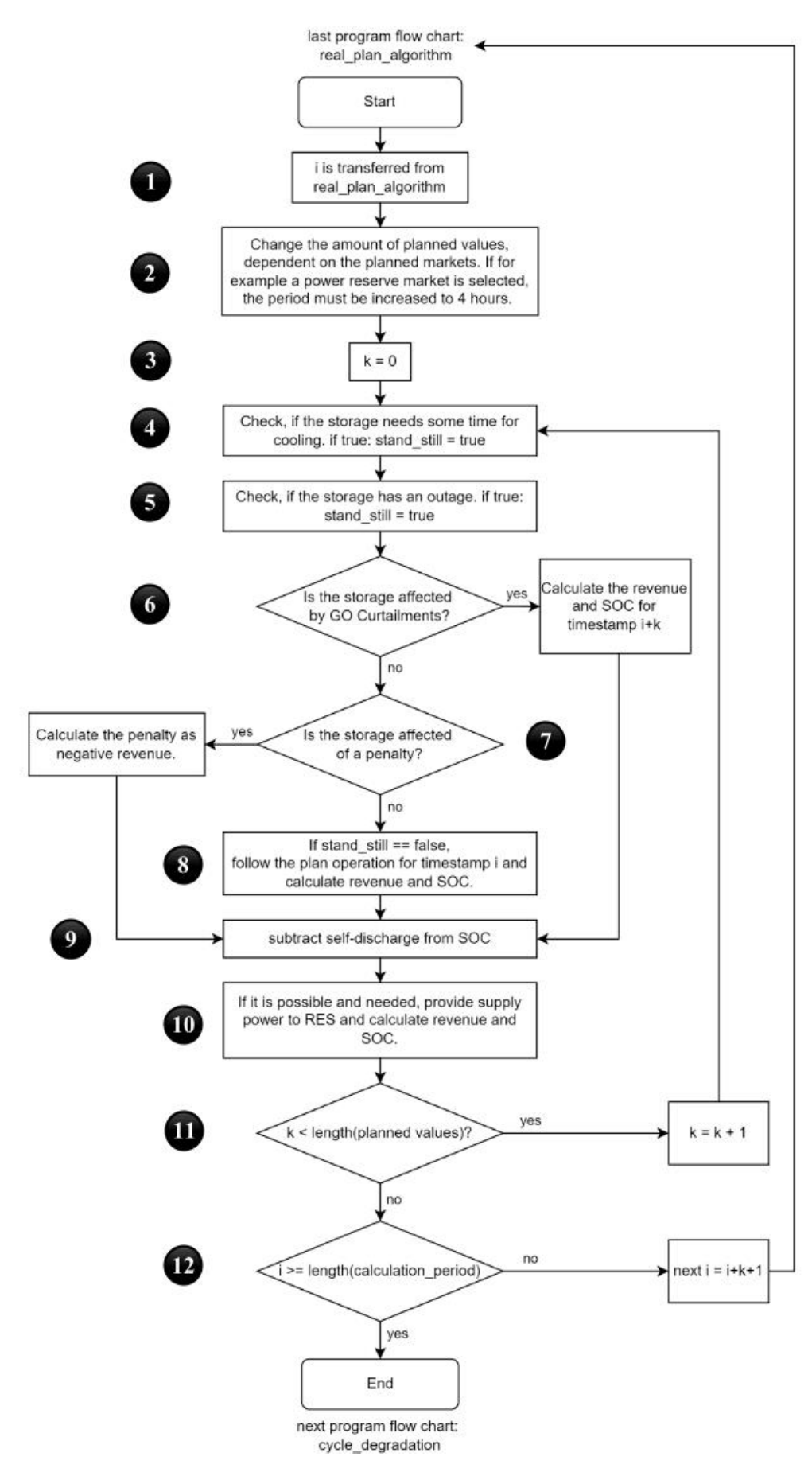


Figure 28 Program Flow Chart 3: Development of Real Operation, SOC and Revenue Based on Real Plan Operation Considering Unexpected Events (own Figure)

Figure 29 exemplifies the output of the main algorithm for the first iteration i = 0 of the process schedules Figure 27 and Figure 28. This example illustrates two nested discharge schedules at rows 13 and 16, whose charging plans occur in rows 4, 10, and 12.

The theoretical schedule within a *prediction\_horizon* of 20, determined based on optimal prices, is contained in column A. Since SR+P is a discharge market and usable SOC = 0, the condition for market participation cannot be met for i = 0. Until i = 15, participation in SR-P markets is also impossible due to the four-hour bid duration. For the remaining markets within the *prediction\_horizon*, nominal prices are developed following the principle outlined in <u>Figure 26</u>.

The maximum achievable profit is obtained by trading on the SR+E discharge market at the two timestamps highlighted in green. These timestamps are transferred to real plan operation in column C. All values beyond row 16 are only considered in the next iteration since no further green-marked operations are planned after row 16. Consequently, from row 17 onward, the subsequent columns outside of plan operation are shaded gray.

Since the usable SOC = 0, the BESS must first be charged to enable a dual discharge operation in the SR+E market. Due to efficiency losses, three charging timestamps are required. These timestamps are selected based on optimal charging prices and must be positioned before the first discharge, which is before row 13. The selected charging timestamps are marked in blue. All belong to the SR-E market with a price of  $140 \frac{\epsilon}{MWh}$  (column I). Column E displays the nominal price.

When the BESS charges in the SR-E market, it receives  $140 \frac{\epsilon}{\text{MWh}}$ . Considering a *simulation\_power* of 1 MW and after deducting taxes and fees, the BESS achieves a profit of  $34.74 \epsilon$  (column D) each charging timestamp. Considering the system RTE, the usable SOC of a 2 MWh BESS increases by 10.858 percentage points per charging timestamp.

A discharge operation decreases the usable SOC by 12.5 percentage points. The profit in column D for discharge is calculated based on the SR+E price in column J, while column G contains the nominal SR+E price. Taxes are not deducted in the case of discharge.

	Α	В	C	D	E	F	G	Н	1	J
	plan operation	usable SOC in %	real operation	revenue in €	nominal revenue charing in €/MW	charging market	nominal revenue discharging in €/MW	discharging market	SR-E price in €/MWh	SR+E price in €/MWh
	SR+P	0,0000	INACTIVE	0	-10,825	SR-E	50,375	SR+E	68,3	226,5
3	SR+P	0,0000	INACTIVE	0	-8,075	SR-E	50,375	SR+E	57,3	226,5
1	SR+P	10,8578	SR-E	34,725	-28,75	SR-E	45,375	SR+E	140	206,5
,	SR+P	10,8576	INACTIVE	0	12,825	RES-P	37,15	SR+E	-60	173,6
5	SR+P	10,8575	INACTIVE	0	-3,75	SR-E	44,25	SR+E	40	202
7	SR+P	10,8573	INACTIVE	0	-3,75	SR-E	25,375	SR+E	40	126,5
3	SR+P	10,8572	INACTIVE	0	-3,75	SR-E	25,375	SR+E	40	126,5
)	SR+P	10,8570	INACTIVE	0	-3,75	SR-E	55,375	SR+E	40	246,5
0	SR+P	21,7147	SR-E	34,725	-28,75	SR-E	64,95	SR+E	140	284,8
1	SR+P	21,7144	INACTIVE	0	-3,75	SR-E	46,825	SR+E	40	212,3
2	SR+P	32,5718	SR-E	34,725	-28,75	SR-E	42,45	SR+E	140	194,8
3	SR+E	20,0716	SR+E	81,625	14,225	RES-P	75,375	SR+E	-60	326,5
4	SR+P	20,0713	INACTIVE	0	11,35	RES-P	60,375	SR+E	-60	266,5
5	SR+P	20,0710	INACTIVE	0	-8,75	SR-E	50,375	SR+E	60	226,5
6	SR+E	7,5709	SR+E	81,625	2,875	SR-E	75,375	SR+E	13,5	326,5
7	SR+P									
8	SR+P									
9	SR+E									
0	SR+P									
1	SR+P							l,		
2										

Figure 29 Detailed Example of Main Simulation Program (own Figure)

#### 4.2.4 Degradation Algorithm

The degradation is referred to **Step 6** of <u>Figure 21</u> and can be divided into capacity and power degradation. It is also assumed that the nominal capacity and power of the battery are constant every replacement period.

To determine capacity degradation, the following dependencies are considered. Some formulas have been simplified by averaging. User-provided inputs are marked in green, while parameters computable by the program at EOL are highlighted in blue:

$$\overline{DOD}(\overline{Q_d}, Q_N) \qquad \qquad \text{Formular (6)}$$

$$\overline{SOC}(Q_N, Q_{loss}(t), Q_d(t)) \qquad \qquad \text{Formular (7)}$$

$$Q_{loss}(\delta(t = EOL), Q_N) \qquad \qquad \text{Formular (4)}$$

$$\delta(t = EOL, cycles, \overline{SOC}, \overline{DOD}) \qquad \text{Formular (3)}$$

In the simulation program, the user specifies the storage capacity  $Q_U$  of the BESS, which is available for usage throughout the plant's lifetime, with the condition  $Q_E \ge Q_U$  (Figure 3).  $Q_d(t)$  is dependent on  $Q_U$  and the battery operation. The user provides an average DOD value along with EOL parameters in terms of cycles and time.

Figure 30 illustrates the program flowchart for determining capacity degradation.

Depending on the operation of the BESS,  $Q_d(t)$  can be determined, as the unused portion of the battery is assumed to be fully charged (<u>Figure 30</u>, **Step 3**). Therefore,  $Q_d(t)$  can be calculated from the SOC time series relative to the usable capacity  $SOC_U(t)$ .

$$Q_d(t)(\text{MWh}) = Q_U(\text{MWh}) \cdot \left[ 1 - \frac{SOC_U(t)(\%)}{100} \right]$$
(36)

Based on formular (6),  $Q_N$  can be derived from  $\overline{Q_d}$  and  $\overline{DOD}$  (Figure 30, Step 4). However,  $Q_N$  may have been incorrectly calculated, as  $\overline{DOD}$  relies on an unverified user input. Consequently, the degradation algorithm validates the calculation of  $Q_N$  and corrects it if necessary.

To compute the degradation,  $\overline{SOC}$  must be estimated based on user inputs while neglecting degradation losses (formular 5) (Figure 30, Step 5):

$$\overline{SOC}(\%) = \left(1 - \frac{\overline{Q_d}(MWh)}{Q_N(MWh)}\right) \cdot 100 \% \tag{37}$$

From the previous assumptions, the idle and cycle degradation factors can be determined (formular 3) and used to calculate the assumed nominal capacity loss  $Q_{loss}$  (formular 4) based on the number of cycles and time within the replacement period. To verify the minimum capacity  $Q_{N,min}$ , the following applies (Figure 30, Step 7):

$$Q_{N,min} = Q_U + Q_{loss} (38)$$

If  $Q_N$  is smaller than  $Q_{N,min}$  it is set to  $Q_N = Q_{N,min}$ , the user input  $\overline{DOD}$  is corrected according to formular (6), and  $\overline{SOC}$  is recalculated, including the computed degradation losses (<u>Figure 30</u>, **Steps 10** and 11). According to <u>Figure 6</u>,  $\overline{SOC}$  has a minor influence on overall degradation. Therefore, formular (7) for SOC calculation is linearized by considering only the start and end degradation:

$$\overline{SOC} = 0.5 \cdot \left[ \left( 1 - \frac{\overline{Q_d}}{Q_N} \right) + \left( \frac{Q_N - Q_{loss}}{Q_N} - \frac{\overline{Q_d}}{Q_N} \right) \right] \cdot 100 \%$$

$$\overline{SOC}(\%) = \left[ 1 - \frac{2 \cdot \overline{Q_d}(MWh)}{Q_N(MWh)} + \frac{Q_N(MWh) - Q_{loss}(MWh)}{Q_N(MWh)} \right] \cdot 50 \%$$
(39)

The loop iterates with the calculation of degradation coefficients and terminates once  $Q_{N,min} \ge Q_N$  (Figure 30, Step 8).

The power coefficients are determined using the corrected SOC and DOD assumptions based on formular (11).

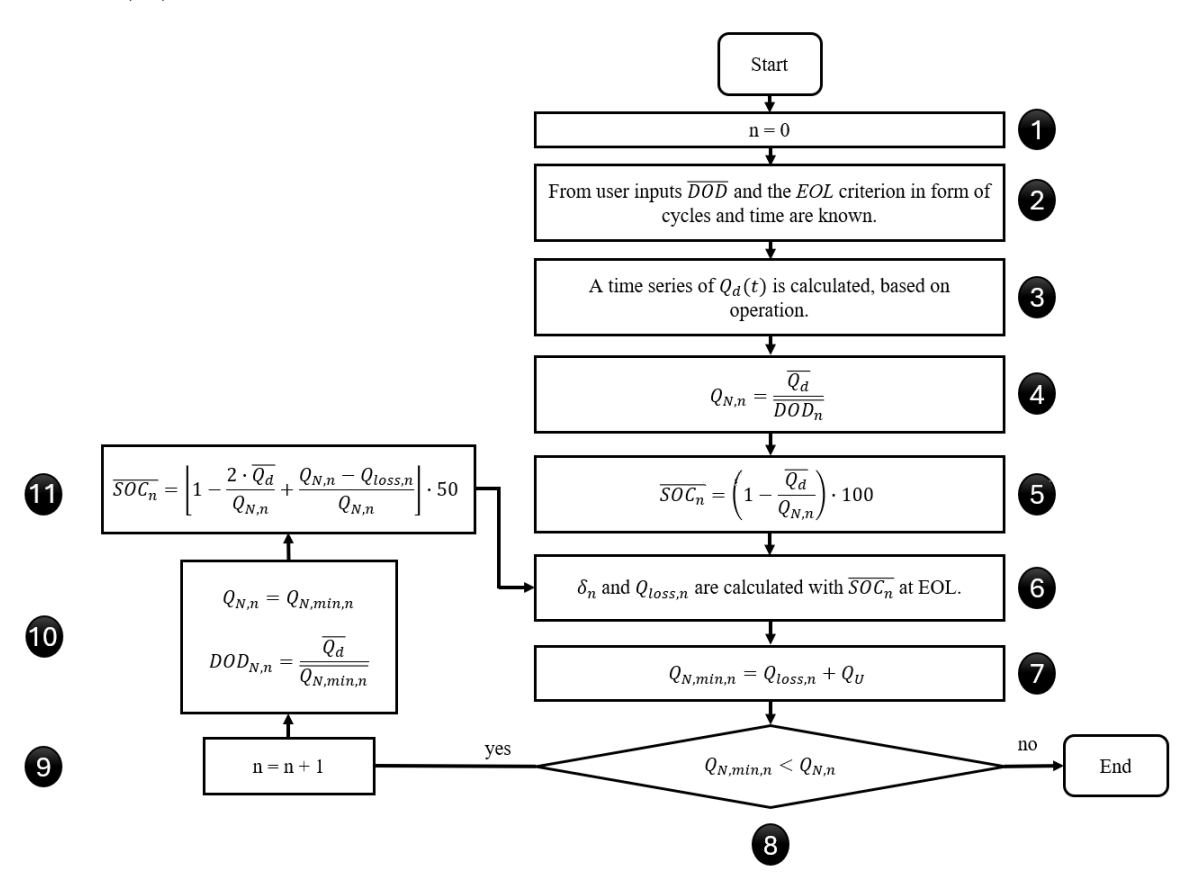


Figure 30 Algorithm of Capacity Degradation (own Figure)

#### 4.2.5 Financial Figures

As financial output variables, annual costs, revenues, and cash flows are relevant. The IRR and NPV can be derived from the cash flows. This represents **Steps 7 and 8** of Figure 21.

To determine the annual revenues, the revenue time series, generated in **Step 5** of <u>Figure 21</u> is aggregated annually. In some cases, single revenues may be negative if penalty payments have been incurred.

Annual costs consist of CAPEX, OPEX, and, optionally, initial costs and discounts. All OPEX values are updated annually based on the predefined input data. Power-dependent CAPEX are paid only at the beginning of the calculation period, whereas capacity-dependent CAPEX are incurred after each replacement period.

Cash flows are calculated for each year *t* based on costs and revenues:

$$cashflow(t) = revenue(t) - cost(t)$$
(40)

IRR and NPV are determined using Python's built-in functions. The NPV calculation additionally requires the input parameter discount rate. <u>Appendix 36</u> contains the formulas for calculating these variables.

Running multiple simulations with varying input parameters alters the financial outcome. The IRR serves as the optimization criterion, with the simulation yielding the highest IRR being the final result.

# 5 Application of the Simulation Tool

## 5.1 Baseline Simulation for

The wind plant with a nominal power of 18.4 MW, is planned to be repowered to approximately 79.2 MW and further expanded by an 85.7 MWp PV plant. Additionally, the implementation of a BESS is considered, with its optimal capacity, power, and operation strategy to be determined using the developed simulation program. The repowering project is shown in <u>Figure 31</u>, where PV-panels are marked blue and wind turbines marked by yellow and green pins.



: Combination Plant Wind + PV (internal Source)

Due to the numerous parameters that need to be considered, a baseline simulation is first conducted. After verifying the present results against literature sources, the key parameters for future operation influencing the IRR are optimized, followed by a sensitivity analysis. The main result of an optimal dimensioned and operated BESS for the is then analyzed and evaluated.

For the wind and PV plant implementation, two separate simulations were conducted in PVSyst and WindPRO, with the respective annual time series, excluding losses from <u>Appendix 42</u>, stored in the files 'power\_pv.xlsx' and 'power\_wind.xlsx.' Additionally, based on the simulation data, self-consumption per plant is assumed to be 57.8 kW. This self-consumption is not included in the annual time series but is provided to the program as an input variable for each plant.

Since GO curtailments are location-dependent, the time series developed in chapter 3.5 is adjusted based on location-specific grid congestions from Appendix 32. is located in Niedersachsen, where, according to Appendix 32, positive Redispatch occurs with average frequency compared to the national average, while negative Redispatch occurs more frequently. In Niedersachsen, the GO curtails more than in any other state. An analysis of the GO curtailments of the existing wind plant shows a slightly above-average curtailment probability compared to other CEE plants.

For the simulation, based on this analysis, it is assumed that the probability of a negative Redispatch curtailment is approximately doubled compared to the average. Using this new probability, the time series 'curtailments GO.xlsx' is generated.

Since planning and permitting take some time, the year 2027 is chosen as the commissioning year, with a calculation period of 20 years, as the PV plant is expected to be repowered after 20 years.

As cross-market optimization yields the highest profit, trading on all implemented markets is allowed in the baseline calculation.

The discount rate is set at 2 %

Since RES and BESS share a grid connection point, grid connection costs, like power-dependent CAPEX, could potentially be reduced. However, for the baseline simulation, the system is simulated according to the plant layout in <u>Figure 1</u>, without a grid limit, and the BESS has its own transformer dimensioned to its nominal power.

For cooling times, the datasheet specifications nominal power, the pause time is 1:30 h.

In the case of penalties, prices are assumed to be 20 % higher than the price would be without a penalty (BDEW, 2018:11).

From preliminary simulations, the degradation costs of the storage system were calculated at  $8.486 \frac{\epsilon}{MW \cdot cvcle}$ . This parameter is only needed for Redispatch renumeration.

A residual value of  $38 \frac{\epsilon}{kWh}$  is set (chapter  $\underline{2.4}$ ) which is approximately 20 % of the purchase price. This value is minimally higher compared to the literature average of  $30 \frac{\epsilon}{kWh}$  because it is assumed that second-life battery markets will grow in the future. (J. Li et al., 2023:4824). Furthermore, the degraded capacity is excluded from the calculation of the residual value.

Using second-life Batteries would also be a chance for the IRR optimization of the BESS. However, the degradation model would have to be adapted for this, which is why the usage of second-life batteries is not considered in this work.

The following parameters have already been explained in previous chapters and therefore remain at their default settings:

• Price RES+P =  $21.04 \frac{\text{ct}}{\text{kWh}}$  (chapter <u>3.3</u>)

- Fees BESS =  $0.11 \frac{\text{ct}}{\text{kWh}}$  (chapter <u>3.3</u>)
- Energy-dependent OPEX =  $0.273 \frac{\epsilon}{MWh}$  (chapter <u>3.2</u>)
- Self-discharge =  $4 \frac{\%}{\text{month}}$  for LFP and  $1 \frac{\%}{\text{month}}$  for NMC (chapter <u>2.3.1</u>)
- Available storage hours to enable participation in PR Market = 0.83 h (chapter <u>2.5</u>), but adjusted for detailed simulations according to <u>Appendix 18</u>.
- Available storage hours to enable participation in SR positive or negative Market = 1 h (Figure 12)
- RTE annual degradation = 0.2 percentage points (chapter 3.3)
- RTE reduction = 26 percentage points at SOC = 100 % (chapter 3.3)

Additionally, the following data developed in chapter  $\underline{3}$  are incorporated into the simulation:

- CAPEX & OPEX
- Grid charges
- Intraday, reserve power, and reserve energy prices
- Reserve power activation probabilities for PR and SR
- Storage and RES outages
- System RTE

For the remaining variables, assumptions must be made for the baseline simulation, which can be optimized in subsequent simulations. The goal is to identify which parameters have the most significant impact on the simulation results and which ones are negligible.

For the baseline simulation, the following parameters are assumed, with the main parameters 'cycles per year', 'capacity' and 'power' based on the simulation from <u>Appendix 2</u>:

- The capacity unit of the BESS is to be replaced every 5 years.
- To ensure that SR energy is fully activated, trading is conducted at 25 €/MWh below the average value.
   Optimizing this value would require long-term experience in direct marketing.
- Storage technology: LFP
- A reduced power usage to increase the RTE is not assumed.
- There are no initial costs or discounts.
- $\overline{DOD} = 80 \%$ . This value is likely to be significantly undercut in practice. In such cases, the specified  $\overline{DOD}$  will be corrected by the program's degradation algorithm (chapter 4.2.4).
- Target cycles per year = 730
- *prediction\_horizon* = 10 values
- During a charging process, 2 % more energy is deliberately charged than would be needed for an
  assigned discharging process, to account for self-discharge and minor discharging losses from
  RES+P.

- For multiple scheduling processes within the same prediction horizon, the comparison price for subsequent schedules must not deviate by more than 50 % from the price of the initial schedule. Otherwise, the subsequent schedules will not be considered.
- It is assumed that, in practice, 11 % less profit can be generated than the optimal profit estimated by the program (Hornek et al., 2025:1).
- Usable power of 1 MW and usable capacity of 2 MWh are assumed.

The baseline simulation results in an IRR of 10 % and an NPV of 551 k€. However, the IRR results represent only potential outcomes based on numerous assumptions. Nevertheless, IRR comparisons can be used to test dependencies and determine the optimal dimensioning and operation strategy, which is the objective of this study.

Costs, revenues, and cash flows from the simulation are presented in <u>Figure 32</u>. The cash flows are calculated by formular (40). The investment costs are considered in year 1 for simplification. Every five years, the capacity unit is replaced, incurring costs. These replacement costs decrease over time because of the learning effects (<u>Figure 8</u>). Revenues decline slightly with increasing market competition.

OPEX is negligible at  $2,152 \frac{\epsilon}{a}$ . Costs are slightly negative in 2046 because the old capacity unit is sold, generating revenue.

Both CAPEX and OPEX were validated using the literature source (Mongird, Kendall et al., 2020:87-90). However, the power-dependent OPEX are assumed to be doubled for the following simulations due to operational experience.

The simulation calculates average annual revenues of  $180 \text{ k} \in$ , with an initial revenue of  $187 \text{ k} \in$  in 2027 and a slightly declining average. A comparison with <u>Appendix 2</u> shows that the profit from cross-market optimization for a 1 MW and 2 MWh BESS is declining from about 250 k $\in$  in 2023 to 200 k $\in$  in 2024. The simulation results are consistent with the historical analysis.

The actual number of full cycles is not provided in the source (Christian Schäfer, 2024). However, in the simulation program, only 392 cycles per year were executed, despite the user-defined 730 target-cycles. This discrepancy is due to the setting of the prediction horizon which will be optimized in chapter <u>5.2</u>.

The user specifies the number of target cycles to be fulfilled in an initial plan. However, this plan does not consider the SOC and market participation conditions, so this plan is adjusted. The adjustment is made within the specified prediction horizon. Each plan value is converted into a comparative price, which are compared with each other. All unfavorable comparative prices that are limited by the matching factor are discarded. For this reason, significantly more target cycles must be planned for high numbers of cycles, because most planned cycles are discarded due to comparative prices that are too unfavorable.

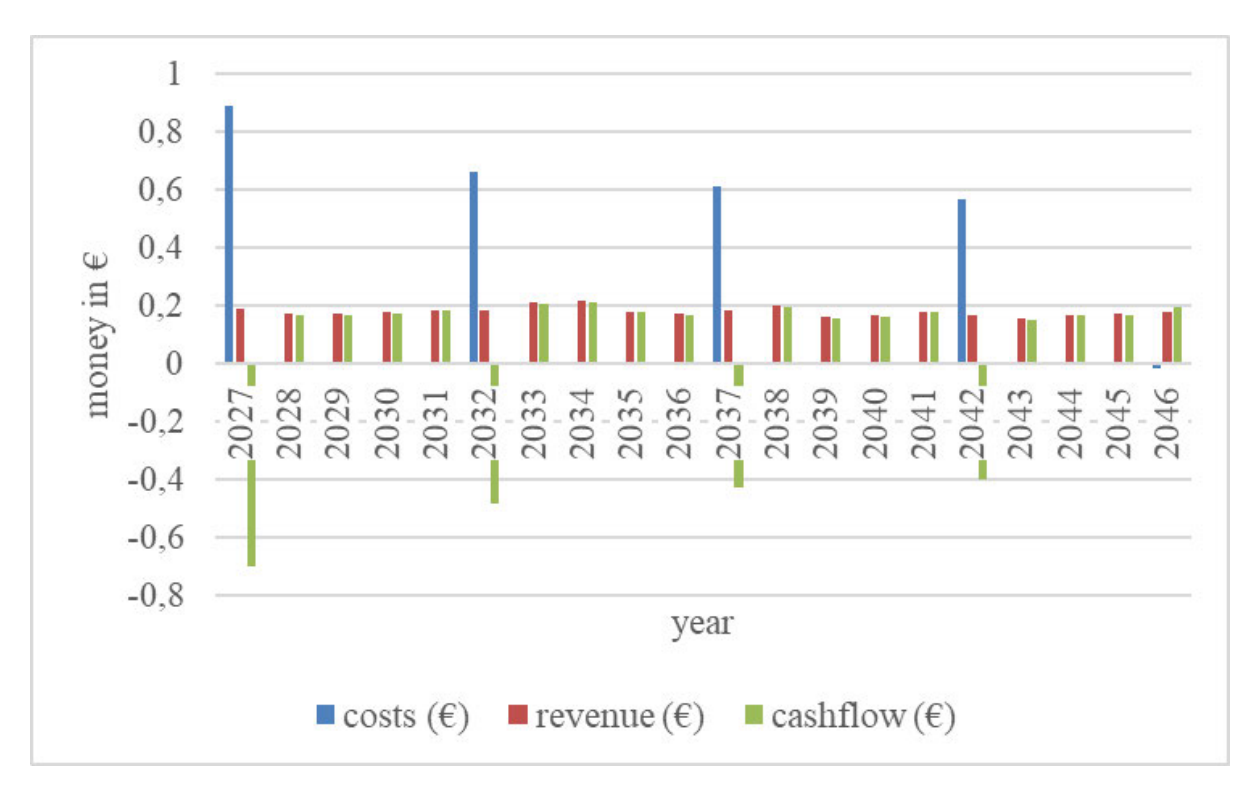


Figure 32 Financial Parameters Costs, Revenue and Cashflow in  $M \in \mathcal{E}$  of BESS-Simulation with 357 Cycles per Year, Usable Power = 1 MW and Usable Capacity = 2 MWh (own Figure)

Power degradation amounts to approximately 0.43 % per replacement over the 5-year period. In contrast, capacity degradation has a significantly greater impact, with around 17.7 % over the 5-year replacement period. The following variables are calculated by the program:  $\overline{DOD} = 33$  % and  $\overline{SOC} = 57$  %.

According to operational analyses in the literature, capacity degradation for NMC is specified as 0.0035 % per full cycle and 0.95 % per year (Feiler, Marcel, 2024:24), resulting in a total degradation of 10.63 % over the 5-year replacement period. Since NMC exhibits a similar degradation behavior to LFP according to Figure 6 and Figure 7 these technologies are comparable.

As  $\overline{DOD}$  and  $\overline{SOC}$  are dependent on the operation of the BESS and have a significant influence on degradation, the degradation result of the simulation program is validated. Figure 7 shows, that the cycling degradation doubles with increasing  $\overline{DOD}$  from 25 % to 40 %.

### 5.2 Parameter Optimization and Sensitivity Analysis

After conducting the baseline simulation, the next step is to optimize parameters.

Less cycles than the target were implemented in the baseline simulation. Because higher cycle utilization leads to higher profits (<u>Figure 34</u>), the losses between the theoretically calculated profit and practical implementation are doubled from 10 % to 20 %. Additionally, the price reduction of the secondary reserve energy markets for assuming 100 % activation probability is increased from 25 to a  $40 \frac{\epsilon}{\text{MWh}}$  lower bid than the average.

To optimize usable power and capacity, various simulations are performed (<u>Figure 33</u>). The other assumptions are retained from the baseline simulation.

A power factor of 2 appears to be optimal for a target of 730 cycles per year, whereas a power factor of 4 results in significant financial losses. However, the real number of cycles implemented by the program may differ significantly from the user-defined target cycles depending on the simulation. Increasing the available capacity up to 20 MWh leads to a notable higher IRR.

For subsequent simulations, only power factors 1 and 2, as well as capacities of at least 20 MWh, will be considered.

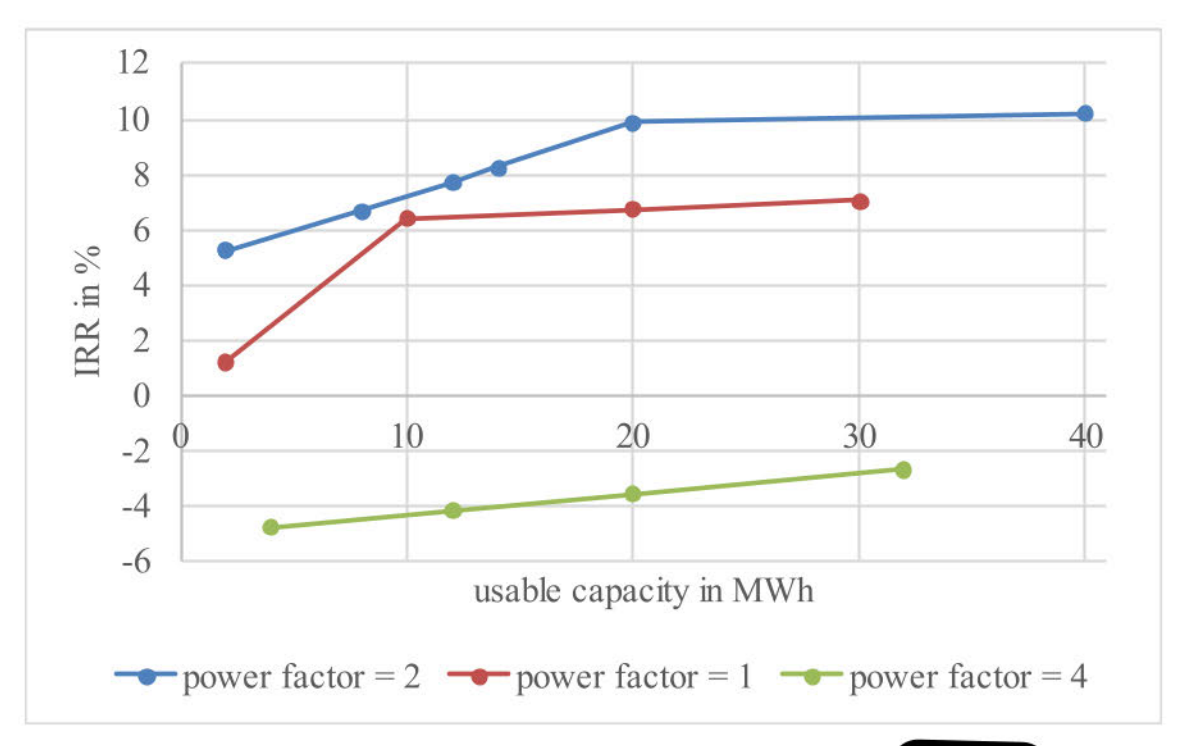


Figure 33 Parameter Optimization of Capacity and Power of BESS for Cycles (own Figure)

To optimize the number of cycles, a 20 MWh BESS with a power factor of 1 (red graph) and 2 (blue graph) was simulated in <u>Figure 34</u>. The choice of annual cycle amount has a strong impact on BESS profitability. For less than 850 cycles per year, a BESS with a power factor of 1 performs better than a power factor of 2. For more than 850 cycles, a BESS with a power factor of 1 performs better.

Operating a BESS with a power factor of 1 and optimizing the cycle amount to 1500 cycles per year can lead to an optimal profit. The IRR is again used as a reference metric; achieving an IRR of 23 % could probably be too high. Furthermore, the actual implementation of 1500 cycles deviates significantly from the intended target, which had to be set to 5,000 cycles for the program to achieve 1300 cycles. This discrepancy arises from a large prediction horizon, which limits the amount of tradable time steps.

Although the target number of cycles is increased further, the program automatically limits the possible number of cycles depending on the prediction horizon. For <u>Figure 34</u>, for example, a simulation with more than 1,500 cycles per year is not possible for *prediction horizon* = 10.

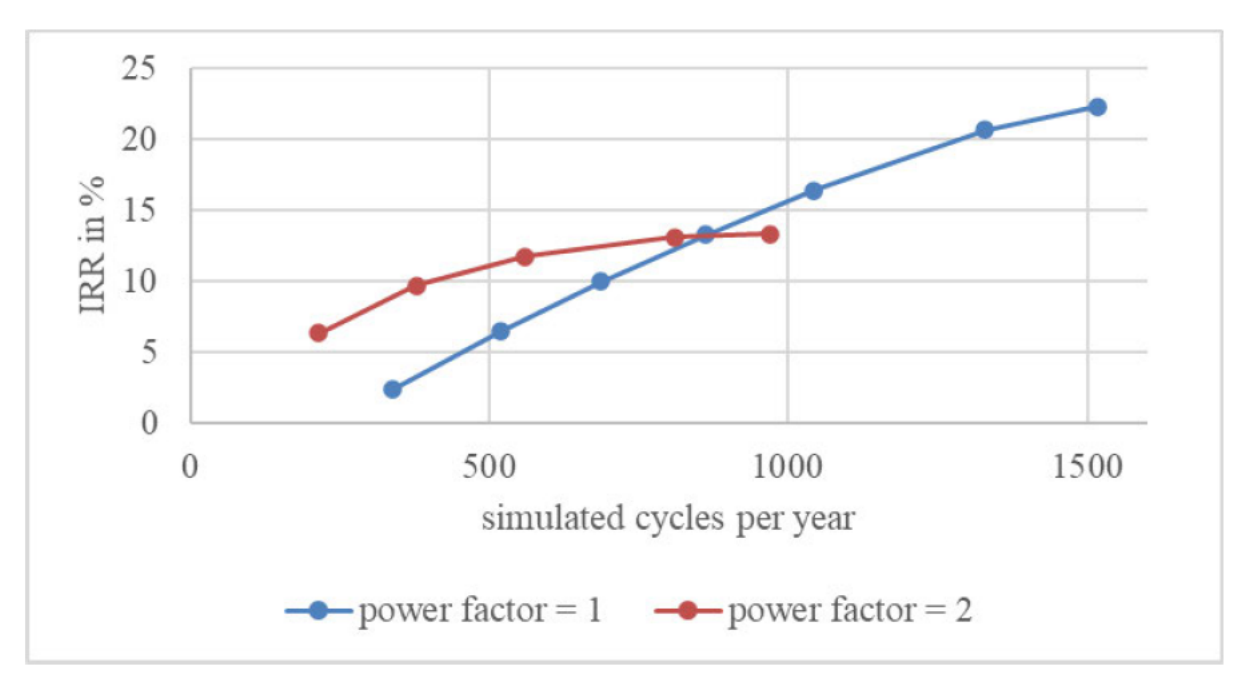


Figure 34 Parameter Optimization of Cycles per Year for BESS of Power Factor 1 and 2 (own Figure)

<u>Figure 35</u> illustrates the impact of the *prediction\_horizon* depending on the simulated cycles per year on the IRR. To enable the program to process large cycle counts at optimum IRR, the *prediction\_horizon* must be reduced. A large prediction horizon limits the number of cycles. The optimum result is 8 predicted values at 1,600 cycles or 4,000 target cycles.

The optimal *prediction\_horizon* changes with the market price prognosis. An increased prediction horizon is advantageous for strongly coupled market price forecasts. For independent price forecasts, a lower prediction horizon is recommended because the increased choice of markets leads to a larger number of cycles utilization.

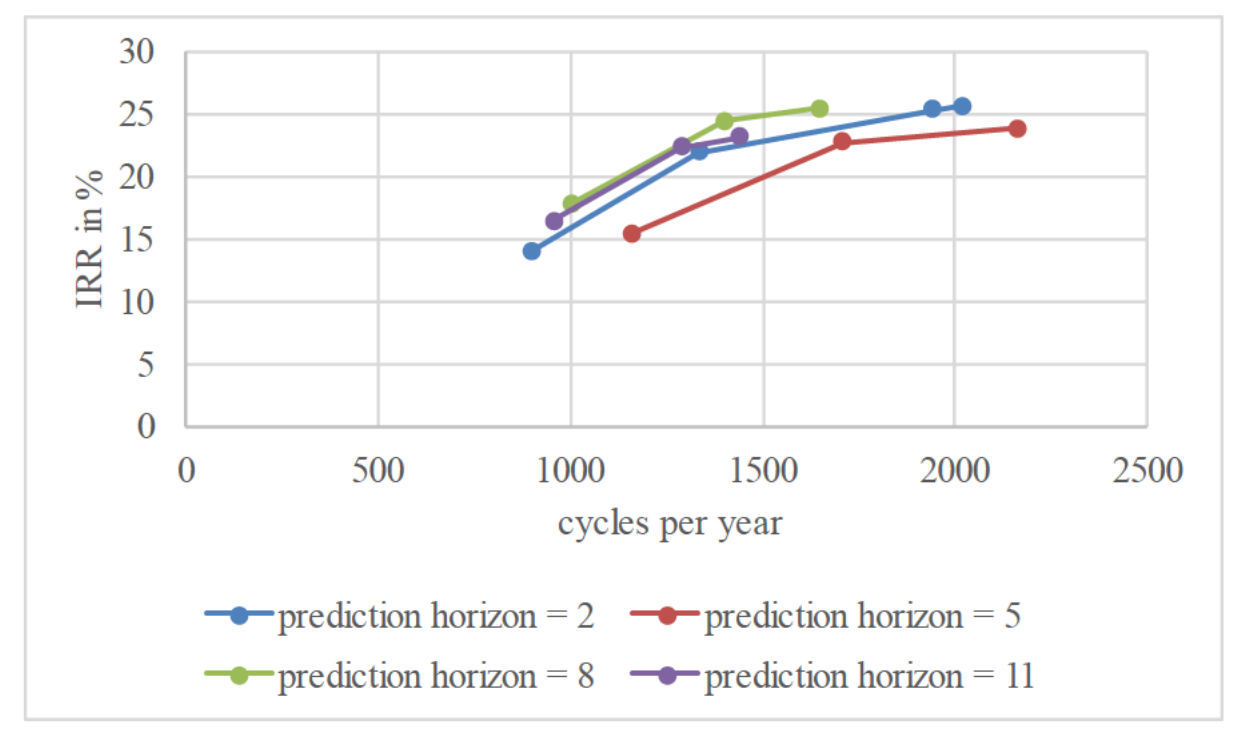


Figure 35 IRR Dependency on Prediction Horizon and Cycles per Year (own Figure)

A simulation comparison is conducted between LFP and NMC with variable cycles per year and otherwise the same input parameters. LFP achieves an IRR that is 1.9 percentage points higher than NMC as an average of all simulations. For this reason, LFP will be used in all subsequent simulations.

The maximum usable power should not be reduced to increase the system RTE. For a simulation of 1643 cycles per year and without any further parameter adjustments, reducing the maximum usable power by 20 % results in a decrease of the IRR by 1.6 percentage points.

Similarly, manually decreasing  $\overline{DOD}$  to mitigate cycle-dependent capacity degradation results in a significant IRR reduction. When the user reduces  $\overline{DOD}$  from 23 % to 15 %, the IRR reduces from 26 % to 5 %. Here, 23 % represents the maximum possible  $\overline{DOD}$ , calculated by the program based on the degradation algorithm (chapter 4.2.4). If the user further reduces the  $\overline{DOD}$ , the EOL capacity will exceed  $Q_U$ . Otherwise, the EOL capacity would equal  $Q_U$  (Figure 3).

The capacity unit should be replaced every 5 years for power factor 1 (<u>Figure 36</u>). Longer replacement periods lead to an almost linear decrease in IRR. For power factor 2 the replacement period can be longer: 10 years are optimal. This is due to a lower cycle utilization for larger power factors (<u>Figure 34</u>). The more cycles per year the storage system utilizes, the faster the capacity degrades and the more often the capacity unit needs to be replaced.

The additional administrative effort of more frequent replacements and the resulting increase in downtimes are not considered in this calculation.

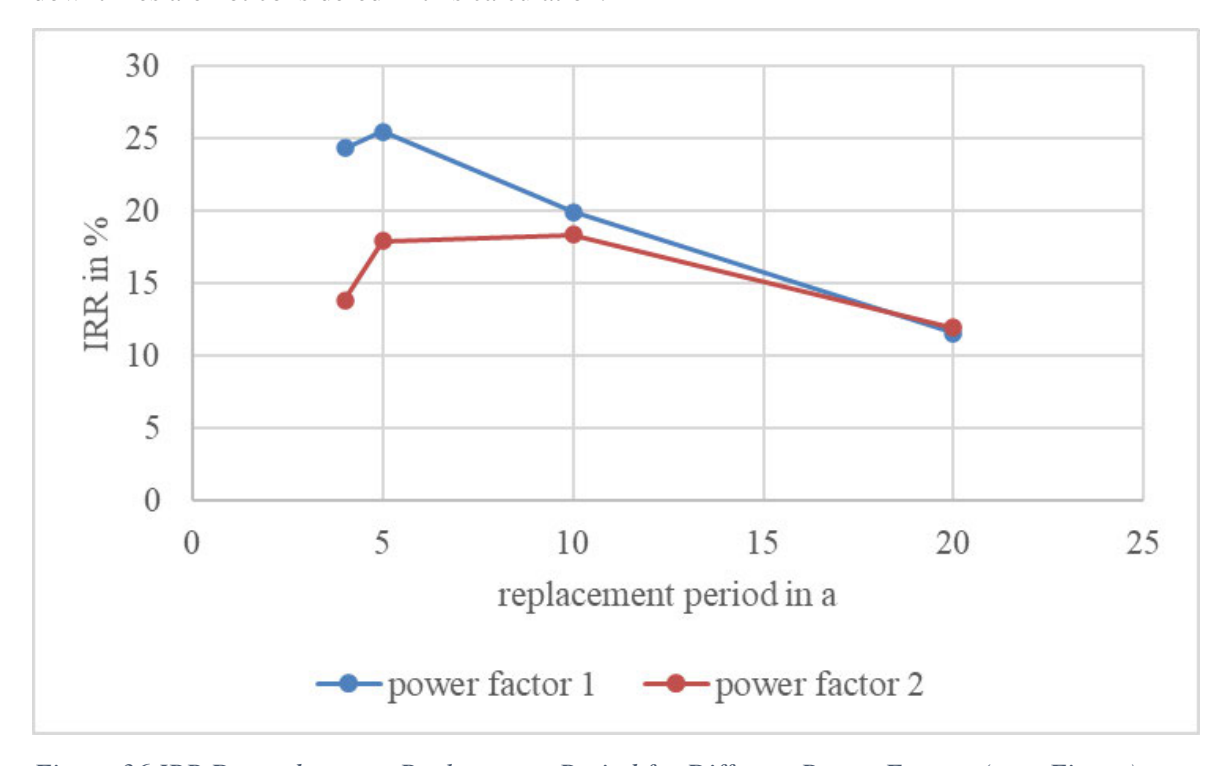


Figure 36 IRR Dependency on Replacement Period for Different Power Factors (own Figure)

For a *prediction\_horizon* of 8, the factor for multiple planning limitation is optimal at 1.5. Increasing or decreasing the factor leads to a reduction of 4 to 5 percentage points for power factor 1. For power factor 2, this factor should be selected between 1.5 and 2. In case of shorter *prediction\_horizon* the multiple planning limitation factor has little impact on the IRR.

The variable representing the safety factor for additional charging to compensate for self-discharge effects and RES+P has a negligible impact on the IRR. If the additional charge is set between 2 % and 4 % of the initial charge, the IRR increases very little.

The supply of RES+P for the simulation with the electricity price of  $21.041 \, \frac{ct}{kWh}$  leads to a reduction in the IRR of 0.08 percentage points. Consequently, the BESS can generate a slightly higher profit on average through the marketing of arbitrage than through the supply of electricity for RES. RES+P is not deactivated for the following simulations to simulate the difference between wind- and PV power supply.

Appendix 39 shows the BESS connected to wind plants, PV plants and both in comparison. Best are a BESS co-located to a wind plant, or a BESS co-located to a combined wind and PV plant. If the BESS is only co-located to a PV plant, the IRR of the BESS is reduced by 1.9 percentage points because more disadvantageous RES+P electricity is traded. If the RES+P price increases, the connection with a PV plant could increase the IRR of the BESS. Additionally, less RES-P electricity can be traded at a discount than if the BESS is co-located to a wind plant.

To operate a BESS in co-location with a wind and PV plant, no additional grid connection power is required, as demonstrated by the simulation results in <u>Appendix 40</u> and <u>Appendix 41</u>. Instead, the BESS could be connected to the same MV transformer as RES, provided that the voltage levels of the RES and BESS inverters are identical. This setup offers the potential to reduce the power-dependent CAPEX of the BESS.

If the BESS is connected to the transformer of the 85.7 MWp PV plant, the IRR of a 20 MW BESS remains unchanged (Appendix 40). Instead, the transformer's operating time is optimally utilized.

When the BESS is connected to the transformer of a wind plant, the grid connection positively impacts the IRR of the BESS (<u>Appendix 41</u>). A detailed analysis shows that a grid limit leads to more inactive periods for the BESS, as it cannot be discharged during grid limits. However, this reduced number of cycles allows the BESS to operate at more favorable prices. The trading volume between RES and BESS are only influenced slightly when connected at the transformer of the wind plant.

If the grid connection power of RES is lower than its nominal capacity, the BESS can significantly benefit from the excess electricity (<u>Appendix 40</u> and <u>Appendix 41</u>), as RES sells this surplus energy to the BESS at a price of  $0 \in$  during these periods.

It was proven that cross-market optimization optimizes profit. The more markets are used, the lower the risk of being dependent on the market prices of a single market. This can also be seen in simulations in which markets are deactivated: Without participation in the SR power markets, the IRR could fall by up to 3.7 percentage points, depending on cycle utilization. If the storage facility is only used on the Intraday market and for trading with RES, the IRR can be reduced by up to 17 percentage points. If only RES-P is to be used for charging the BESS and only INT+P for discharging, the IRR can be reduced by up to 19 percentage points.

Comparison simulations were conducted, initially reducing the mean and subsequently the volatility of market price forecasts. Both a halving of the mean and a halving of volatility each result in approximately a halving of the IRR. The dependencies of the IRR indicated in <u>Figure 33</u> to <u>Figure 36</u> remain largely unchanged.

However, if the market price forecast fundamentally changes, which can be expressed by different assumptions of future market coupling effects (chapter 3.4.2), key parameters such as the optimal

number of cycles per year, the optimal *prediction\_horizon*, and the optimal power factor may be affected.

This was determined based on comparative data from internal market forecasts of the CEE, which serve to validate the simulation results. Cost assumptions remain consistent with those in chapter 3.2. The following conclusions can be drawn:



#### 5.3 Main Simulation, Analysis and Validation

Based on the analysis of the previous chapter, a main simulation is to be carried out to dimension and determine the optimum operating strategy of a BESS. The following section describes the determination of the input parameters for the main simulation.

To determine the system size of the BESS , the usable capacity and power of the BESS must be specified. A power factor of 1 was evaluated as optimal. Figure 33 shows that the IRR for capacities greater than 20 MWh changes only slightly. However, the BESS should not be selected too large As a compromise, a BESS of 30 MW usable power and 30 MWh usable capacity will be planned. The area required is estimated at 2.4 km<sup>2</sup> According to Figure 33, there is enough space between the module fields of the PV plant to implement the project.

According to Appendix 18, this allows for specifying the minimum capacity required for participation in the PR market. For a 1-hour storage system, the minimum storage duration required for each charging and discharging is approximately 0.25 hours. Since the program cannot simulate intermediate recharging within the 4-hour power period, the minimum storage duration is increased to 0.5 hours for each charging and discharging for the 1-hour system to prevent penalty charges in case of PR activation. Storage duration = 1 h for the PR market is interpreted by the program in terms of 2 charges and 2 discharges being possible. Participation is in this case only permitted with SOC = 50 %.

The BESS is to be connected to the PV plant's existing transformer of 85.7 MW to save the costs of an additional transformer. Appendix 40 shows that this does not reduce the IRR of the BESS. Instead, the operating time of the transformer is increased. Although in practice the PV plant and the BESS would share the costs, the cost savings for the simulation are only credited to the BESS.

The transformer cost savings are assumed to be 564 k€ (Ghorbi and Toopchi-Nezhad, 2025:17). These are considered as an initial discount.

To ensure that BESS trading with RES-P from wind and PV remains possible, the grid limit for the simulation is set to 164.9 MW, corresponding to the combined power of the wind and PV plant. The total production data of both renewable technologies is used.

Although RES+P is disabled in the simulation for more economically efficient arbitrage marketing, BESS power supply for RES should still be feasible in practice if electricity prices increase.

The optimal number of cycles per year was determined based on the input data from chapter 3, resulting in 1,600 simulated cycles per year.

This deviation is attributable to the different structures of market price forecasts. The more strongly the markets are coupled, the less cycles per year can be realized. An analysis of historical data does not reveal a high correlation between secondary reserve energy prices and Intraday market prices. Historically, secondary reserve energy prices tend to follow a more random pattern, whereas Intraday market prices exhibit the standard daily pattern shown in Figure 13. It can be assumed that prices will become more closely linked in the future, but this has not been proven. Therefore, both the price forecast of this study and the company's internal price forecasts each represent a possible future, requiring a compromise between them. As a compromise, 668 cycles per year are set for the main simulation. This agrees also with literature, where between 560 and 720 cycles were calculated as optimal in a very similar study (Kyrimlidou et al., 2024:16).

With an adjusted cycle number per year, the replacement period is optimized to 10 years. This is also the replacement period calculated as optimal in a literature BESS simulation (Kyrimlidou et al., 2024:15).

The remaining input parameters for the main simulation were derived based on the analyses in the previous chapter. The visually grouped parameter list of <u>Figure 37</u> shows the input parameters of the main simulation. Columns and rows do not combine any elements:

BESS technology = LFP	year commissioning = 2027	calculation period = 20 a	
replacement period = 10 a	trading on all markets possible except RES+P. For power factor 1, SR ± P must be deactivated too.	usable capacity = 30 MWh	
usable power = 30 MW	grid limit = 164.9 MW	RES+P price = 21.04 ct / kWh	
fees BESS = 0.11 ct / kWh	discount rate = 2 %	initial discount = 564 k€	
RES = Wind and PV	energy dependent OPEX = 0.273 € / MWh	DOD = calculated by program	
target cycles per year = 1300 results in simulated cycles per year = 668	recovery time = 90 min	recovery activation = after 2 full cycles	
no power limitation to increase efficiency	self consumption wind and PV = each 57.8 kW	self-discharge = 4 % / month	
penalty payments are considered 20 % more expensive than without penalty	prediction horizon = 8 values	storage duration for PR participation = 1 h	
storage duration for SR power market participation = 1 h	storage degradation costs = 8.486 € / MW / cycle	charge 2 % more than needed for safty	
losses between theoretical calculation and praxis = 20 %	multiple planning limitation factor = 1.5	residual value = 38 € / kWh	
system RTE annual degradation = 0.2 %	system RTE reduction = 26 percentage points at SOC = 100 %	all market price vectors as developed in chapter 3	
vectors of activation propabilities, system RTE, CAPEX, OPEX and losses as developed in chapter 3, but fixed OPEX doubled.	curtailments of GO as corrected in chapter 5.1	wind and PV production data from WindPRO and PVSyst exports as time-dependent vector output	

Figure 37 Simulation Input Data for Main Simulation (own Figure)

The financial results are presented in <u>Figure 38</u>, expressed through costs, revenues, and cash flow. The project's IRR amounts to 26 %, while the NPV is 32 M€. However, these values should be considered only as an orientation, as the financial outcome is strongly influenced by the numerous assumptions of input parameters.

A forecast simulation from literature determines the optimal IRR of a very similar RES and BESS project for a capacity of 10 MW with an optimal power factor. For the combined RES and BESS plants, the project IRR is stated as 15 % (Kyrimlidou et al., 2024:19).

After appropriate scaling, <u>Figure 38</u> shows a similar progression to <u>Figure 32</u>, as the same market price assumptions were used, despite the significantly higher usable capacity and power. 1 MW / 2 MWh were used in the baseline simulation in contrast to 30 MW / 30 MWh in the main simulation. One key difference lies in the considerably higher initial investment due to the increased capacity and power, despite the transformer costs saved. After 10 years, the capacity unit is replaced, which is reflected in the increased costs in 2037. Additionally, revenues differ due to 668 cycles executed per year in <u>Figure 38</u> compared to 357 cycles in <u>Figure 32</u>.

After accounting for efficiency losses, approximately 20 GWh per year are sold from the BESS. This result was validated based on the simulated annual cycle count and the usable capacity.

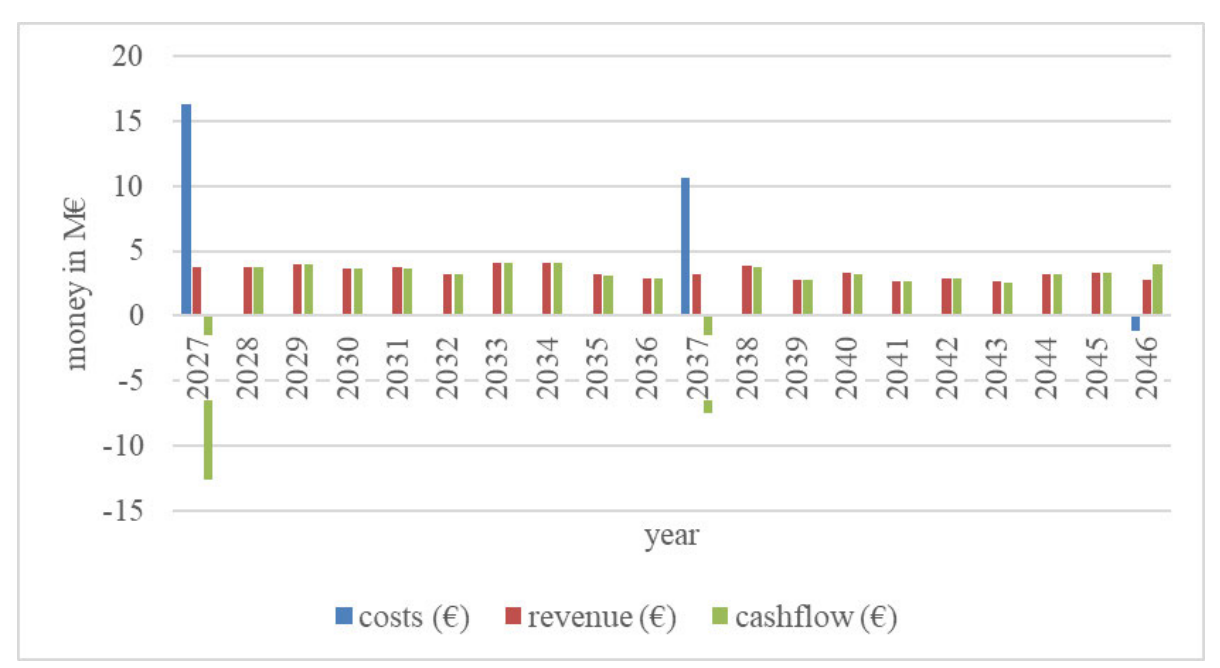


Figure 38 Financial Result of Main Simulation (own Figure)

The capacity degradation amounts to 38 %, and the power degradation is 1 % within 10 years, resulting in a nominal power of 30.3 MW and a nominal capacity of 48.6 MWh. These values were determined using the degradation algorithm from chapter 4.2.4 with the parameters  $\overline{DOD} = 27$  % and  $\overline{SOC} = 53$  %.

For a BESS with a similar operational strategy than in the literature, a capacity degradation of 33.7 % was assumed under simplified linearization for a 10-year operational period (Kyrimlidou et al., 2024:17). Consequently, the calculated capacity degradation appears plausible.

The system RTE is 84 % initially and 85 % after the capacity unit replacement. In the literature, the system RTE is slightly higher at 88 % (Kyrimlidou et al., 2024:13).

The market analysis in <u>Figure 39</u> shows that the BESS remains inactive for about half of its operational time. Charging is primarily conducted by negative curtailments and the SR-E market, while discharging mainly occurs in the INT+P market and, to a lesser extent, by positive curtailments. Approximately 18 % of the time, the system participates in the secondary reserve power markets SR+P and SR-P. Participation in the SR  $\pm$  P market is not permitted for a 1-hour storage system. Downtime also accounts for a significant share of 5 %. Markets with minimal trading activity are SR+E, PR, and RES-P.

Since RES+P is economically unfavorable for the BESS under the current price assumptions and RES-P is used only to a negligible extent, the primary benefit of combining RES and BESS lies in reducing costs through a shared grid connection. If RES would be restricted to feeding in at nominal power, a substantial financial advantage arises when a BESS uses this excess power (<u>Appendix 40</u>). Furthermore, co-location with RES provides security against unfavorable market prices and increased taxes and fees, as these could be mitigated by avoided grid usage.

Penalty payments and cooling times are also minimal. If penalties influence the BESS's operation significantly, certain reserve power markets should be deactivated in the simulation, as the BESS can only restore its SOC after the 4-hour reserve power activation period. If cooling times take up a disproportionate share, the air conditioning system should be redesigned to optimize cooling parameters.

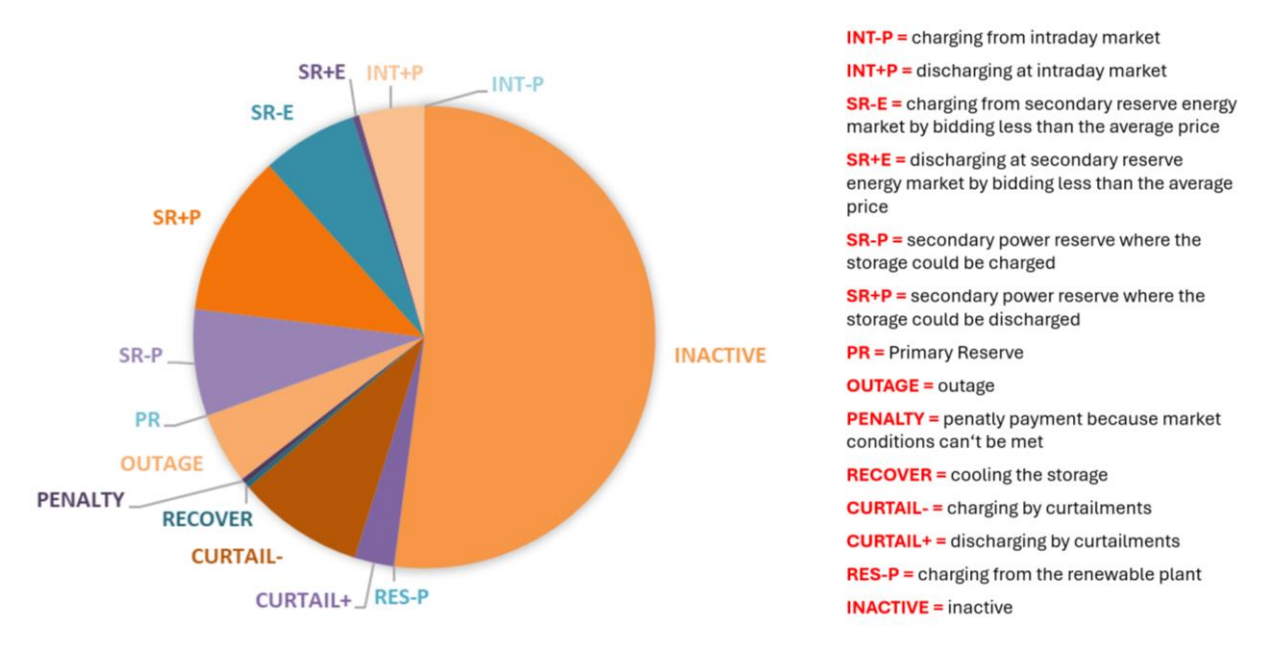


Figure 39 Market Utilization of Main Simulation Result (own Figure)

<u>Figure 40</u> illustrates the BESS revenue distribution across different markets. The primary profit driver is electricity sales in the INT+P market. Charging is predominantly performed through the SR-E market, where the average charging price must be paid, as evidenced by the negative revenue. However, negative curtailments offer an opportunity to improve the IRR, as they generate a net positive revenue. Consequently, it is generally more advantageous to charge the BESS via CURTAIL- rather than through the SR-E market. However, the curtailment remuneration structures for BESS are still in the development phase, so the result may change in future.

The average yield and the standard deviation were determined for the most frequently used markets INT+P and SR-E per 15-min timestamp. For a charging process on the INT+P market, the BESS generates an average revenue of 1,640 € with a standard deviation of 449 €. For a charging process on the SR-E market, the BESS pays an average of 682 € with a standard deviation of 433 €.

A cross-market optimization study from 2021 and 2022 found that the BESS is mainly charged by the Day-Ahead market and discharged at the SR+E Market (Finhold et al., 2023:9-10). However, the Intraday market was not considered in that study. The estimated average daily revenue ranged between  $4,000 \in$  and  $14,000 \in$  for a 10 MW BESS with almost infinite storage capacity (Finhold et al., 2023:9). In this work, the daily revenue is approximately  $10,000 \in$  for a 30 MW / 30 MWh BESS. Considering increasing future market competition, the simulated results are within a possible range.

Even though the financial calculations exhibit significant uncertainties, the potential of a BESS installation in its substantial and can be optimized using the identified operating strategy.



Figure 40 Market Revenue of Main Simulation Result (own Figure)

### 6 Summary and Outlook

In this thesis, a simulation program was developed for the dimensioning and determination of an optimal operating strategy for lithium battery energy storage systems by cross-market optimization. The battery storage system is co-located with a renewable plant. The main advantage of this simulation tool is its transparency: It reveals the results of intermediate calculations. Additionally, all stored data is both accessible and modifiable without programming knowledge. Using the tool, the optimal system size and operating strategy for the PV and wind farm in were determined.

The development of the simulation program requires fundamental knowledge in the fields of engineering, legal and economics. The technical structure of a battery energy storage system and its potential grid connection are presented. Technical parameters and their dependencies are explained to calculate degradation effects and efficiencies. A cost analysis includes forecasting investment costs, operating costs, and residual value. It was presented that taxes and levies have been significantly reduced by the government in recent years. Battery storage systems can be traded on various markets, provided that market-specific participation requirements are met. An overview is given of the historically volatile market prices and the influence of future installed battery storage systems on these prices. The program enables the consideration of grid operator curtailment which will significantly affect the future operation of battery storages.

Based on these fundamentals, the relevant parameters for the simulation program were developed. Approximately 34 parameters and 20 vectors are required as input for the simulation program. The findings from the fundamental analysis were used to explain how they are converted into a format usable by the simulation program. Market price forecasting is based on historical analyses and the projected influence of increasing battery storage market competition. The mean value and volatility were forecasted separately for each market and subsequently linked to the Intraday market price.

After implementing all necessary data, the simulation program was developed. The program is user-friendly and provides considerable assistance for required input. A scheduled operation is generated based on the user-defined number of cycles and participating markets. The program considers technical conditions and constraints, such as state of charge or requirements for market participation. Unplanned outages or curtailments by the grid operator are considered as well. A variety of possible operating strategies are predicted based on the scheduled operation. The most profitable strategy is executed. As a result, the actual operation time series and the associated revenue are calculated. After considering capacity and power degradation, storage costs can be determined. The internal rate of return serves as the optimization metric for multiple simulations with variable parameters. Flowcharts and examples illustrate the methodology.

For the application example of a baseline scenario was developed. Its financial revenue and degradation results were validated through historical literature analysis. An analysis of multiple simulations enables the following key findings regarding battery storage systems:

- The storage system's power should be at least 20 MW. If installed power is lower, the IRR
  decreases significantly.
- The storage duration should be 1 or 2 hours, depending on the number of cycles.
- A 1-hour storage duration can achieve the highest IRR.
- About 668 cycles per year were chosen as optimal, dependent on the analysis of three different market forecasts: The market forecast from this thesis, an internal market forecast and a literature review.
- The replacement period depends on the number of cycles per year: for 668 cycles per year, the battery storage capacity unit should be replaced after 10 years. For higher cycle numbers, the optimal replacement period decreases.
- Lithium-iron-phosphate demonstrated a slightly higher IRR compared to nickel-manganesecobalt lithium battery storage.
- Minimal trading is conducted with the renewable plant. Supplying power to the renewable plant
  is not economically viable at an electricity price of 21 ct/kWh or lower.
- A significant advantage of combining the battery storage system with renewable generation is
  the reduction of grid connection costs. Connecting a battery storage system to a transformer of
  a much larger PV plant allows for optimal utilization of the transformer's operating time without
  negatively impacting the battery storage internal rate of return. In the case of grid limits for the
  renewable plant, the battery storage system can benefit financially.
- If the mean value and volatility of the market price forecast change, all dependencies fundamentally remain the same. However, if the market price coupling changes, then the optimally calculated parameters, such as the number of cycles per year or storage hours, can also change.
- If cross-market optimization is not applied, significant financial losses for the battery storage system will occur. Operational analyses indicate that the primary profit can be achieved by charging from the secondary reserve power market and discharging by Intraday market participation.

• Increased curtailments, where the storage system is charged, can positively impact the storage system's revenue.

For a lithium-iron-phosphate battery storage system with a constant usable capacity and power of 30 MWh and 30 MW over its lifetime is proposed. It is designed to perform 668 cycles per year and is connected to the transformer of an 81.7 MWp PV plant, reducing grid connection costs. Over a 20-year operating period, a capacity unit replacement is planned after 10 years. The capacity degradation after 10 years is approximately 38 %, resulting in an installed capacity of 48 MWh. Power degradation can be neglected.

The internal rate of return of the simulation is 27 % with a net present value of 32 M $\in$  and a daily revenue is approximately 10,000  $\in$ . These results exceed literature values which report about 15 % IRR. However, the forecast uncertainty of market simulations is significant, meaning that the result falls within a reasonable tolerance range.

The simulation program, in its currently developed version, can already be used for the technical and economic optimization of battery storage projects. However, the use of market price forecast data from market specialists is recommended, as market price forecasts have a significant impact on the optimal operation strategy and financial outcome. Forecast data should be updated annually due to rapidly changing market prices.

Furthermore, the program is not limited to lithium battery storage but can also incorporate alternatives such as sodium-ion accumulators. All short-term storage technologies can be implemented within the program code. By adjusting the degradation model, the potential of second-life batteries can also be simulated. For the correct implementation of reserve power markets, multiple operating states should be possible simultaneously to enable the calculation of recharging or discharging during reserve power provision.

This thesis not only enabled the design of the battery storage system for but also provides a simulation tool capable of optimizing a wide range of future battery storage projects.

#### References

- 50hertz, Amprion, Tennet, Transnet BW, 2024a. § 19 StromNEV-Umlage 2024 [WWW Document]. URL https://www.netztransparenz.de/de-de/Erneuerbare-Energien-und-Umlagen/Sonstige-Umlagen/Aufschlag-f%C3%BCr-besondere-Netznutzung-19-StromNEV-Umlage/%C3%9Cbersicht-Aufschlag-f%C3%BCr-besondere-Netznutzung/-19-StromNEV-Umlage-2024 (accessed 07.11.2024).
- 50hertz, Amprion, Tennet, Transnet BW, 2024b. Netztransparenz > Home [WWW Document]. Netztransparanz. URL https://www.netztransparenz.de/de-de/ (accessed 15.12.2024).
- 50hertz, Amprion, Tennet, Transnet BW, 2020a. Musterprotokoll PR. [WWW Document]. URL https://www.regelleistung.net/xspproxy/api/StaticFiles/Regelleistung/Allgemeine%20Infos/Ar ten\_der\_Regelreserve/01\_FCR/Musterprotokoll%20zum%20Nachweis%20der%20Erbringun g%20von%20Primärregelleistung.pdf (accessed 25.03.2025).
- 50hertz, Amprion, Tennet, Transnet BW, 2020b. Musterprotokoll SR. [WWW Document]. URL https://www.regelleistung.net/xspproxy/api/StaticFiles/Regelleistung/Allgemeine%20Infos/Ar ten\_der\_Regelreserve/02\_aFRR/Musterprotokoll\_zum\_Nachweis\_der\_Erbringung\_von\_Seku ndärregelleistung.pdf (accessed 25.03.2025).
- 50hertz, Amprion, Tennet, Transnet BW, 2020c. Musterprotokoll TR. [WWW Document]. URL https://www.regelleistung.net/xspproxy/api/StaticFiles/Regelleistung/Allgemeine%20Infos/Ar ten\_der\_Regelreserve/03\_mFRR/Musterprotokoll\_zum\_Nachweis\_der\_Erbringung\_von\_Min utenreserveleistung.pdf (accessed 25.03.2025).
- 50hertz, Aprion, Tennet, Transnet BW, 2023. Prognose des Umfangs und der Kosten der Maßnahmen für Engpassmanagement nach § 13 Abs. 10 EnWG (2023). [WWW Document]. URL https://www.bundesnetzagentur.de/SharedDocs/Downloads/DE/Sachgebiete/Energie/Unterneh men\_Institutionen/Versorgungssicherheit/Netzreserve/PrognoseNetzSystemsicherheitskosten2 023.pdf?\_\_blob=publicationFile&v=1 (accessed 25.03.2025).
- 50hertz, Tennet, Amprion, Transnet BW, 2024c. regelleistung.net [WWW Document]. URL https://www.regelleistung.net/de-de/ (accessed 28.11.2024).
- Agentur für Erneuerbare Energien, 2024. Durch Abregelung verlorene Stromerzeugung aus Erneuerbaren Energien [WWW Document]. URL https://www.unendlich-vielenergie.de/mediathek/grafiken/durch-abregelung-verlorene-stromerzeugung-aus-erneuerbarenenergien (accessed 15.11.2024).
- BDEW, 2023. Installierte Leistung Photovoltaik in Deutschland bis 2045 [WWW Document]. URL https://www.bdew.de/service/publikationen/installierte-leistung-photovoltaik-in-deutschland-bis-2045/ (accessed 25.11.2024).
- BDEW, 2018. Modalitäten für Regelreserveanbieter gemäß Artikel 18 Abs. 5 Konsultation BNetzA. [WWW Document]. URL https://www.bundesnetzagentur.de/DE/Beschlusskammern/1\_GZ/BK6-GZ/2018/BK6-18-004/Stellungnahme\_bdew\_pdf.pdf?\_\_blob=publicationFile&v=1 (accessed 25.03.2025).
- Benjamin Blat Belmonte, Panagiotis Mouratidis, Georg Franke, Stephan Rinderknecht, 2023.

  Developments in the cost of grid balancing services and the design of the European balancing market ScienceDirect [WWW Document]. URL https://www.sciencedirect.com/science/article/pii/S2352484723011253?ref=pdf\_download&fr=RR-2&rr=8f2c9b614f0e44fe (accessed 16.12.2024).
- Böttcher, J., Nagel, P., 2018. Batteriespeicher: Rechtliche, Technische und Wirtschaftliche Rahmenbedingungen. Walter de Gruyter GmbH, Berlin/München/Boston, GERMANY. [WWW Document]. URL http://ebookcentral.proquest.com/lib/hawhamburg-ebooks/detail.action?docID=5156901 (accessed 25.03.2025).
- Bundesamt der Justiz, Bundesministeriums der Justiz, 2024. § 51 EEG 2023 Einzelnorm [WWW Document]. URL https://www.gesetze-im-internet.de/eeg\_2014/\_\_51.html (accessed 18.11.2024).
- Bundesministerium für Wirtschaft und Klimaschutz BMWK, 2023. Stromspeicher-Strategie. [WWW Document]. URL https://www.bmwk.de/Redaktion/DE/Downloads/S-T/stromspeicherstrategie-231208.pdf?\_\_blob=publicationFile&v=8 (accessed 25.03.2025).

- Bundesministeriums der Justiz, Bundesamt der Justiz, 2024a. EnFG nichtamtliches Inhaltsverzeichnis [WWW Document]. URL https://www.gesetze-im-internet.de/enfg/(accessed 04.11.2024).
- Bundesministeriums der Justiz, Bundesamt der Justiz, 2024b. UStG nichtamtliches Inhaltsverzeichnis [WWW Document]. URL https://www.gesetze-im-internet.de/ustg\_1980/(accessed 09.11.2024).
- Bundesministeriums der Justiz, Bundesamt der Justiz, 2024c. EnWG nichtamtliches Inhaltsverzeichnis [WWW Document]. URL https://www.gesetze-im-internet.de/enwg\_2005/(accessed 07.11.2024).
- Bundesministeriums der Justiz, Bundesamt der Justiz, 2023a. StromStG nichtamtliches Inhaltsverzeichnis [WWW Document]. URL https://www.gesetze-iminternet.de/stromstg/index.html#BJNR037810999BJNE000700307 (accessed 04.11.2024).
- Bundesministeriums der Justiz, Bundesamt der Justiz, 2023b. StromNEV nichtamtliches Inhaltsverzeichnis [WWW Document]. URL https://www.gesetze-im-internet.de/stromnev/(accessed 09.11.2024).
- Bundesministeriums der Justiz, Bundesamt der Justiz, 2006. KAV nichtamtliches Inhaltsverzeichnis [WWW Document]. URL https://www.gesetze-im-internet.de/kav/ (accessed 07.11.2024).
- Bundesnetzagentur, 2024a. SMARD | So funktioniert der Strommarkt [WWW Document]. URL https://www.smard.de/page/home/wiki-article/446/384 (accessed 13.12.2024).
- Bundesnetzagentur, 2024b. SMARD | Marktdaten [WWW Document]. SMARD. URL https://www.smard.de/home/downloadcenter/download-marktdaten/ (accessed 03.11.2024).
- Bundesnetzagentur, 2024c. SMARD | Netzengpassmanagement im 1. Quartal 2024 [WWW Document]. URL https://www.smard.de/page/home/topic-article/444/213808 (accessed 15.11.2024).
- Bundesnetzagentur, 2024d. Anlage 1 zur Bestimmung des finanziellen Ausgleichs für Anpassung der Wirkleistungserzeugung oder des Wirkleistungsbezugs. [WWW Document]. URL https://www.bundesnetzagentur.de/DE/Beschlusskammern/1\_GZ/BK8-GZ/2022/2022\_4-Steller/BK8-22-0001/Anlagen/BK8-22-0001-A\_Festlegung\_Anlage1\_Download\_BF.pdf?\_\_blob=publicationFile&v=3 (accessed 25.03.2025).
- Bundesnetzagentur, 2024e. Bundesnetzagentur Kraftwerksliste [WWW Document]. URL https://www.bundesnetzagentur.de/DE/Fachthemen/ElektrizitaetundGas/Versorgungssicherhei t/Erzeugungskapazitaeten/Kraftwerksliste/start.html (accessed 16.12.2024).
- Bundesverband der Energie- und Wasserwirtschaft, 2024. BDEW-Strompreisanalyse Juli 2024 [WWW Document]. URL https://www.bdew.de/service/daten-und-grafiken/bdew-strompreisanalyse/ (accessed 04.11.2024).
- Buratynskyi, I., Nechaieva, T., Leshchenko, I., Shulzhenko, S., 2023. Profitability of the PV Plant and BESS Joint Operation on the Electricity Market, in: Zaporozhets, A. (Ed.), Systems, Decision and Control in Energy V. Springer Nature Switzerland, Cham, pp. 543–554. https://doi.org/10.1007/978-3-031-35088-7\_29 (accessed 25.03.2025).
- Bürklin, B., Latz, T., Schenk, L., Degen, F., Diehl, M., Krätzig, O., Paulsen, T., Wessel, S., Kampker, A., Lackner, N., Neef, C., Wicke, T., 2022. Umfeldbericht zum europäischen Innovationssystem Batterie 2022. https://doi.org/10.24406/publica-749 (accessed 25.03.2025).
- Christian Schäfer, 2024. Regelleistung Online Die Analyseplattform für den Regelleistungsmarkt. URL https://www.regelleistung-online.de/ (accessed 13.12.2024).
- Connor Thelen, Hannah Nolte, Markus Kaiser, Patrick Jürgens, Paul Müller, Charlotte Senkpiel, Christoph Kost, 2024. Wege zu einem klimaneutralen Energiesystem [WWW Document]. Fraunhofer-Inst. Für Solare Energiesysteme ISE. URL https://www.ise.fraunhofer.de/de/veroeffentlichungen/studien/wege-zu-einem-klimaneutralenenergiesystem.html (accessed 15.11.2024).
- Crawford, A.J., Viswanathan, V.V., Wu, D., Barbaro dos Santos, A.F., 2022. Energy Northwest Horn Rapids Solar and Storage: An Assessment of Battery Technical Performance (No. PNNL-ACT-10122). Pacific Northwest National Lab. (PNNL), Richland, WA (United States). https://doi.org/10.2172/1877859 (accessed 01.10.2024).
- Dr. Balaram Bora, 2015. COMPARISON BETWEEN NET PRESENT VALUE AND INTERNAL RATE OF RETURN. [WWW Document] URL

- $https://d1wqtxts1xzle7.cloudfront.net/41051869/comparison\_between\_NPV\_and\_IRR-libre.pdf?1452577364=\&response-content-$
- disposition=inline%3B+filename%3DComparison\_Between\_Net\_Present\_Value\_And.pdf&E xpires=1740557835&Signature=MdPn7uAL~1GEqtb~wJKuR1YQXyEzCWju7zqNpbYMMc xOlmAtJA8HaHFLr7x1JB9vctrPTJxyWHUnoMNAfnP18D5uAlXsvA-
- 4DJ9p2LHbowbpR51eKyHlzNt4V3MCofWlBkScDjmyWOXA6H0SaqpNf~aCOVrhQc7m2 3jcVX5Hn3t-
- dMCKPIaCgqH5LEIM8oGYbKgDFmqBEscLFYRY55xYdSPN8avbhzfb6Z4V6me-Cii2-8DyWSUDkq-
- YkGYFolhaGIUiAz4VBPbP3iZqZXIvdvVqoM1jiOIkukLBwXCSr52pdY5dkiGwvaOGmBY xt7Hh7XLTnqH5AaWR7GfgaWqT2w\_\_&Key-Pair-Id=APKAJLOHF5GGSLRBV4ZA [WWW Document]. Comp. Net Present Value Intern. Rate Return. URL
- $https://d1wqtxts1xzle7.cloudfront.net/41051869/comparison\_between\_NPV\_and\_IRR-libre.pdf?1452577364 = \& response-content-$
- $\label{lem:disposition} disposition=inline% 3B+filename% 3DComparison\_Between\_Net\_Present\_Value\_And.pdf\&E xpires=1740557835\&Signature=MdPn7uAL~1GEqtb~wJKuR1YQXyEzCWju7zqNpbYMMc xOlmAtJA8HaHFLr7x1JB9vctrPTJxyWHUnoMNAfnP18D5uAlXsvA-$
- $4DJ9p2LHbowbpR51eKyHlzNt4V3MCofWlBkScDjmyWOXA6H0SaqpNf\sim aCOVrhQc7m2\\3jcVX5Hn3t-$
- dMCKPIaCgqH5LEIM8oGYbKgDFmqBEscLFYRY55xYdSPN8avbhzfb6Z4V6me-Cii2-8DyWSUDkq-
- YkGYFolhaGIUiAz4VBPbP3iZqZXIvdvVqoM1jiOIkukLBwXCSr52pdY5dkiGwvaOGmBY xt7Hh7XLTnqH5AaWR7GfgaWqT2w\_\_&Key-Pair-Id=APKAJLOHF5GGSLRBV4ZA (accessed 26.02.2025).
- Ekman, C.K., Jensen, S.H., 2010. Prospects for large scale electricity storage in Denmark. Energy Convers. Manag. 51, 1140–1147. https://doi.org/10.1016/j.enconman.2009.12.023 (accessed 25.03.2025).
- EMD International A/S, 2024. windPRO Best Software for Wind Farm and PV Project DesignEMD International. URL https://www.emd-international.com/windpro/ (accessed 18.11.2024).
- European Energy Exchange AG, 2024. European Energy Exchange AG (EEX) [WWW Document]. URL https://www.eex.com/de/ (accessed 13.12.2024).
- Fallahifar, R., Kalantar, M., 2023. Optimal planning of lithium ion battery energy storage for microgrid applications: Considering capacity degradation. J. Energy Storage 57, 106103. https://doi.org/10.1016/j.est.2022.106103 (accessed 25.03.2025).
- Fan, F., Zorzi, G., Campos-Gaona, D., Burt, G., Anaya-Lara, O., Nwobu, J., Madariaga, A., 2021. Sizing and Coordination Strategies of Battery Energy Storage System Co-Located with Wind Farm: The UK Perspective. Energies 14, 1439. https://doi.org/10.3390/en14051439 (accessed 25.03.2025).
- Feiler, Marcel, 2024. Potenzialanalyse zur Kombination von netzgekoppelten Photovoltaik-Großprojekten mit Batteriespeichersystemen. [WWW Document]. URL https://opus4.kobv.de/opus4-haw/files/5126/I002175428Abschlussarbeit.pdf (accessed 25.03.2025).
- Finhold, E., Gärtner, C., Grindel, R., Heller, T., Leithäuser, N., Röger, E., Schirra, F., 2023. Optimizing the marketing of flexibility for a virtual battery in day-ahead and balancing markets: A rolling horizon case study. Appl. Energy 352, 121667. https://doi.org/10.1016/j.apenergy.2023.121667 (accessed 25.03.2025).
- Fraunhofer ISE, 2025. Öffentliche Stromerzeugung 2024: Deutscher Strommix so sauber wie nie Fraunhofer ISE [WWW Document]. Fraunhofer-Inst. Für Solare Energiesysteme ISE. URL https://www.ise.fraunhofer.de/de/presse-und-medien/presseinformationen/2025/oeffentliche-stromerzeugung-2024-deutscher-strommix-so-sauber-wie-nie.html (accessed 12.02.2025).
- Fraunhofer ISE, 2024. Energy-Charts [WWW Document]. URL https://www.energy-charts.info/index.html (accessed 13.12.2024).
- Fraunhofer ISI, Consentec GmbH, ifeu gGmbH, Technische Universität Berlin, 2024.

  Langfristszenarien für die Transformation des Energiesystems in Deutschland [WWW Document]. URL https://langfristszenarien.de/enertile-explorer-

- wAssets/docs/LFS3\_T45\_Webinar\_Feb\_2024\_Dezentral\_final\_presented.pdf (accessed 25.03.2025).
- Ghorbi, E., Toopchi-Nezhad, H., 2025. Seismic-isolation of a high-voltage power transformer with pseudo-rolling elastomeric isolators: Design, evaluation, and implementation. Eng. Struct. 329, 119753. https://doi.org/10.1016/j.engstruct.2025.119753 (accessed 25.03.2025).
- Graf von Luckner, Kiesel, 2019. Hawkes processes for market order arrivals on the German intraday power market and their application in optimal market maker pricing. [WWW Document]. URL https://www.strommarkttreffen.org/2019-06-07\_Luckner\_Hawkes\_processes\_for\_modeling\_event\_arrivals\_on\_intraday\_market\_and\_optimal\_market\_maker\_pricing.pdf (accessed 25.03.2025).
- Hornek, T., Lee, Y., Menci, S.P., Pavić, I., 2025. The Value of Battery Energy Storage in the Continuous Intraday Market: Forecast vs. Perfect Foresight Strategies. https://doi.org/10.48550/arXiv.2501.07121 (accessed 25.03.2025).
- International Renewable Energy Agency IREA, 2017. Electricity storage and renewables: costs and markets to 2030 [WWW Document]. URL https://www.irena.org/publications/2017/Oct/Electricity-storage-and-renewables-costs-and-markets (accessed 28.10.2024).
- International Renewable Energy Agency IREA, 2012. Electricity Storage and Renewables for Island Power: A Guide for Decision Makers. [WWW Document]. URL https://www.irena.org/-/media/Files/IRENA/Agency/Publication/2012/Electricity-Storage-and-RE-for-Island-Power.pdf (accessed 25.03.2025).
- Koch, C., 2021. Intraday imbalance optimization: incentives and impact of strategic intraday bidding behavior. Energy Syst. 13, 409–435. https://doi.org/10.1007/s12667-021-00445-9 (accessed 25.03.2025).
- Kyon Energy, 2024. Stellungnahme Vergütung von Redispatch-Maßnahmen [WWW Document]. URL https://www.kyon-energy.de/blog/stellungnahme---vergutung-von-redispatch-massnahmen (accessed 19.11.2024).
- Kyrimlidou, P.T., Simoglou, C.K., Biskas, P.N., 2024. Optimal sizing and long-term operation of a hybrid RES-BESS station in a competitive electricity market. Sustain. Energy Grids Netw. 39, 101450. https://doi.org/10.1016/j.segan.2024.101450 (accessed 25.03.2025).
- Li, J., He, S., Yang, Q., Wei, Z., Li, Y., He, H., 2023. A Comprehensive Review of Second Life Batteries Toward Sustainable Mechanisms: Potential, Challenges, and Future Prospects. IEEE Trans. Transp. Electrification 9, 4824–4845. https://doi.org/10.1109/TTE.2022.3220411 (accessed 25.03.2025).
- Li, R., Bao, L., Chen, L., Zha, C., Dong, J., Qi, N., Tang, R., Lu, Y., Wang, M., Huang, R., Yan, K., Su, Y., Wu, F., 2023. Accelerated aging of lithium-ion batteries: bridging battery aging analysis and operational lifetime prediction. Sci. Bull. 68, 3055–3079. https://doi.org/10.1016/j.scib.2023.10.029 (accessed 25.03.2025).
- Liebau, B., 2012. Der deutsche Strommarkt: Marktdesign und Anbieterverhalten. [WWW Document]. URL https://www.uni-muenster.de/Ebooks/index.php/series/catalog/book/140 (accessed 25.03.2025).
- Lo Franco, F., Morandi, A., Raboni, P., Grandi, G., 2021. Efficiency Comparison of DC and AC Coupling Solutions for Large-Scale PV+BESS Power Plants. Energies 14, 4823. https://doi.org/10.3390/en14164823 (accessed 25.03.2025).
- Marie Wettingfeld, Peter Martin, Florin Collmer, 2023. Kurzstudie für die EWS Elektrizitätswerke Schönau eG Redispatch im deutschen Stromsystem Hintergründe, Kostenverteilung, Emissionen. [WWW Document]. URL https://foes.de/publikationen/2023/2023\_09\_FOES\_Redispatch.pdf (accessed 25.03.2025).
- Martinez-Bolanos, J.R., Udaeta, M.E.M., Gimenes, A.L.V., Silva, V.O. da, 2020. Economic feasibility of battery energy storage systems for replacing peak power plants for commercial consumers under energy time of use tariffs. J. Energy Storage 29, 101373. https://doi.org/10.1016/j.est.2020.101373 (accessed 25.03.2025).
- Mauler, L., Duffner, F., G. Zeier, W., Leker, J., 2021. Battery cost forecasting: a review of methods and results with an outlook to 2050. Energy Environ. Sci. 14, 4712–4739. https://doi.org/10.1039/D1EE01530C (accessed 25.03.2025).

- Merten, M., Olk, C., Schoeneberger, I., Sauer, D.U., 2020. Bidding strategy for battery storage systems in the secondary control reserve market. Appl. Energy 268, 114951. https://doi.org/10.1016/j.apenergy.2020.114951 (accessed 25.03.2025).
- Mohammad Shahjalal, Probir Kumar Roy, Tamanna Shams, Ashley Fly, Jahedul Islam Chowdhury, Kailong Liu a, Md. Rishad Ahmed, 2021. A review on second-life of Li-ion batteries: prospects, challenges, and issues ScienceDirect [WWW Document]. URL https://www.sciencedirect.com/science/article/pii/S0360544221031303 (accessed 03.03.2025).
- Mongird, K., Fotedar, V., Viswanathan, V., Koritarov, V., Balducci, P., Hadjerioua, B., Alam, J., 2019. Energy Storage Technology and Cost Characterization Report [WWW Document]. URL https://www.pnnl.gov/publications/energy-storage-technology-and-cost-characterization-report (accessed 20.10.2024).
- Mongird, Kendall, Viswanathan, Vilayanur, Alam, Jan, Vartanian, C., Baxter, R., 2020. Energy Storage Grand Challenge Cost and Performance Assessment 2020 [WWW Document]. URL https://www.pnnl.gov/sites/default/files/media/file/Final%20-%20ESGC%20Cost%20Performance%20Report%2012-11-2020.pdf (accessed 20.10.2024).
- NREL, 2024. System Advisor Model SAM [WWW Document]. Syst. Advis. Model SAM. URL https://sam.nrel.gov/ (accessed 13.02.2025).
- Philipp Götz, Dr. Johannes Henkel, Thorsten Lenck, Dr. Konstantin Lenz, Energy Brainpool GmbH & Co. KG, 2014. Negative Strompreise Ursachen und Wirkungen. Forstwiss. Cent. 38, 295–296. https://doi.org/10.1007/BF01769436 (accessed 25.03.2025).
- Pregnolato, S., 2019. Real-Time Battery Conditions Estimation. [WWW Document]. URL https://webthesis.biblio.polito.it/secure/12495/1/tesi.pdf (accessed 25.03.2025).
- PVsyst SA, 2024. PVsyst. URL https://www.pvsyst.com/ (accessed 18.11.2024).
- SMA Solar Technology AG, 2023. MV Power Station [WWW Document]. URL https://files.sma.de/downloads/MVPS-S2-SCS2xxx-DS-de-20.pdf (accessed 27.10.2024).
- Statista, 2025. Anzahl der Stunden mit negativen Strompreisen in Deutschland in den Jahren 2014 bis 2024 [WWW Document]. Statista. URL https://de.statista.com/statistik/daten/studie/618751/umfrage/anzahl-der-stunden-mit-negativen-strompreisen-in-deutschland/#:~:text=Anzahl%20der%20Stunden%20mit%20negativen%20Strompreisen%20 in%20Deutschland%20bis%202024&text=Im%20Jahr%202024%20lag%20der,457%20Stunden%20im%20negativen%20Bereich. (accessed 15.11.2024).
- Stroe, D.-I., Knap, V., Swierczynski, M., Stroe, A.-I., Teodorescu, R., 2017. Operation of a Grid-Connected Lithium-Ion Battery Energy Storage System for Primary Frequency Regulation: A Battery Lifetime Perspective. IEEE Trans. Ind. Appl. 53, 430–438. https://doi.org/10.1109/TIA.2016.2616319 (accessed 25.03.2025).
- Sun, S., Guan, T., Cheng, X., Zuo, P., Gao, Y., Du, C., Yin, G., 2018. Accelerated aging and degradation mechanism of LiFePO4/graphite batteries cycled at high discharge rates. RSC Adv. 8, 25695–25703. https://doi.org/10.1039/C8RA04074E (25.03.2025).
- Swierczynski, M., Stroe, D.-I., Stan, A.-I., Teodorescu, R., Kær, S.K., 2015. Lifetime Estimation of the Nanophosphate \hboxLiFePO\_4\hbox/C Battery Chemistry Used in Fully Electric Vehicles. IEEE Trans. Ind. Appl. 51, 3453–3461. https://doi.org/10.1109/TIA.2015.2405500 (accessed 25.03.2025).
- tagesschau.de, 2024. USD/EUR Kurs aktuell [WWW Document]. tagesschau.de. URL https://www.tagesschau.de/wirtschaft/boersenkurse/xc0009666410-25216210/ (accessed 20.10.24).
- Tanim, T.R., Yang, Z., Colclasure, A.M., Chinnam, P.R., Gasper, P., Lin, Y., Yu, L., Weddle, P.J., Wen, J., Dufek, E.J., Bloom, I., Smith, K., Dickerson, C.C., Evans, M.C., Tsai, Y., Dunlop, A.R., Trask, S.E., Polzin, B.J., Jansen, A.N., 2021. Extended cycle life implications of fast

- charging for lithium-ion battery cathode. Energy Storage Mater. 41, 656–666. https://doi.org/10.1016/j.ensm.2021.07.001 (accessed 25.03.2025).
- Tennet, Amprion, Transnet BW, 50hertz, 2022. Präqualifikationsverfahren für Regelreserveanbieter (FCR, aFRR, mFRR) in Deutschland ("PQ-Bedingungen"). [WWW Document]. URL https://www.regelleistung.net/xspproxy/api/staticfiles/regelleistung/pqbedingungen(stand03.0 6.2022).pdf (accessed 25.03.2025).
- Timur Sayfutdinov, Mazhar Ali, Oleg Khamiso, 2020. Alternating direction method of multipliers for the optimal siting, sizing, and technology selection of Li-ion battery storage. [WWW Document]. URL https://www.sciencedirect.com/science/article/pii/S0378779620301942?via%3Dihub
- (accessed 25.03.2025).

  Tobias Reuther, Dr. Christoph Kost, 2024. Kurzstudie: Photovoltaik- und Batteriespeicherzubau in Deutschland Fraunhofer ISE [WWW Document]. Fraunhofer-Inst. Für Solare Energiesysteme ISE. URL
  - https://www.ise.fraunhofer.de/de/veroeffentlichungen/studien/photovoltaik-und-batteriespeicherzubau-in-deutschland.html (accessed 30.11.2024).
- UL Solutions, 2024. HOMER Hybrid Renewable and Distributed Generation System Design Software [WWW Document]. URL https://homerenergy.com/ (accessed 13.02.2025).
- Westnetz GmbH, 2024a. Netzentgelte Strom [WWW Document]. URL https://www.westnetz.de/de/ueber-westnetz/unser-netz/netzentgelte-strom.html (accessed 09.11.2024).
- Westnetz GmbH, 2024b. Netzentgelte Strom 2024 Preisblatt [WWW Document]. URL https://www.westnetz.de/content/dam/revu-global/westnetz/documents/ueber-westnetz/unsernetz/netzentgelte-strom/preisblaetter-westnetz-strom-01-01-2024.pdf (accessed 26.03.2025).
- Zheng, Y., Wu, H., Yi, W., Lai, X., Dai, H., Han, X., Ouyang, M., 2020. A novel classification method of commercial lithium-ion battery cells based on fast and economic detection of self-discharge rate. J. Power Sources 478, 229039. https://doi.org/10.1016/j.jpowsour.2020.229039 (accessed 25.03.2025).

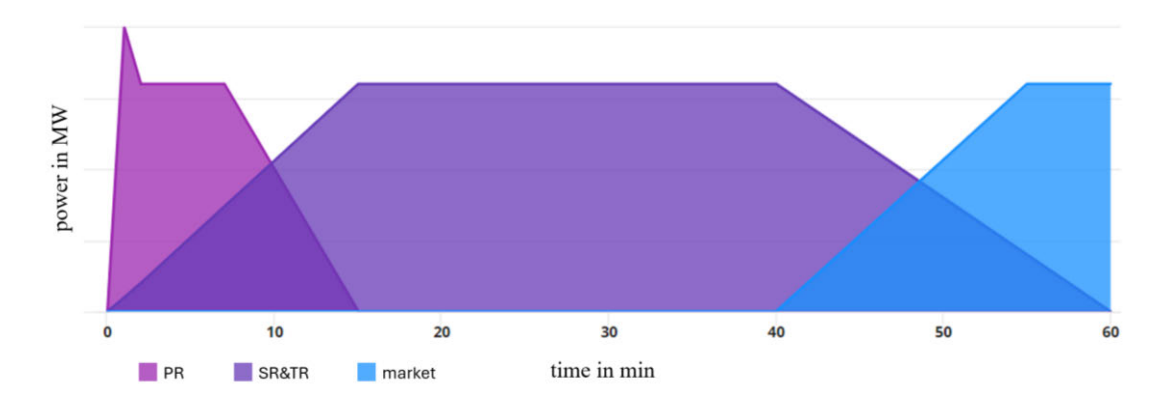
# Appendix

# Appendix Table of Contents

Appendix 1 A	ctivation of Reserve Power	III
	xample Revenue of a BESS Using the Cross-Market Strategy	
	traday Market Volatility	
	verage Quarter-Hourly Intraday Market Prices Monthly Corrected	
	ourly Dependency of Volatilities of Intraday Market Prices	
	Ionthly Dependency of Intraday Market Prices	
Appendix 7 L	ong-term Development of Intraday Market Prices	VI
Appendix 8 L	ong-term Development of Activated PR-Power	VI
	ong-term Development of Tendered and Activated SR Power	
Appendix 10 l	Long-term Development of SR Energy Prices	VII
Appendix 11 l	Long-term Development of SR Power Prices	VIII
Appendix 12 l	Influence of C-rate on Capacity Degradation of LFP Cells	VIII
Appendix 13 l	Power Degradation of the BESS dependent on the Number of Cycles and Do	DDIX
Appendix 14	CAPEX Components for LFP in 2020 for Different Power and Capacity I the Battery	•
Appendix 15	CAPEX Comparison of NMC and LFP Price Components in 2020 for Diffund Capacity Layouts of the Battery	
Appendix 16	Development of Maximum Power-Dependent Grid Fee for MV connection	
Appendix 17	Germanys Electricity Market Prices of Intraday and Day Ahead Market in	_
Appendix 18 (	Capacity Reserve PR Market Dependent on Storage Hours and SOC	XII
Appendix 19 l	Historical Negative Day-Ahead Market Price Periods in Germany	XII
Appendix 20 I	Forecast Battery Storage Installed Power in Germany	XIII
Appendix 21 l	Development of GO Curtailments for RES in Germany	XIII
Appendix 22 l	Forecast Operation of BESS in Germany in July 2045	XIV
Appendix 23 l	Forecast Germanys Electricity Generation for different Technologies	XV
Appendix 24 l	Forecast of Energy-Dependent Grid Fees for MV Connection for BESS	XV
Appendix 25	Time-dependent Volatility Development of Primary Reserve Prices	XVI
Appendix 26 l	Idling and Cycling Degradation of an NMC Cel	XVII
Appendix 27 l	Forecast Primary Reserve Prices Example for Simulation	XVII
Appendix 28	Time-dependent Volatility Development of Intraday Prices with Increase Participants	
Appendix 29 l	Historical Monthly Production Outages of German Wind- and PV-Plants	XIX
Appendix 30 l	Forecast Outage Time Series of RES and BESS for Simulation	XX
Appendix 31 l	Forecast Monthly Distribution of GO Curtailments in Germany in 2045	XXI
Appendix 32 l	Maps of Positive and Negative Redispatch Energy in Germany in 2021	XXI
Appendix 33 I	Prognosis of PR Tendered Power in Germany - Example Periods	XXII

XXII
XXIII
XXIII
XXIII
XXIV
XXIV
XXV
t XXV
XXVI
g XVII
XVII
XXX

Appendix 1 Activation of Reserve Power



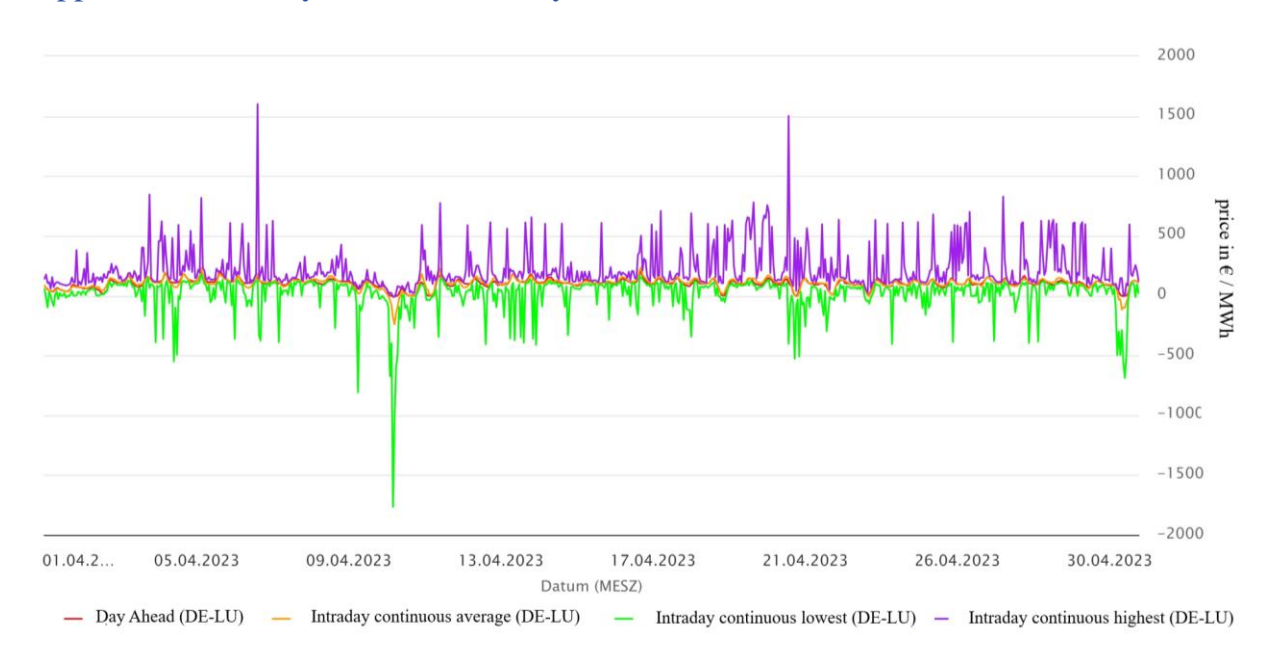
To stabilize a frequency deviation, reserve power is activated. PR is utilized within the first 15 min minutes of a frequency deviation, followed by SR, and subsequently TR for up to one hour. Finally, the frequency deviation is balanced by the balance responsible party through trading on the electricity markets (50hertz et al., 2024c).

Appendix 2 Example Revenue of a BESS Using the Cross-Market Strategy



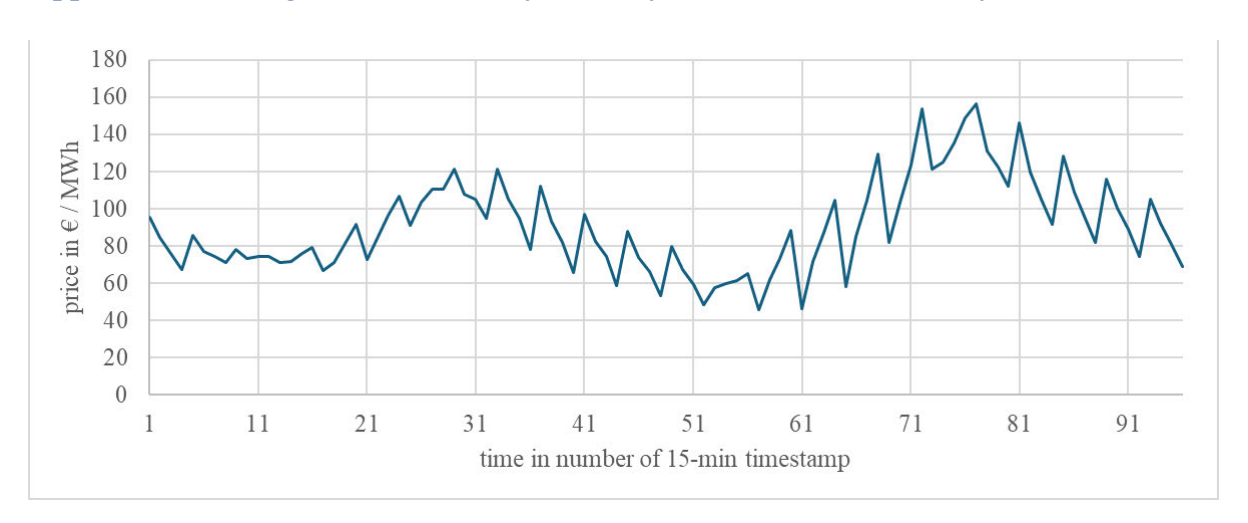
The potential annualized revenue in  $k \in MW$  of a 2-hour BESS with a maximum of 2 cycles per day, 100% DOD and 90% system-RTE in Germany in 2024 is presented (Christian Schäfer, 2024). Different markets and market combinations were investigated. The maximum revenue is achieved through a combination of different markets (black graph). If trading were limited to a single market, such as the PR market (light blue graph), the revenue during the example period would be only half as high (Christian Schäfer, 2024).

#### Appendix 3 Intraday Market Volatility



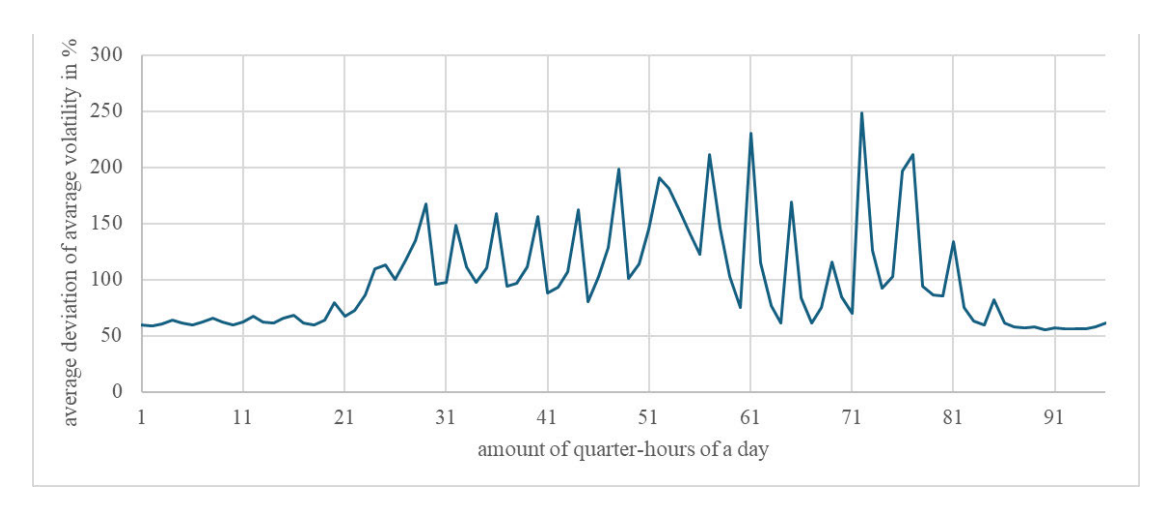
Trading on the Intraday market is conducted based on the pay-as-bid principle (Koch, 2021:409). In addition to the average price of the 15-minute auction, minima and maxima (green and purple graphs) are also observable. For example, on April 6, 2023, these could briefly deviate up to 883 % from the average (orange graph). This significantly increases the volatility of the Intraday market prices (Fraunhofer ISE, 2024).

Appendix 4 Average Quarter-Hourly Intraday Market Prices Monthly Corrected



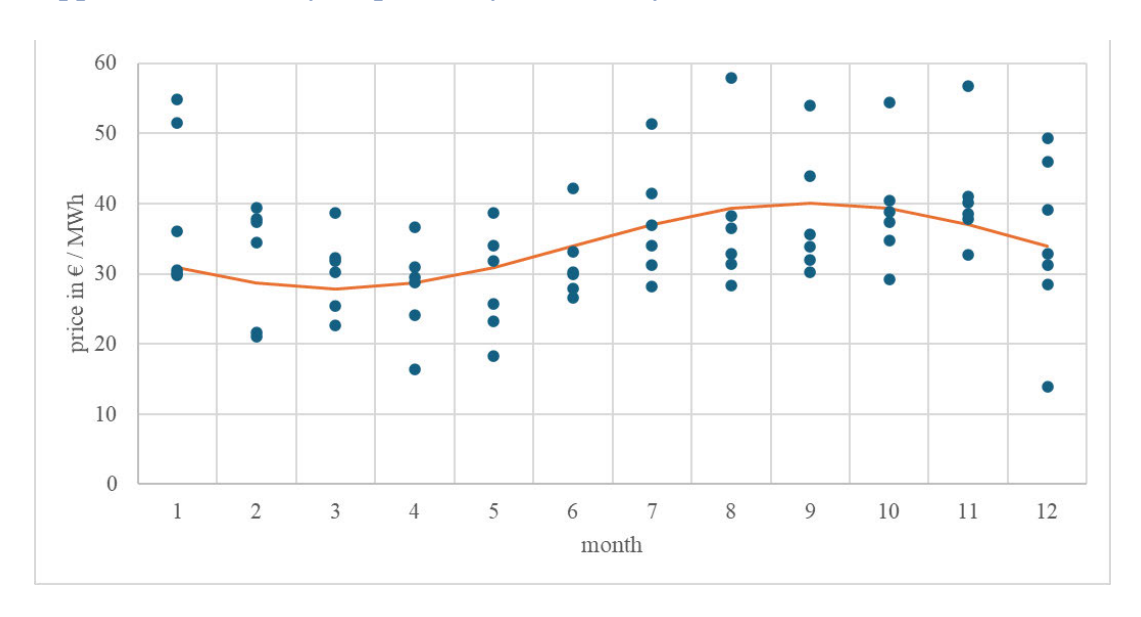
After correction of the monthly variation of the Intraday market prices, all market prices are comparable with each other regardless of the month. The mean price per time of day can now be determined in quarter-hourly resolution in the unit  $\epsilon$ /MWh, which is shown in the diagram. These values would be approximately valid for the month of June, for example, as June in <u>Appendix 6</u> has approximately the mean value of the balancing function. For all other months, the calculated time-dependent prices must be corrected using the monthly adjustment function from <u>Appendix 6</u> (own Figure).

Appendix 5 Hourly Dependency of Volatilities of Intraday Market Prices



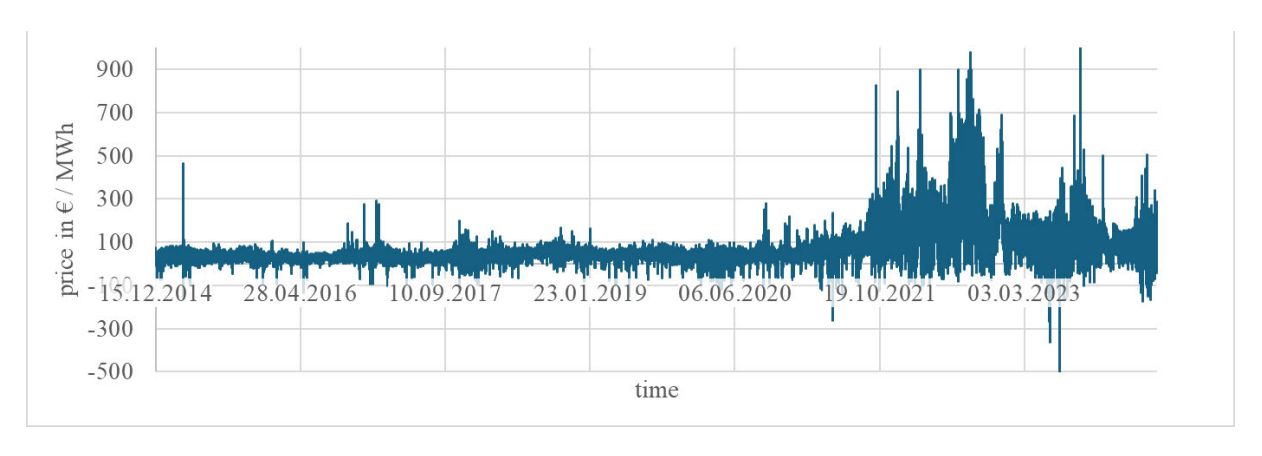
The quarter-hourly volatilities are determined by formular (18) with g=1. The means of the quarter-hourly volatilities are expressed as a percentage relative to the mean of all volatilities. A value of 100 % on the y-axis indicates that the quarter-hourly volatility does not differ from the daily mean. During the day, volatility is elevated, whereas at night, fewer deviations from the average price are expected. The jagged pattern is due to the hourly bids on the Day-Ahead market, which are balanced on the Intraday Market. As the Intraday market trades in 15-minute resolution, a maximum occurs every four values. (European Energy Exchange AG, 2024).

#### Appendix 6 Monthly Dependency of Intraday Market Prices



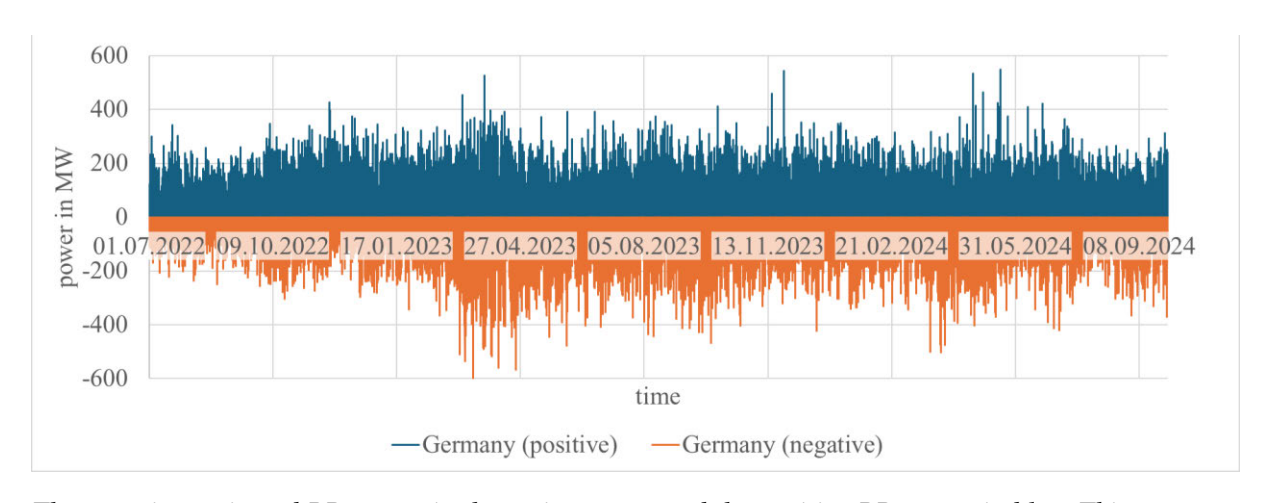
The Intraday market prices of various years are represented as monthly average prices in the form of blue dots. A sinusoidal fitting function with an amplitude of 18 % was determined. In April, the Intraday market price is lower than in September (European Energy Exchange AG, 2024).

Appendix 7 Long-term Development of Intraday Market Prices



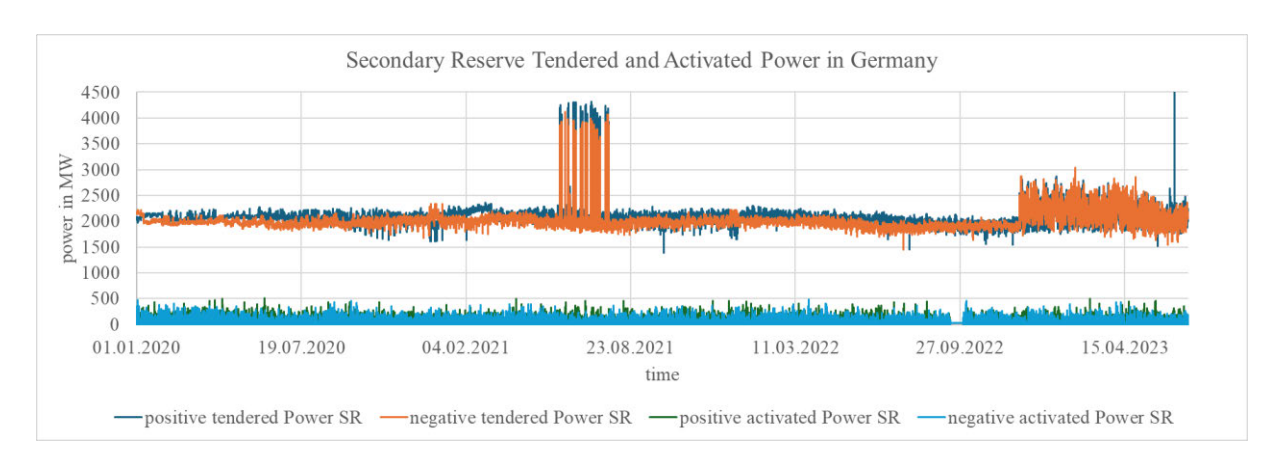
The Intraday market shows a sharp increase in the average price and volatility since October 2021. In 2024, the market has already stabilized but is on a significantly higher price level than before 2021. Before 2021, the average price was around  $35 \in /MWh$ , currently at  $70 \in /MWh$  (European Energy Exchange AG, 2024).

#### Appendix 8 Long-term Development of Activated PR-Power



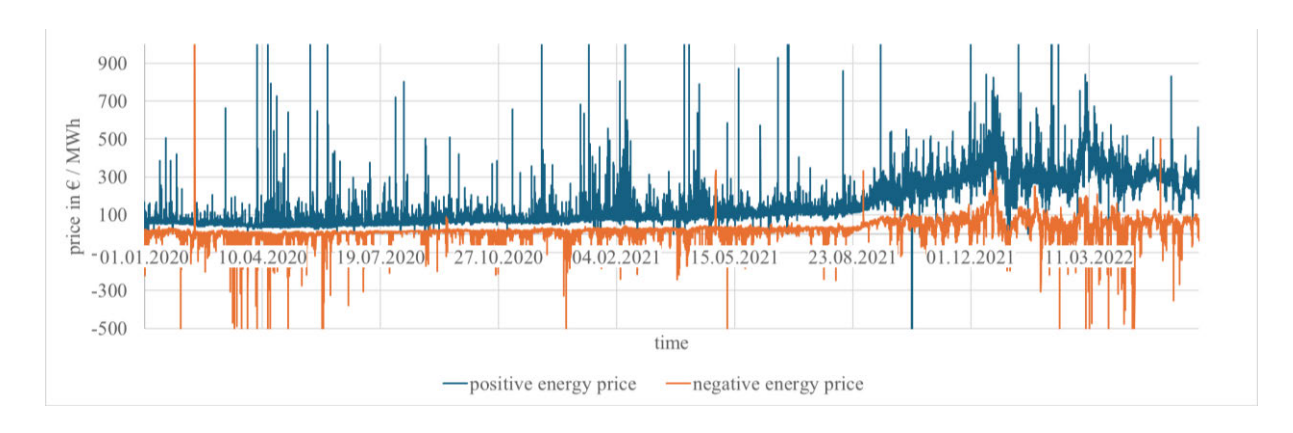
The negative activated PR power is shown in orange and the positive PR power in blue. This averages 34 MW for both positive and negative PR but is highly volatile. From 2022 to 2024, the activated PR power decreased by around 9 % per year (50hertz et al., 2024b).

#### Appendix 9 Long-term Development of Tendered and Activated SR Power



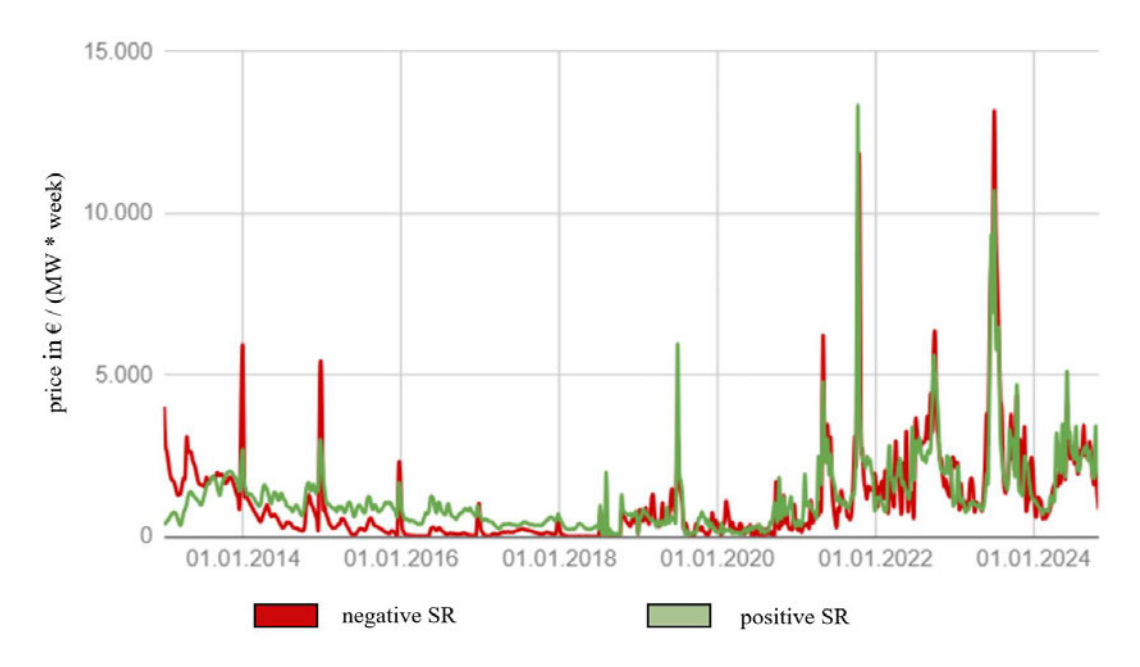
The development of the positive and negative tendered power of SR is shown in dark blue and orange and that of the activated power in light blue and green. The activated power has remained largely constant historically. In July 2021, there were short-term sharp increases in the tendered powers, which could be due to the decommissioning of conventional power plants (Bundesnetzagentur, 2024e). From December 2022, the volatility in tendering powers increased significantly, which is due to the conversion of the European balancing energy market structure (Benjamin Blat Belmonte et al., 2023:915). The activation probabilities of positive and negative SR have decreased by around 0.05 percentage points per year during the analysis period (own Figure, data from: Bundesnetzagentur, 2024b).

#### Appendix 10 Long-term Development of SR Energy Prices



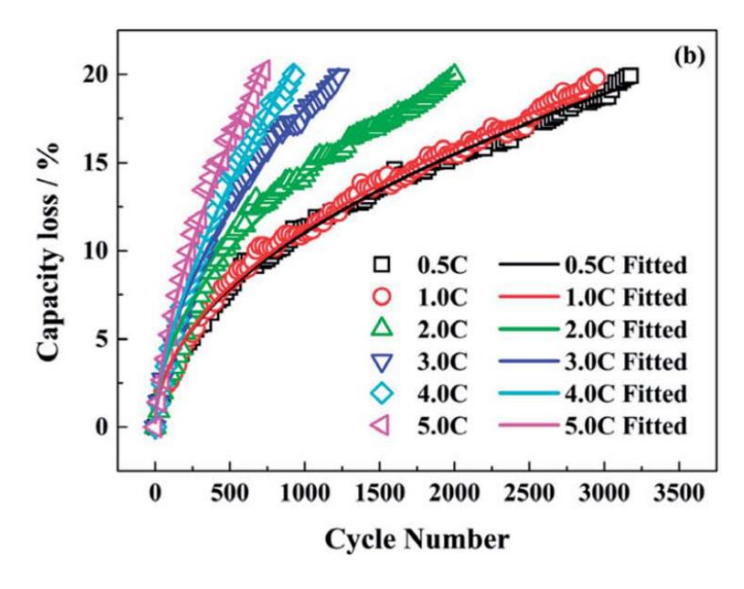
The energy price development of positive SR in  $\epsilon$  / MWh is shown in blue and that of negative SR in orange. Prices have risen sharply since 2021, especially for positive SR. The volatility has increased significantly. The average prices for positive SR of 296  $\frac{\epsilon}{MWh}$  in the years 2021 to 2022 are significantly higher than those of the Intraday market. The average price for negative SR is 62  $\frac{\epsilon}{MWh}$ . The operator of the BESS must pay money to charge the BESS at negative prices from SR (Bundesnetzagentur, 2024b).

Appendix 11 Long-term Development of SR Power Prices



The development of the power prices of positive SR is shown in green and negative SR in red. Similar to PR, an increase in the average price and volatility can be seen from 2021 onwards. Positive and negative SR have undergone a very similar development since 2019. The price has leveled off at circa  $2,500 \frac{\epsilon}{MW \cdot week}$ , which is a significantly higher price level than between 2015 and 2019 (Christian Schäfer, 2024).

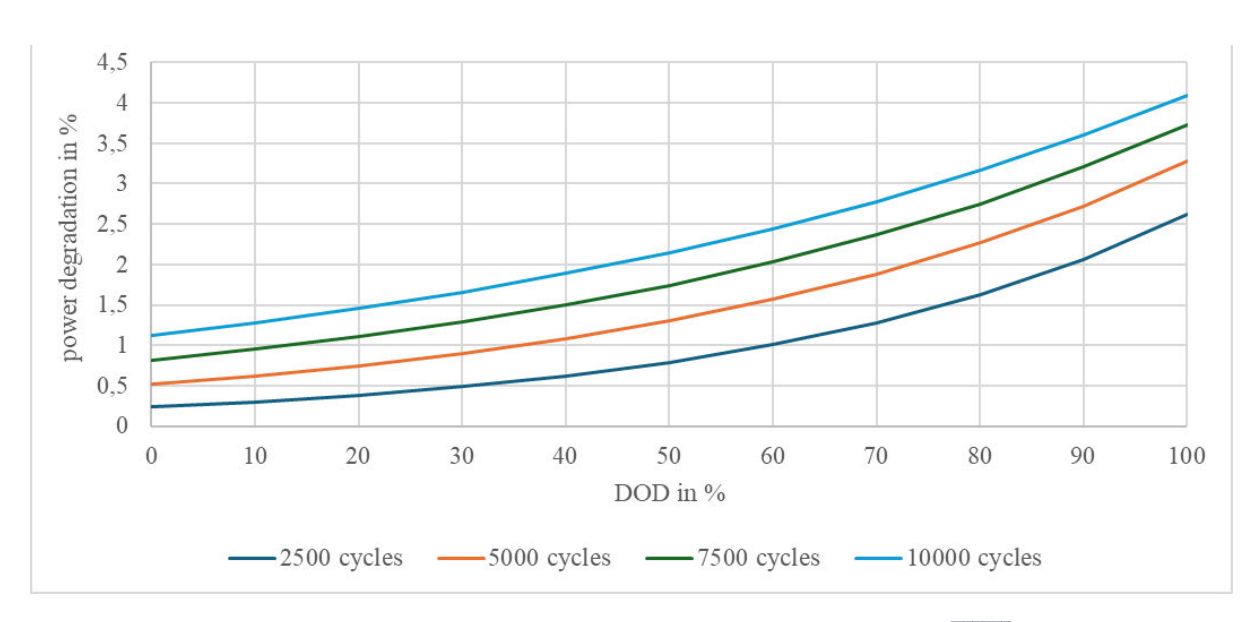
Appendix 12 Influence of C-rate on Capacity Degradation of LFP Cells



The influence of the C-rate on  $\delta_{cyc}$  of LFP cells is shown. The number of cycles are plotted against percentage capacity losses. The C-rate significantly impacts  $\delta_{cyc}$  for C-rates greater than 1, but since operations assume C-rates of  $\leq 1$ , the effect of the C-rate on  $\delta_{cyc}$  is neglected. This is shown by comparing the red curve to the black one (Sun et al., 2018:25697).

Appendix 13 Power Degradation of the BESS dependent on the Number of Cycles and

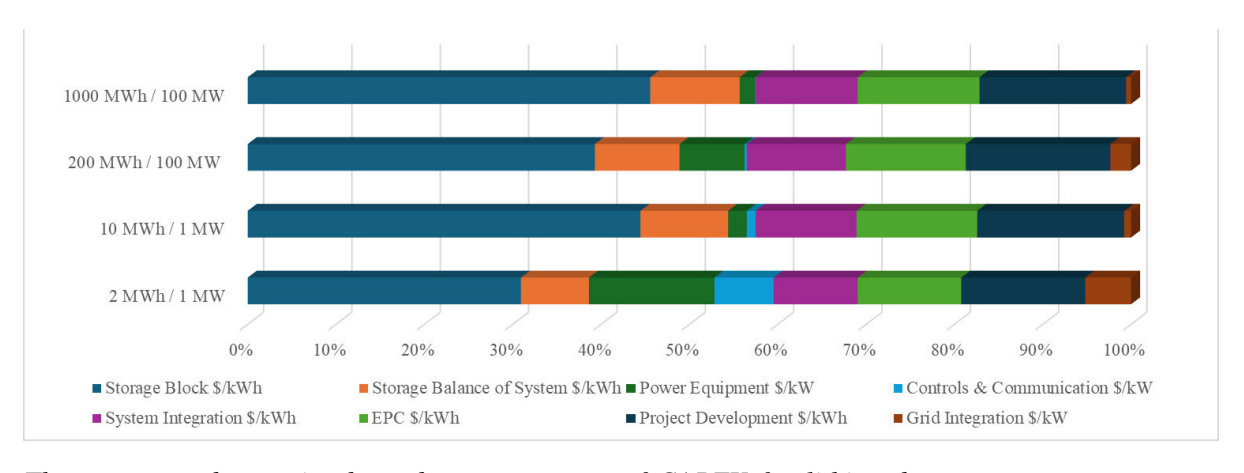
#### DOD



The power degradation of LFP in percentage relative to  $P_N$  as a function of  $\overline{DOD}$  and the number of cycles at a temperature of 20 °C is illustrated. As the DOD increases, power degradation rises exponentially, whereas the increase in power degradation with a rising number of cycles is approximately linear (own Figure, values from: (Swierczynski et al., 2015:3457))

Appendix 14 CAPEX Components for LFP in 2020 for Different Power and Capacity

#### Layouts of the Battery

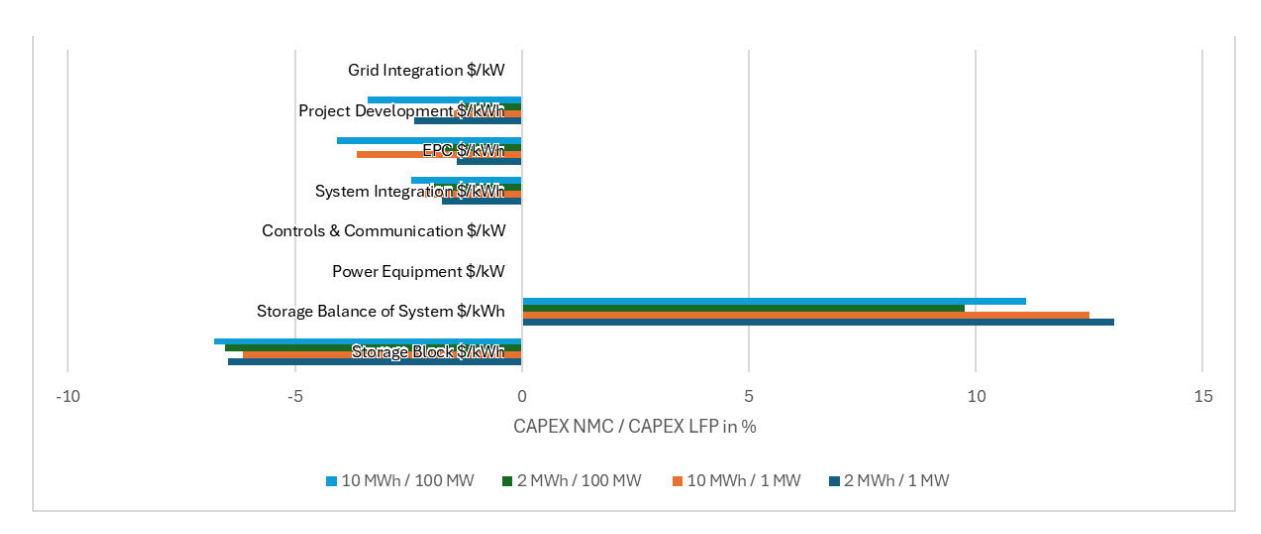


The power- and capacity-dependent components of CAPEX for lithium battery storage systems are shown, using LFP BESS as an example for the year 2020. Batteries with varying capacities and power levels are analyzed regarding their percentage contribution to total CAPEX. The components are color-coded below the graph, and their units indicate whether they are energy- or power-dependent cost components. Each component was calculated using the specific capacity- and power-dependent costs based on Formular (12). The absolute CAPEX for the systems under consideration vary significantly.

They were converted to euros using the formula (14). This results in 544 k $\in$  for a 1 MW / 2 MWh storage system, 3.7 M $\in$  for a 1 MW / 10 MWh storage system, 77.8 M $\in$  for a 100 MW / 2 MWh storage system, and 323.5 M $\in$  for a 100 MW / 10 MWh storage system. The cost components also vary: The costs of the storage block always account for the largest share. With increasing capacity or power installation for storage hours > 1, the proportion of power-related costs decreases (own Figure, based on: Mongird et al., 2020:87.f).

Appendix 15 CAPEX Comparison of NMC and LFP Price Components in 2020 for

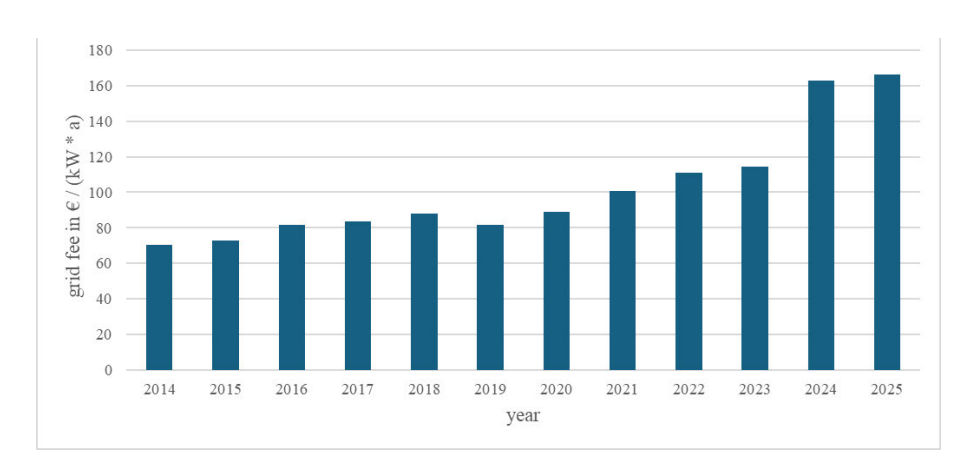
Different Power and Capacity Layouts of the Battery



NMC and LFP CAPEX are compared for different CAPEX components on the y-axis and different system sizes of installed capacity and power, shown in different colors. A positive percentage cost ratio indicates a cost advantage for NMC compared to LFP. It can be observed that only the capacity-dependent CAPEX change slightly, with BOS and battery block costs showing the largest variation of up to 13 %. The capacity-dependent CAPEX of LFP are lower than NMC for each component except BOS costs. The power-dependent CAPEX are assumed to be technology-independent (own Figure, based on: Mongird et al., 2020:87.ff).

#### Appendix 16 Development of Maximum Power-Dependent Grid Fee for MV

#### connection of BESS



The development of maximum power-dependent grid fees in  $\frac{\epsilon}{kW \cdot a}$  of BESS with medium-voltage connection is shown. 'Maximum' refers to a grid utilization factor of 1 according to Formula (15)(16). The grid fees from the published rate sheets of the grid operator Westnetz GmbH were investigated. Over the past 10 years, power-dependent grid fees have approximately doubled. Since 2019, there has been a strong increase in grid fees, attributed to grid expansion resulting from the integration of RES. The power-dependent grid fees differ only minimally between the possible voltage levels of the BESS grid connection (Westnetz GmbH, 2024a). In addition to medium voltage, high-voltage grid connections with transformation to medium voltage and high-voltage connection are also possible for BESS (own Figure, data source: (Westnetz GmbH, 2024a)).

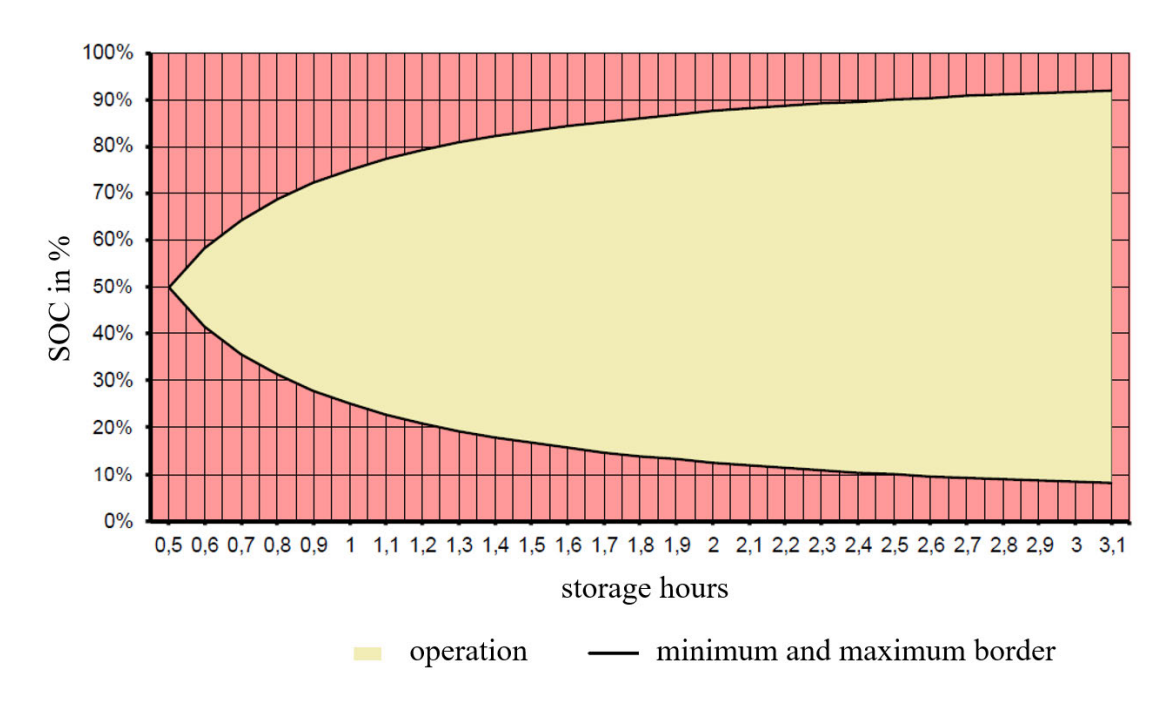
Appendix 17 Germanys Electricity Market Prices of Intraday and Day Ahead Market

in April 2023



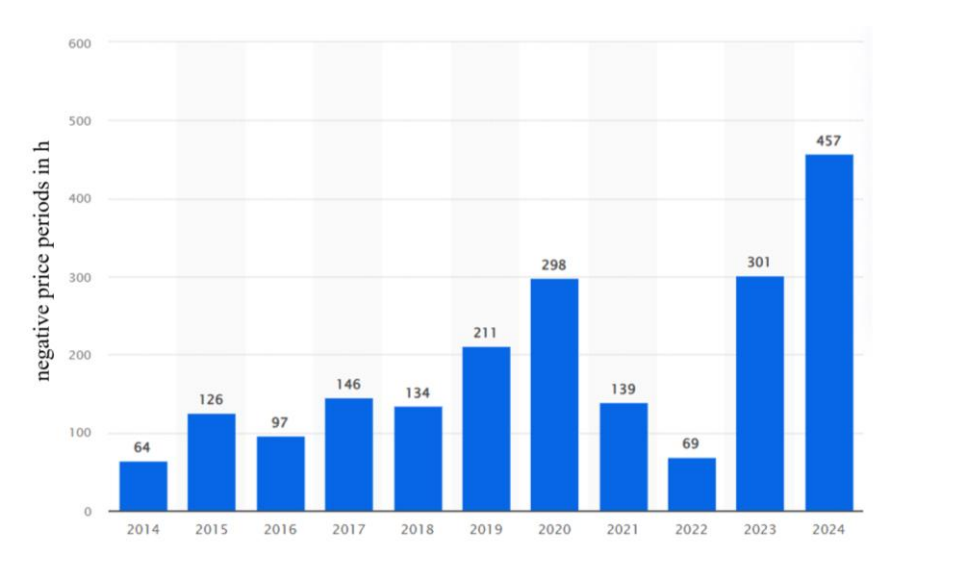
The Day-Ahead and Intraday market prices in € / MWh are presented as continuous average prices for April 2023. Although the average prices of the Day-Ahead and Intraday auctions are approaching each other, greater volatility is noticeable in Intraday trading (Christian Schäfer, 2024)(Fraunhofer ISE, 2024).

Appendix 18 Capacity Reserve PR Market Dependent on Storage Hours and SOC



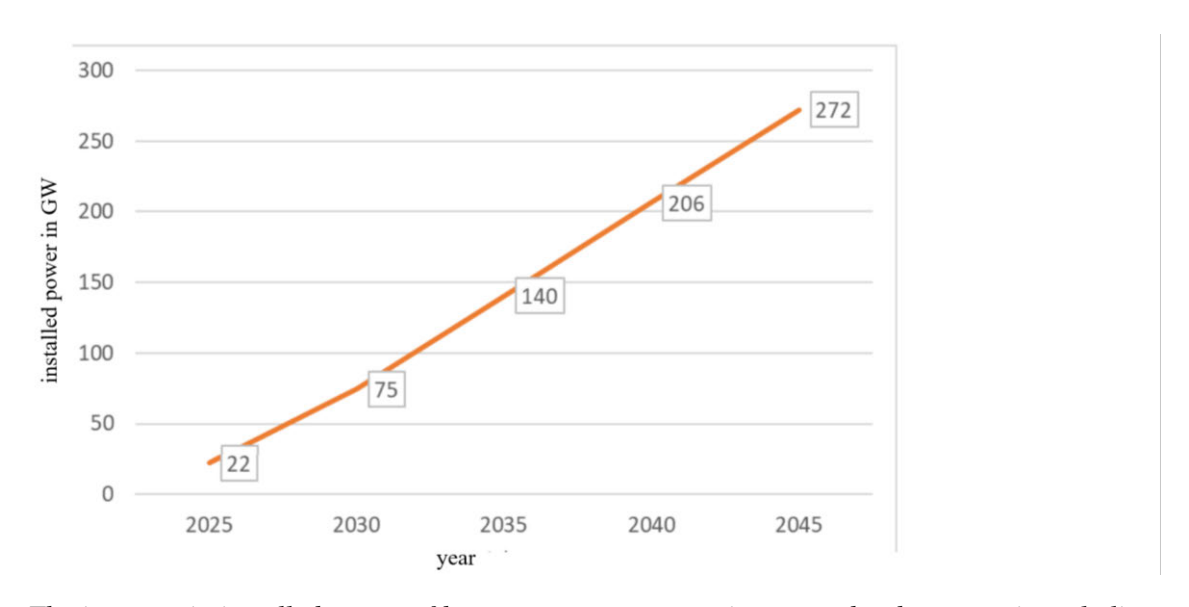
A BESS may participate in the PR market if it is operated in the yellow area of the diagram. Operation depends on the SOC and the storage hours (formular (13). For example, a symmetrically prequalified 1 MW and 0.5 MW storage facility could only participate in the PR market with SOC = 50 % according to the diagram. However, there are other additional requirements for market participation that increase the minimum requirement for  $Q_N$ . For example, the working capacity of a previous activation and the delayed effect of storage management measures are considered. This increases the minimum capacity for the 1 MW storage facility to 0.83 MWh (Tennet et al., 2022:64.ff).

Appendix 19 Historical Negative Day-Ahead Market Price Periods in Germany



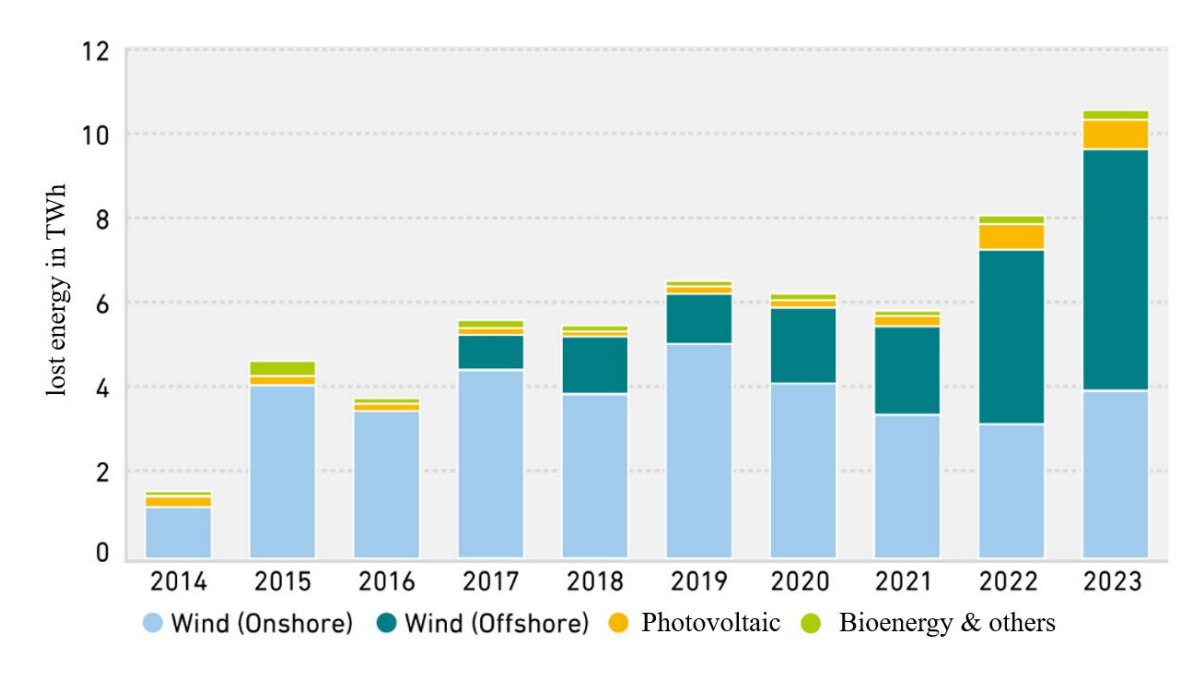
The amount of negative electricity price periods on the German Day-Ahead market fluctuates annually, but has reached record levels in the past two years. The trend of negative electricity price periods is increasing (Statista, 2025).

Appendix 20 Forecast Battery Storage Installed Power in Germany



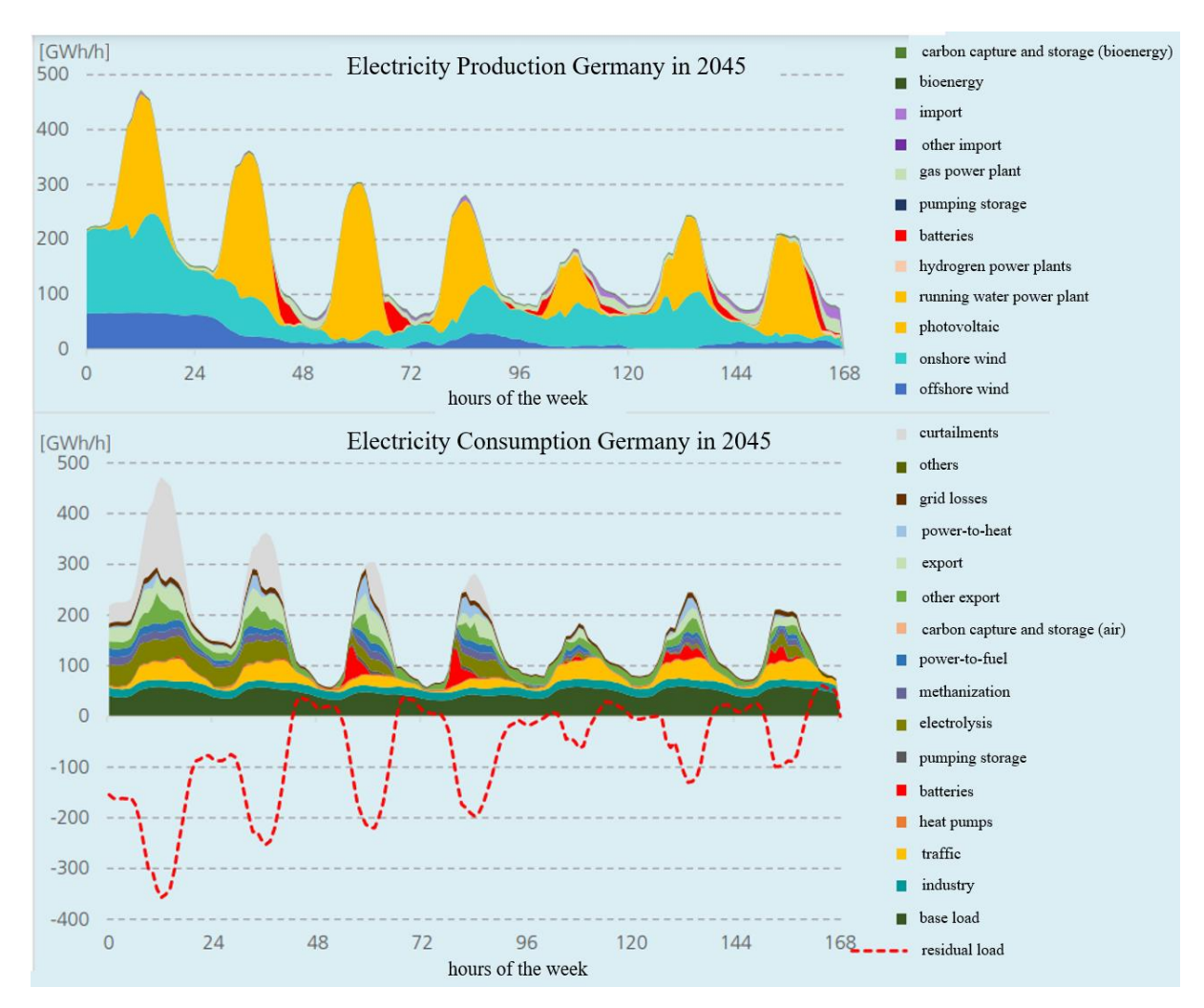
The increase in installed power of battery storage systems is assumed to be approximately linear with an installation rate of around 13.2 GW per year. In 2045, the installed power of battery storage systems is expected to amount to 272 GW with a capacity of 544 GWh (Fraunhofer ISI et al., 2024:28).

Appendix 21 Development of GO Curtailments for RES in Germany



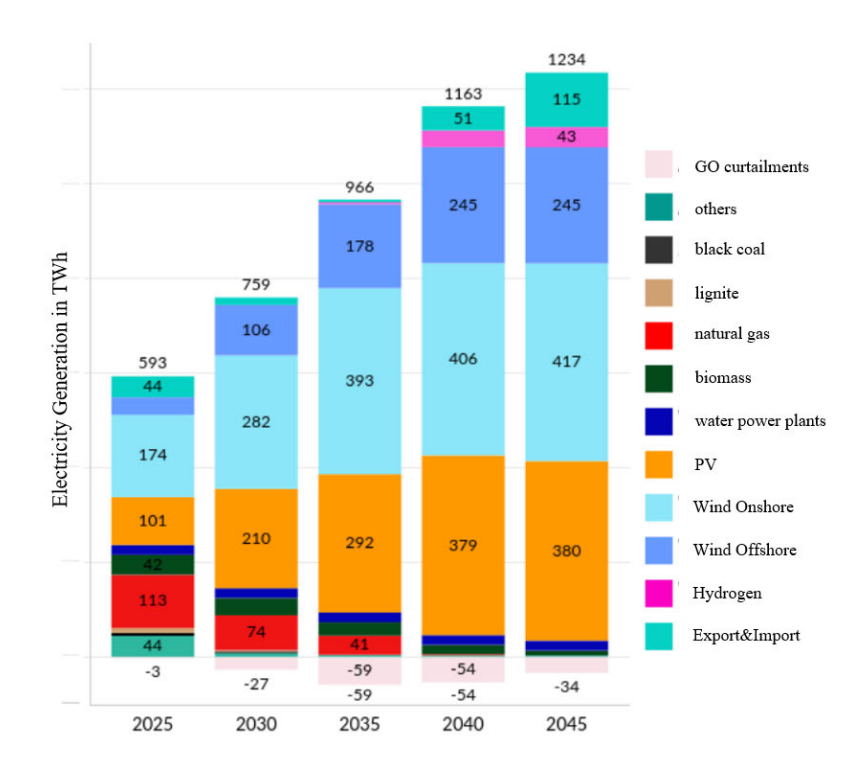
The development of curtailments in TWh by the grid operators for different types of RES over the years is shown. A significant increase is evident: over nine years, the curtailed energy volumes have increased approximately fivefold. While onshore wind energy curtailments have remained relatively stable over the past nine years, PV and offshore wind energy curtailments have shown a sharp increase in recent years (Agentur für Erneuerbare Energien, 2024).

Appendix 22 Forecast Operation of BESS in Germany in July 2045



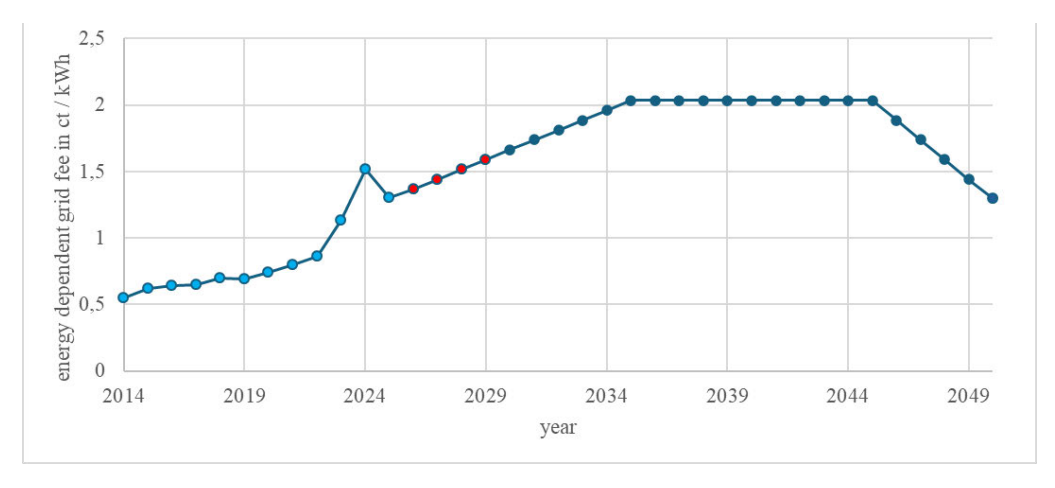
The projected electricity production and usage in Germany during a week in July 2045 is forecasted. Large production peaks occur at midday on cloudless days, necessitating renewable energy curtailments, indicated in grey. Significantly less curtailment is expected during winter (Connor Thelen et al., 2024:56). The forecast shows the operation of battery storage systems in 2045: on sunny days in summer, battery storage systems are expected to be charged in the morning or at noon and discharged in the evening. If the energy produced from renewable sources is low, battery storage systems will also be discharged during the day to cover the energy demand (Connor Thelen et al., 2024:58).

Appendix 23 Forecast Germanys Electricity Generation for different Technologies



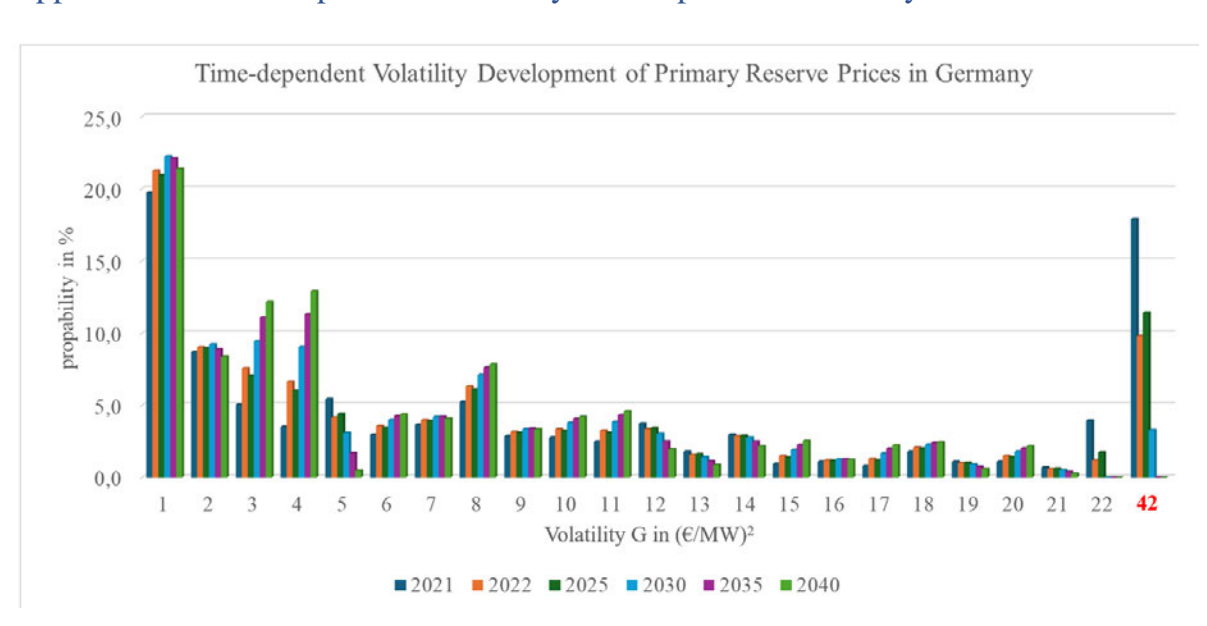
Germanys electricity generation in TWh is forecasted for different technologies. GO curtailment volumes of 59 TWh could be possible in 2035, decreasing to 34 TWh by 2045 in a 100 % renewable energy system. However, the study highlights that with accelerated PV expansion, GO curtailments could reach up to 199 TWh annually by 2045 (Fraunhofer ISI et al., 2024:32), corresponding to 14 % of Germany's total electricity production. This demonstrates significant forecasting uncertainty. Given that GOs anticipate a PV capacity of 453 GW by 2045 (BDEW, 2023), it is assumed that curtailments of RES will far exceed 34 TWh in 2045 (Fraunhofer ISI et al., 2024:15).

Appendix 24 Forecast of Energy-Dependent Grid Fees for MV Connection for BESS



The historical development of energy-dependent grid fees in ct / kWh from GO Westnetz for MV connection are visualized in light blue. Forecast values for linear extrapolation are represented in red and dark blue. For installations commencing from 2030 onwards, all dark blue values are applicable,

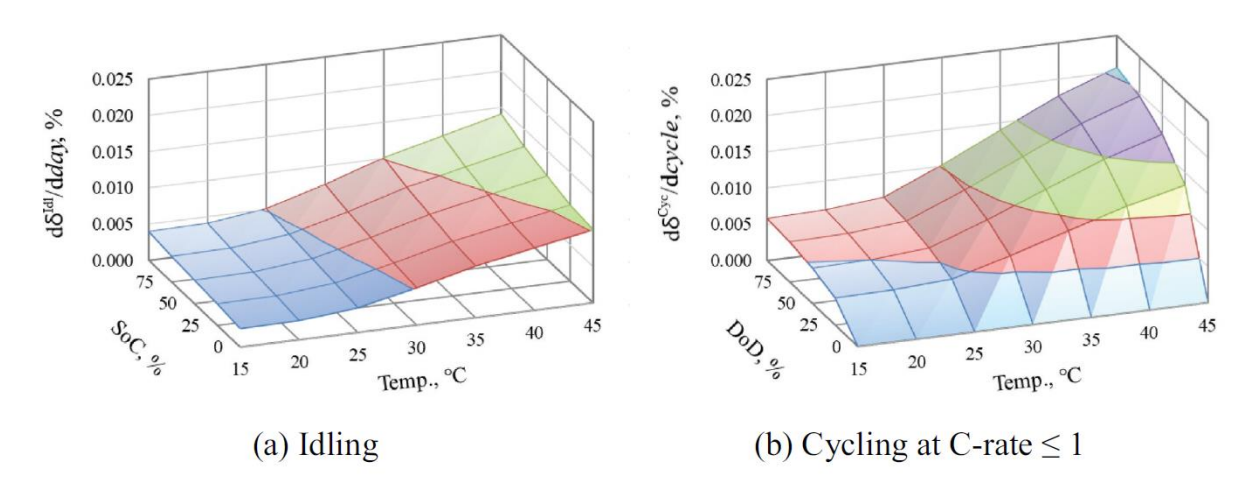
whereas for installations before 2030, the red and dark blue values could be relevant, depending on the commissioning date. An exemption from ernergy-dependent grid fees for BESS applies for 20 years until commissioning before 2030. To incorporate the special regulation on the waiver of energy-dependent grid fees, the projected energy-dependent grid fees for BESS are presented as an annual matrix in the Excel file. Rows in the Excel matrix denote the commissioning year, while columns represent the years post-commissioning. The values provided apply exclusively to MV connections. Compared to connections of higher voltage levels, energy-dependent grid fees average approximately 25% of those at medium voltage. High-voltage and high-voltage with transformation to medium voltage behave similarly. If MV connection is not used, users must adjust the values in the Excel matrix. For instance, in the case of a high-voltage connection, the simplest adjustment would be to multiply all values by a factor of 0.25 (Westnetz GmbH, 2024a).



Appendix 25 Time-dependent Volatility Development of Primary Reserve Prices

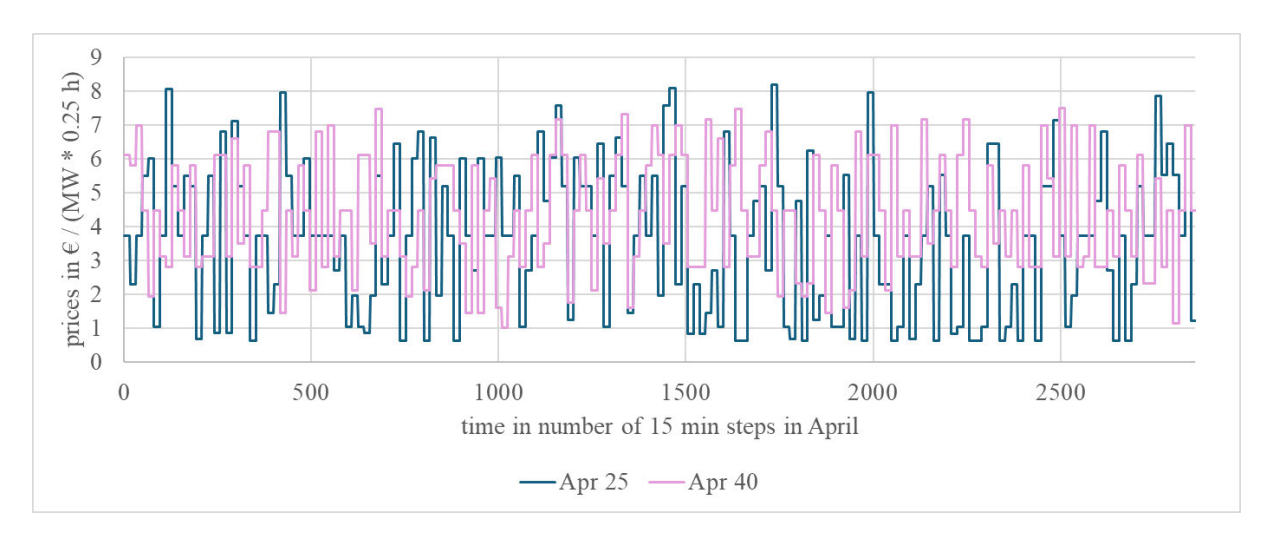
The deviations of the PR market prices from the mean value are shown in the form of volatility G according to formula (18) expressed in intervals on the x-axis. The factor g of the formula (18) is 1. The volatility equals the interval numbers except the last interval. The last interval summarizes all G(t) > 22 and is indicated by the mean value 42. Based on historical data, the histograms of G were created for the years 2021 in dark blue and 2022 in orange. The data was then extrapolated linearly by assuming the probability changes of the years 2021 and 2022 for each interval for a 5-year period. A stabilization of the market can be observed through an increase in lower G(t) and a decrease in higher G(t) (own Figure).

## Appendix 26 Idling and Cycling Degradation of an NMC Cel



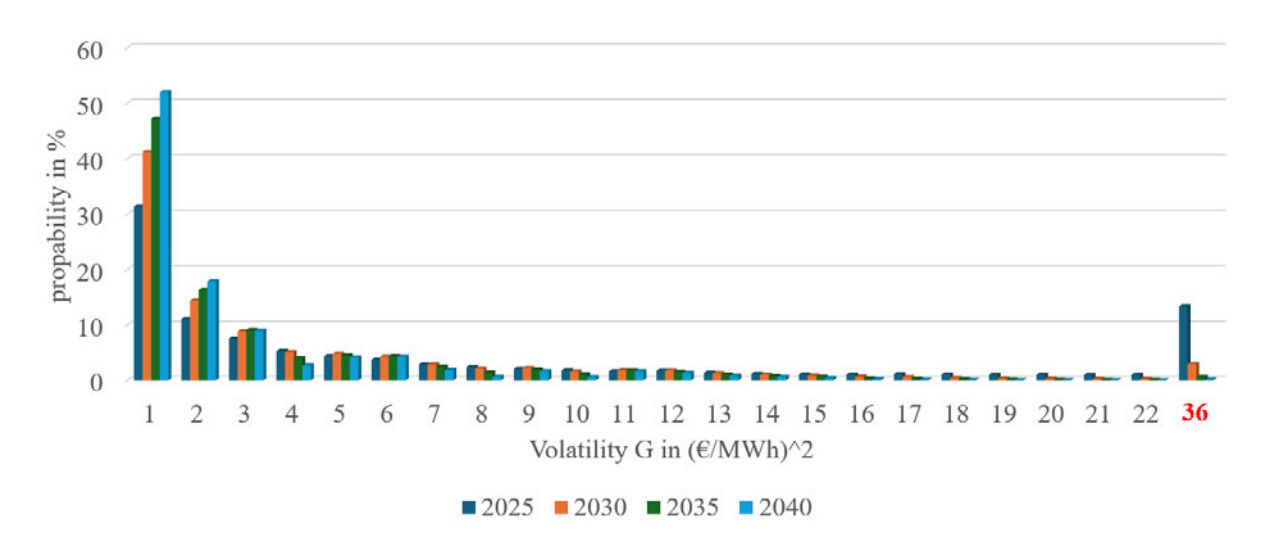
The idling and cycling degradation per day (a) and per cycle (b) is illustrated for NMC battery cells. Degradation effects are dependent on temperature, SOC and DOD. Temperature has the most significant impact on both types of degradation, with sharp degradation increases at temperatures above 25 °C (Timur Sayfutdinov et al., 2020:3).

#### Appendix 27 Forecast Primary Reserve Prices Example for Simulation



The PR market forecasts for April 2025 and are shown in the diagram. The mean value increases from  $3.65 \frac{\varepsilon}{MW \cdot 0.25 \, h}$  in 2025 to  $4.35 \frac{\varepsilon}{MW \cdot 0.25 \, h}$  in 2040. The standard deviation decreases from  $2.1 \frac{\varepsilon}{MW \cdot 0.25 \, h}$  in 2025 to  $1.8 \frac{\varepsilon}{MW \cdot 0.25 \, h}$  in 2040 (own Figure).

Appendix 28 Time-dependent Volatility Development of Intraday Prices with Increase of Arbitrage Participants

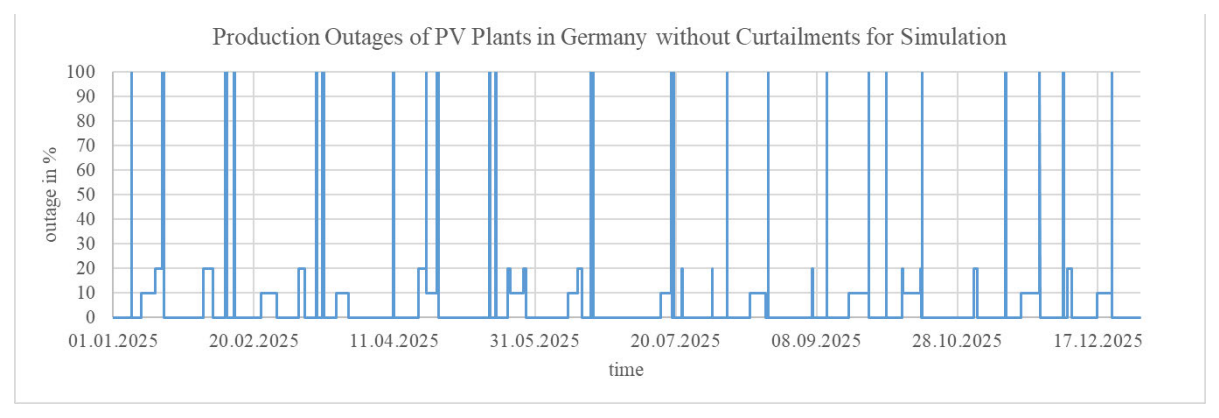


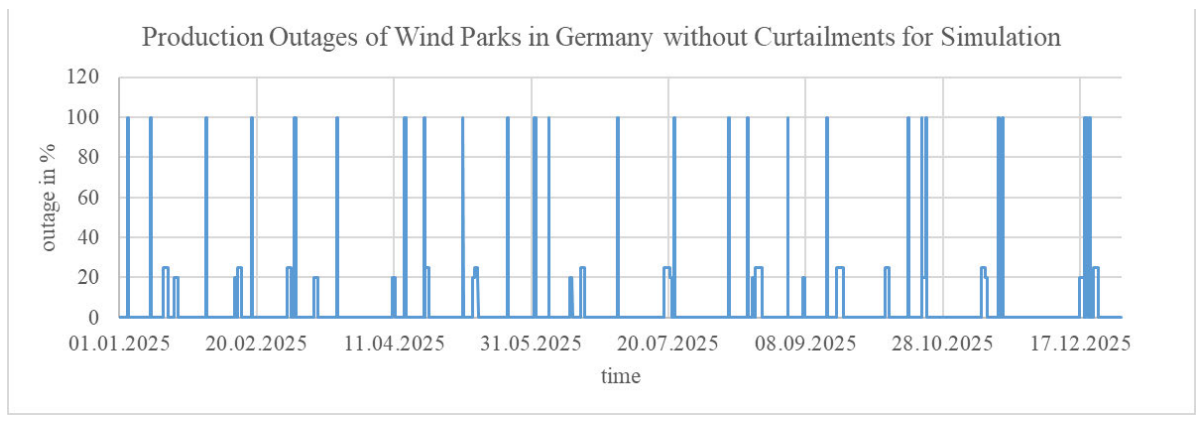
Using the method of chapter 3.4.1, the volatility G was divided into different intervals for the analysis of the Intraday Market and extrapolated linearly for each interval. After normalization to 100 %, all volatilities G > 10 are reduced manually to show the increase in BESS market competition. A stabilization of the market can be seen due to the increase in probability of lower volatility intervals (own Figure).

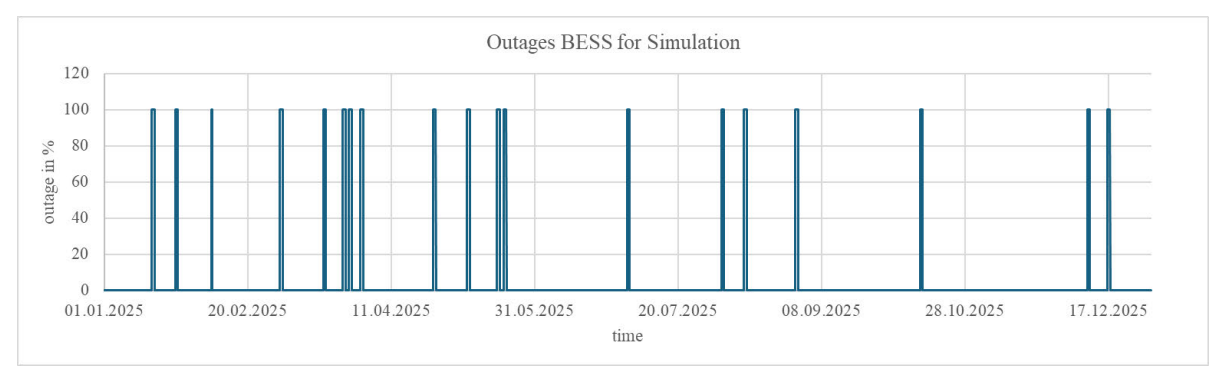
opendix 29 Histor	rical Monthly Produ	ction Outages of	German Wind- a	and PV-Plant
	ows monthly production		it 9/ Jaggag way wing	I am and a am

The lower diagram shows monthly production outages in the unit % losses per wind speed corrected planned yield in the years 2021 to 2023 of 29 German wind plants. The upper diagram shows the same for 11 German PV plants with irradiation corrected planned yield. The adjustment of the planned yield is necessary because irradiation and wind speeds vary over time. PV plants show greater seasonal variability, with higher percentage outages in winter and spring due to maintenance and grid outages. For wind plants, technical defects are more common in late summer, but planned shutdowns show no clear monthly trend (own Figures).

# Appendix 30 Forecast Outage Time Series of RES and BESS for Simulation

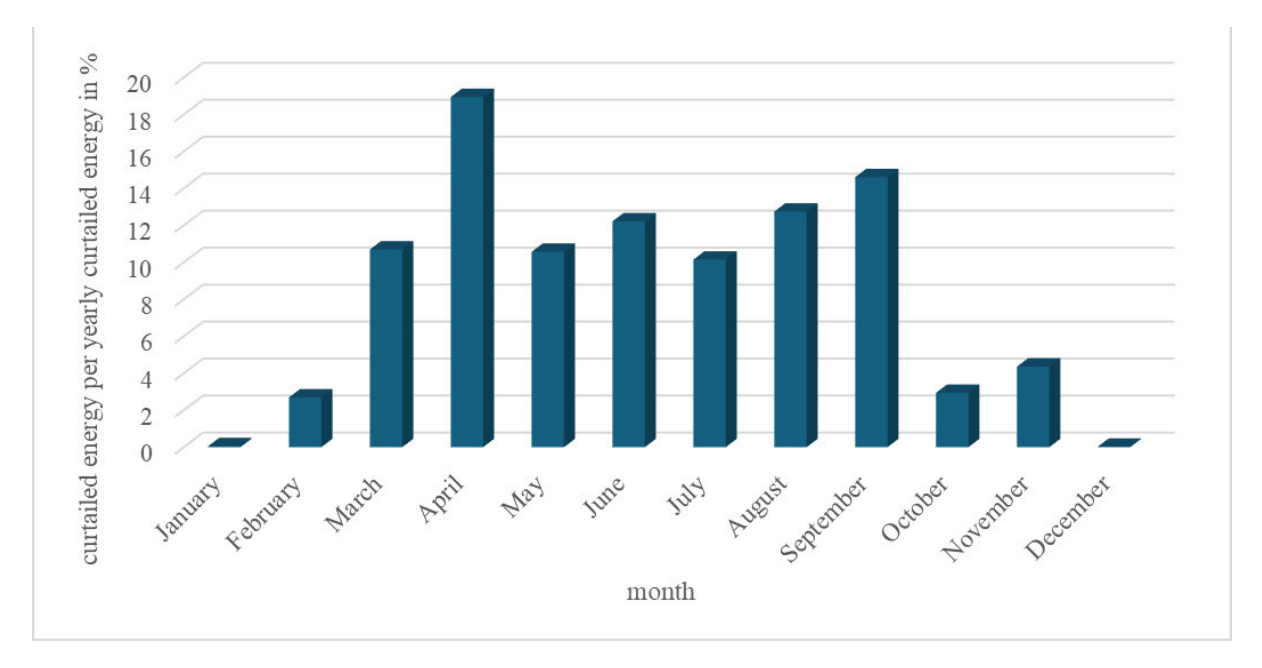






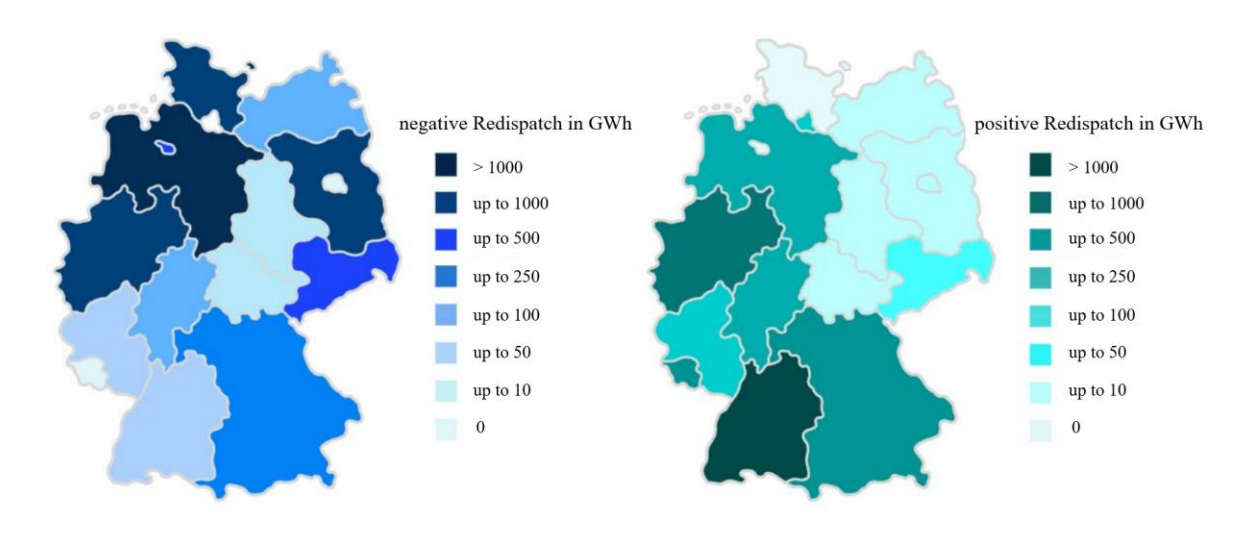
The three figures show predicted production outages in % of total production without curtailments in Germany for RES and BESS in 2025. For the BESS, 5 % of the theoretical annual production is considered as a total outage. For wind and PV, the outage time series are based on historical analysis of <u>Appendix 29</u> (own Figures).

Appendix 31 Forecast Monthly Distribution of GO Curtailments in Germany in 2045

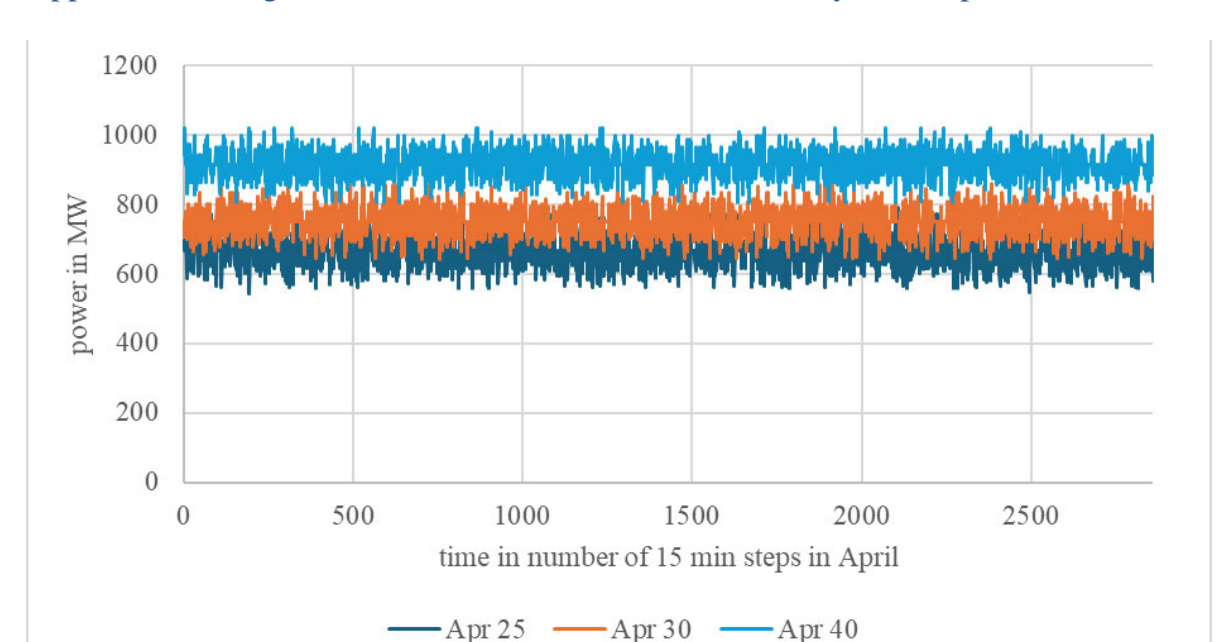


The forecast of monthly distribution of GO curtailments in the unit monthly curtailed energy per yearly curtailed energy in Germany in 2045 is shown (own Figure, based on: Fraunhofer ISI et al., 2024:16).

Appendix 32 Maps of Positive and Negative Redispatch Energy in Germany in 2021

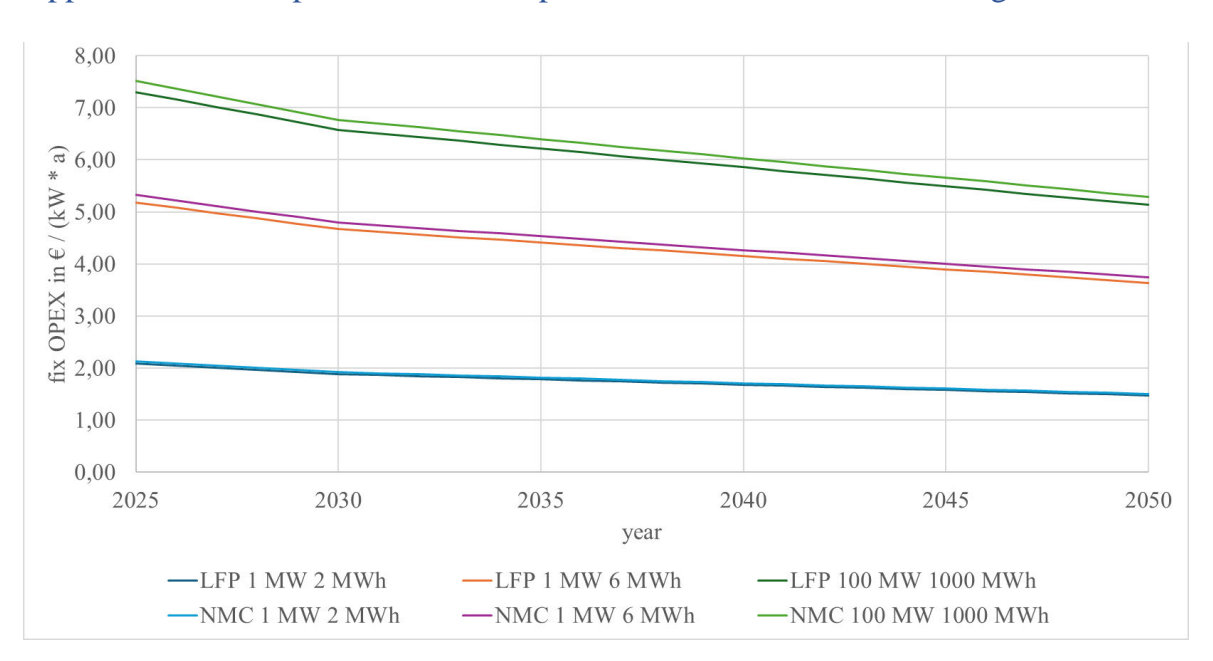


The maps indicate positive and negative Redispatch energy in GWh of transmission grid operators in Germany in 2021. While negative Redispatch measures are generally more probable in the north of Germany, positive Redispatch measures are more probable in the south. The maps are only an indicator of the real Redispatch measures at the specific location of the plant (Marie Wettingfeld et al., 2023:11).



Appendix 33 Prognosis of PR Tendered Power in Germany - Example Periods

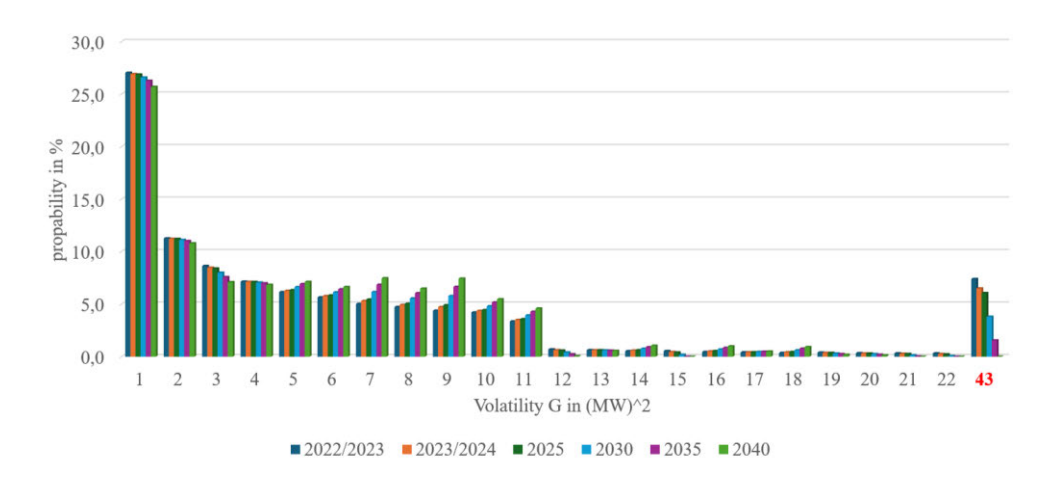
An example of tendered PR power in MW in April of three years 2025, 2030 and 2040, with a 15-minute resolution is shown. The standard deviation decreases from 42 MW in 2025 to 35 MW in 2040 (own Figure).



Appendix 34 Examples for Power-dependent OPEX Stored in the Program

The diagram shows examples of LFP and NMC BESS of different installed capacity and power for power-dependent OPEX in  $\frac{\epsilon}{kW \cdot a}$  stored in the program, depending on time. The difference between LFP and NMC is very small (own Figure).

### Appendix 35 Time-dependent Volatility Development of Activated PR Power



The Diagram shows the time-dependent volatility development of activated PR positive and negative power considering formular (18) with g = 418. Values outside the scale were aggregated with G = 43 on average (own Figure).

### Appendix 36 Formulars for calculation of NPV and IRR

The NPV in the unit € describes the current value of the future cash-flows (Dr. Balaram Bora, 2015:63):

$$NPV = \sum_{t=1}^{n} \frac{C_t}{(1+k)^t} - C_0 \tag{41}$$

The variable t indicates the number of years, n stands for the last year, k describes the discount factor and C equals the cash-flows.  $C_0$  is the initial investment. For the IRR calculation, NPV in formular (41) is set to 0 and the formal will be solved for k = IRR (Dr. Balaram Bora, 2015:63). To reduce programming effort, the initial investment is offset against operating year 1.

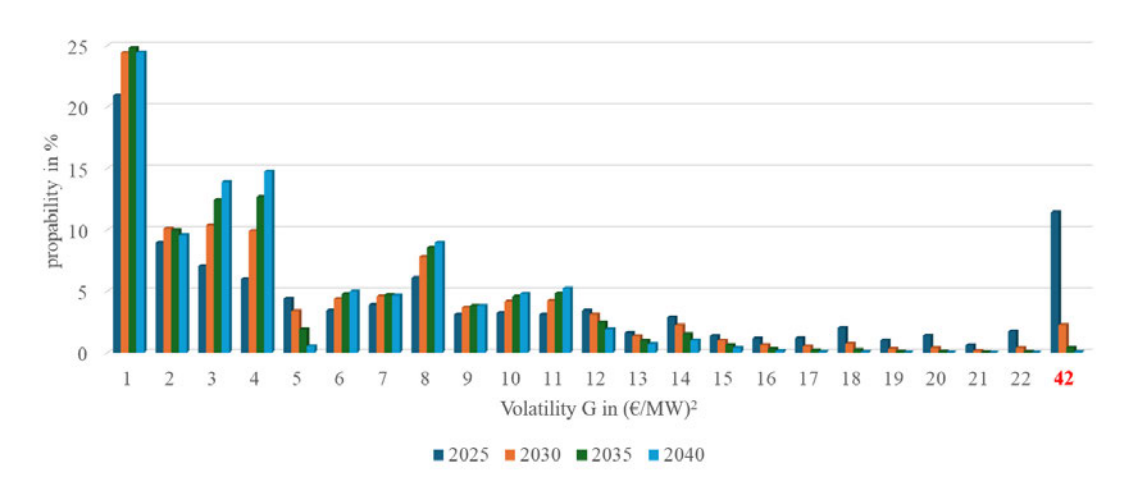
#### Appendix 37 Starting the Simulation via Program Environment

```
305
          # This is the main function where all starts. Dependent on program usage, choose
306
307
          # The main program includes the grafical user input inclusive input validation a
308
309
         #start_main_program()
310
311
          # To simulate a sensitivity analysis of variable capacity and power, select the
          #optimum_IRR_capacity_power()
312
313
314
                              sitivity analysis of variable cycles and prediction horizon,
         optimum_IRR_cycles_predict()
315
316
          # Add here other possible functions to test parameter variation or simular.
317
```

To start the program as a developer, for example, for sensitivity analysis, the main function in 'main.py' must be modified by commenting out the main program execution ('start\_main\_program', red cycled) and uncommenting other user-defined functions cycled in yellow and blue. The uncommented function 'optimum\_IRR\_cycles\_predict()' outputs a matrix of multiple simulation results, dependent on the annual cycles and the prediction horizon of the simulation. The input variables are defined in the function 'gra.fast\_init()' (own Figure).

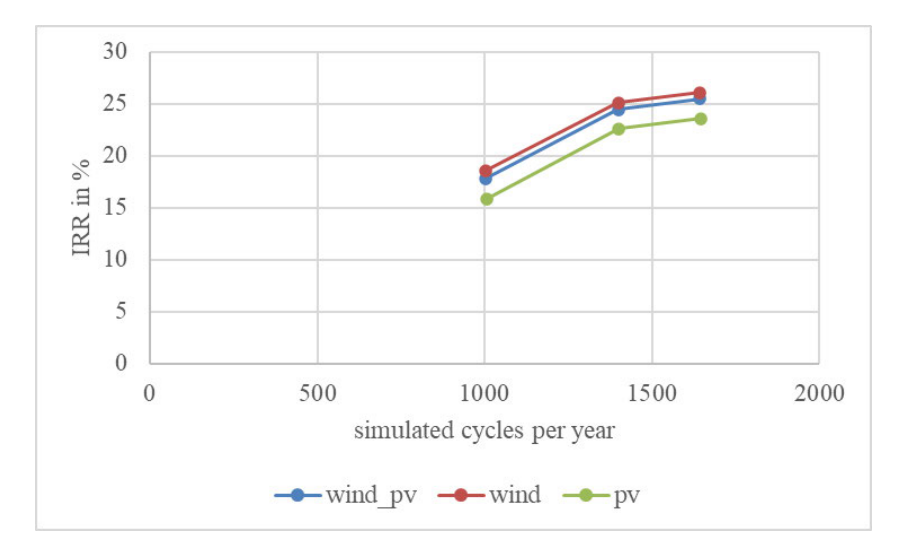
Appendix 38 Histogram Analysis of Volatility Development of PR Prices with

### Increase of Arbitrage Participants



The histogram analysis of <u>Appendix 25</u> of Primary Reserve market price volatilities is corrected by the expected strong increase in BESS and other arbitrage-model participants in the future. This influence cannot be derived from historical trends. These participants would exploit price peaks in the PR market or shift to other markets, thereby reducing the likelihood of extreme volatility. From 2030 onwards, the probability of volatility levels  $G > 10 \left( \frac{\epsilon}{MW} \right)^2$  is manually reduced. Larger volatilities are adjusted by a greater factor than smaller ones, resulting in the modified probabilities shown in the Diagram (own Figure).

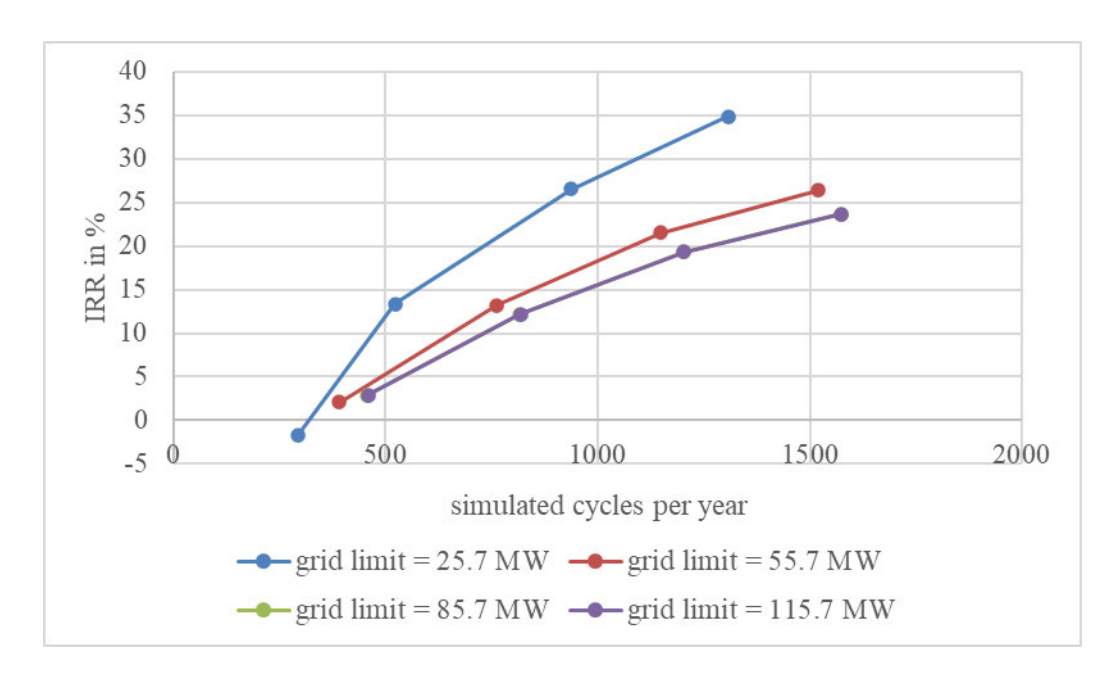
#### Appendix 39 BESS in Combination with Wind, PV or Wind and PV Plant



The diagram indicates the IRR dependent on the renewable technology and the cycles per year. In a simulation with activated power supply of RES, a BESS can achieve the highest IRRs with a co-located wind plant and combined wind- and PV plant (red and blue graph). If the BESS is only co-located to a PV plant, the IRR of the BESS decreases by 1.9 percentage points. This is because of a more disadvantageous RES+P price in comparison to the average price, the BESS sells its energy on the arbitrage markets (own Figure).

Appendix 40 Influence of Grid Limit and Cycles per Year on the IRR of BESS and PV

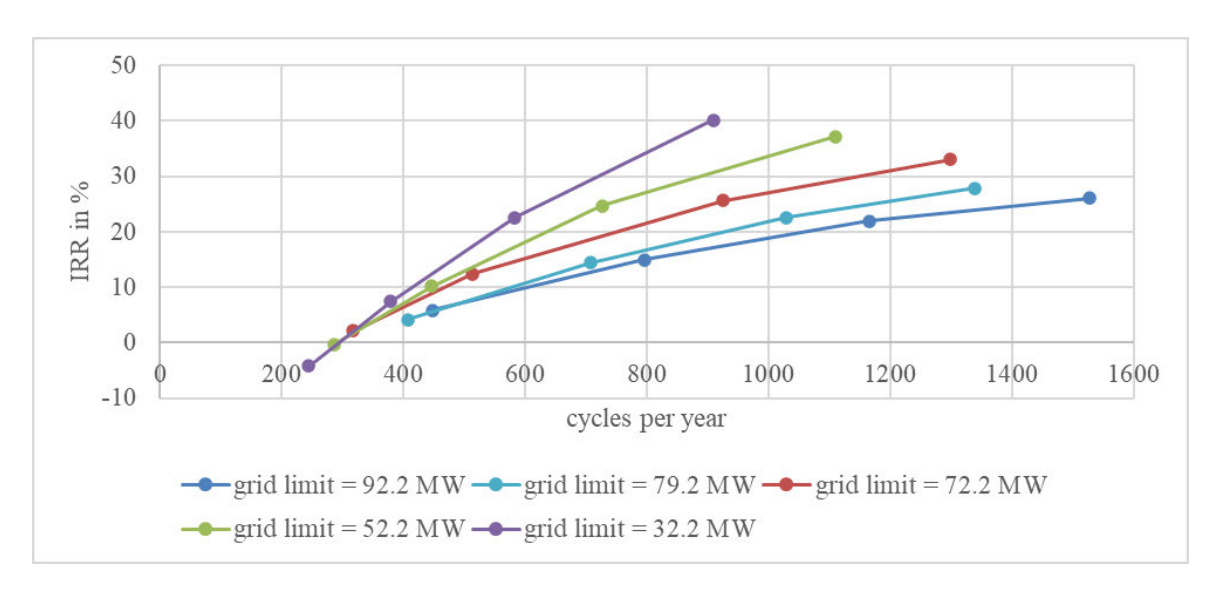
#### Plant Connected at the Same Transformer



The diagram shows the IRR in % dependent on the simulated cycles per year and the grid limit. It is assumed that the 85.7 MW PV plant and the BESS are connected to the same transformer. For dimensioning, the question arises whether the transformer needs to be enlarged. The diagram negates this question for a 20 MW / 20 MWh BESS, as the IRR remains unchanged if the storage system is connected to the 85.7 MW transformer which is dimensioned for the PV plant only. This is shown by the green graph which is behind the purple one. A feed-in limit that is lower than the nominal power of the PV plant has a beneficial effect on the IRR of the BESS, because the PV plant sells the electricity to the BESS at  $0 \in W$  when its nominal power is exceeded (own Figure).

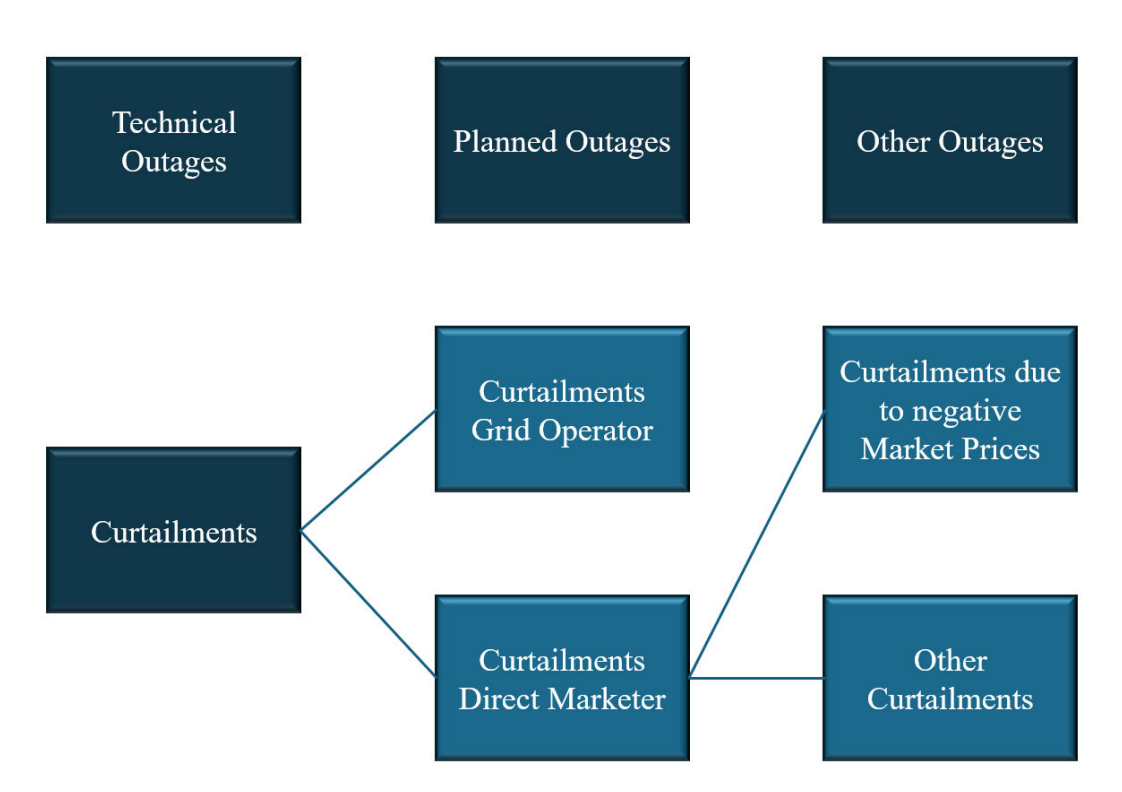
Appendix 41 Influence of Grid Limit and Cycles per Year on the IRR of BESS and

#### Wind Plant Connected at the Same Transformer



The IRR in % is plotted dependent on the simulated cycles per year and the grid limit. It is assumed that the 79.2 MW wind plant and the BESS are connected to the same transformer. For dimensioning, the question arises whether the transformer needs to be enlarged. Because of the difference between the dark and light blue graph, a reduced transformer power influences the IRR of the BESS positively. If the transformer's nominal power is lower than that of the wind plant, the BESS can benefit significantly because the wind plant sells the electricity to the BESS for  $0 \frac{\epsilon}{MWh}$  when the transformer's nominal power is exceeded (own Figure).

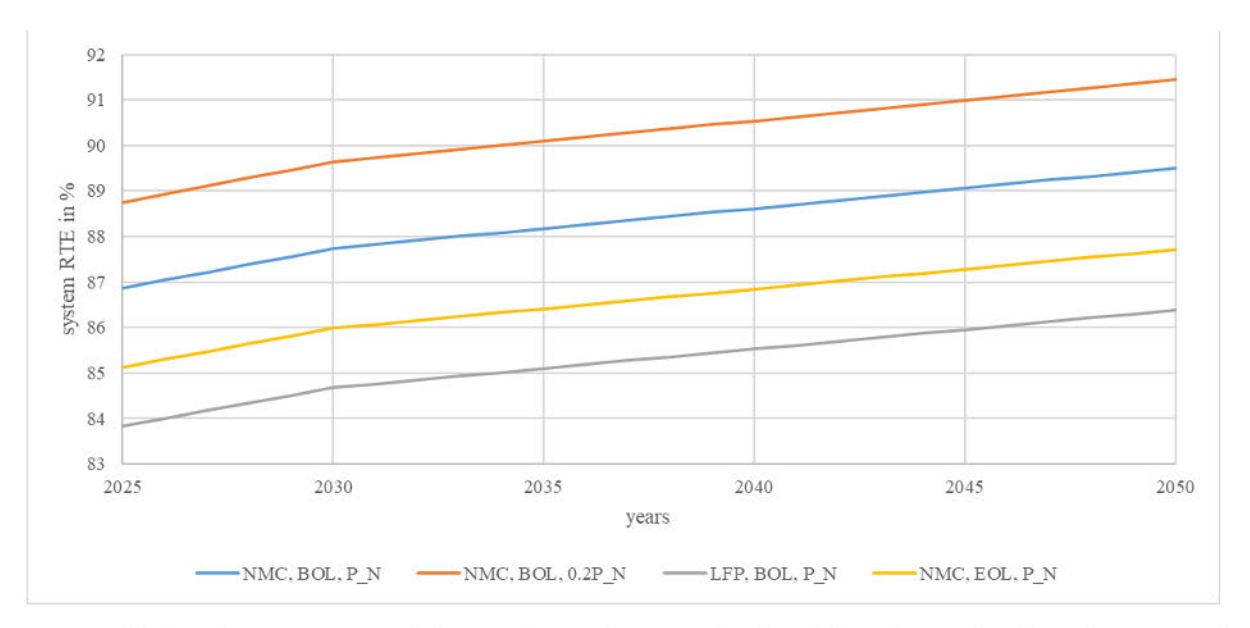
Appendix 42 Production Outages of Wind and PV Plants



Outages of PV and wind plants can be divided into the categories Technical Outages, Planned Outages, Other Outages and Curtailments. The GO can curtail to stabilize the grid. The DM curtails in cases of avoiding negative prices or if the electricity could not be sold on the market. A more detailed explanation of the individual categories is contained in chapter 2.6 (own Figure).

Appendix 43 System RTE Dependent on Technology, Degradation, Usable Power and

## Learning Rate



Some calculated system RTEs of the simulation data are displayed based on technology (NMC, LFP), learning rate, degradation (BOL, EOL), and  $P_U$  (as percentages of  $P_N$ ) in comparison. The largest difference is technology-specific, by comparing NMC (blue curve) to LFP (gray curve). When comparing the blue and orange curves,  $P_U$  appears to have a significant effect.

 $0.5P_N$  can be assumed minimal. The comparison between the blue and yellow curves shows the development of system RTE from BOL to EOL, with EOL occurring after 10 years of operation. The impact of degradation is as large as the reduction from  $P_U = P_N$  to  $P_U = 0.2P_N$  (own Figure).

## Appendix 44 Development of Independent Price Forecasts for PR, SR and Intraday

#### Markets

Because of page limitations the development of the market price forecasts are summarized here, following the principle stated in chapter <u>3.4.1</u>.

The average price of the PR market for 2025 is assumed to be 2,500  $\frac{\epsilon}{\text{MW} \cdot \text{week}}$  based on historical price trends (<u>Figure 14</u>). A slight linear increase to 3,000  $\frac{\epsilon}{\text{MW} \cdot \text{week}}$  by 2035 is projected to follow the prevailing trend since 2020, after which the price is kept constant.

Not only long-term price developments but also annual trends influence the market price, as shown by the gray function in <u>Figure 14</u>. These annual trends are expressed by a sine function with an amplitude of 0.1 and an offset of 1 which is multiplied by the price forecast. The period length of the function corresponds to four years. This results in a price deviation by up to 10 % from the long-term mean. Since other price time series exhibit similar annual price fluctuations, the same function is also applied to the SR and Intraday price forecasts.

The development of volatility is analyzed using histograms, as shown in <u>Appendix 25</u>. The results indicate market stabilization through a reduction in extreme prices and an increase in lower volatility levels near the mean value.

However, the forecast must be adjusted due to the expected strong increase in BESS and other arbitrage participants in the future. This influence cannot be derived from historical trends. These participants would exploit price peaks in the PR market or shift to other markets, thereby reducing the likelihood of extreme volatility.

From 2030 onwards, the probability of volatility levels  $G > 10 \left(\frac{\epsilon}{MW}\right)^2$  is manually reduced. Larger volatilities are adjusted by a greater factor than smaller ones, resulting in the modified probabilities shown in Appendix 38.

The time series of the projected PR prices must maintain the same price for 16 quarter-hour periods, as this corresponds to the market's bid duration (Figure 12). Additionally, positive and negative volatilities are symmetrically distributed around the mean value. However, a minimum price of  $0.63 \frac{\epsilon}{MW \cdot week}$  is imposed, as this threshold has not been historically undershot.

<u>Appendix 27</u> presents projected price development examples of the PR Market. Although the mean price has increased slightly and volatility has significantly decreased, the example months of 2025 and 2040 show only minor price differences.

In the analysis of SR, unlike PR, four different markets are considered. A distinction is made between power and energy prices, as well as different auctions for positive and negative SR (<u>Appendix 9</u>).

The activation probability in the SR market is even lower than in the PR market, historically averaging 1.23 % for both positive and negative SR (<u>Appendix 9</u>). Since a low activation probability results in low cycle utilization, the SR power market is highly suitable for BESS because low cycle utilization leads to less degradation of the BESS.

The approach to determine activation probabilities and prices follows the same methodology as for PR, separately to the four markets. The activation probabilities for negative and positive SR are analyzed separately.

Historical data analysis indicates a declining activation probability for SR (<u>Appendix 9</u>). For the coming years, it is assumed that the average activation probability of positive and negative SR will decrease linearly until 2035 and remain constant thereafter.

For the analysis of the SR activation probability, raw tendered and activation power data is converted into activation probabilities using formula (20) and then evaluated for historical trends in mean values and volatility changes.

Since the activation duration of SR is approximately 45 minutes according to <u>Appendix 1</u>, the probability means of three consecutive timestamps are calculated, and activation is applied for 45 minutes if the randomization algorithm determines SR activation. The result is an average probability of 0.87 % for positive SR and 0.96 % for negative SR over the period from 2025 to 2050.

The price development of the SR power market in recent years is comparable to that of the PR market (<u>Appendix 11</u>). The same average power price is assumed for both positive and negative SR, as their trends have been very similar.

The mean value and volatility of SR power prices have increased significantly in recent years (Appendix 11). Between 2020 and 2023, the mean value has increased elevenfold. Since such a steep increase is not expected in the future, data analysis begins in April 2021, when the price increase was significantly lower. The mean power price is set at  $3000 \frac{\epsilon}{MW \cdot week}$  for both positive and negative SR, as in the PR market. The minimum price of SR power is set at  $0.08 \frac{\epsilon}{MW \cdot week}$ , corresponding to the historically lowest value.

No time-of-day dependent probabilities were considered in the forecast. Due to the constant price within the 4-hour period, time-of-day effects are negligible.

Data analysis of SR energy prices starts in November 2021, when an increase in the price level becomes evident. Since 2021, SR energy prices have risen significantly, particularly for positive SR (Appendix 10). Positive and negative prices must be analyzed separately. The volatility of negative SR prices has increased considerably. As with the SR power prices, no clear time-of-day dependency for SR energy prices can be observed. A slight overall reduction in energy prices is observed for both positive and negative SR.

As BESS participation in the SR market increases while a reduction of CAPEX is expected, a long-term reduction in energy SR prices is anticipated. For positive SR positive energy, a linear reduction of the mean price from  $26 \frac{ct}{kWh}$  to  $14 \frac{ct}{kWh}$  is extrapolated based on historical trends, after which it remains constant (<u>Appendix 10</u>). The price for negative SR energy has historically varied between 4 to  $6 \frac{ct}{kWh}$  (<u>Appendix 10</u>), so the future mean value is set at a constant  $4 \frac{ct}{kWh}$  for the calculation period.

As with PR, SR volatility forecasts are derived from histogram evaluations. Large volatilities are manually reduced because of anticipated BESS market competition.

Due to similar power prices, lower activation probabilities which lead to lower degradation, and an additional energy price, SR is on average more attractive than PR for BESS.

The Intraday market also exhibits a significant increase in average price and a sharp rise in volatility from October 2021 onward (<u>Appendix 7</u>). Therefore, data analysis is conducted only after price stabilization in 2023.

For future projections, as assumed for reserve market prices, the average price level is expected to be slightly higher than before the price surge in 2021. The average price is assumed to be  $8.6 \, \frac{\text{ct}}{\text{kWh}}$ . In contrast to reserve markets, the Intraday market shows a time-of-day dependent price development (<u>Figure 13</u>) and monthly dependency (<u>Appendix 6</u>). Consequently, the price forecasting methodology is adjusted.

The mean price function of the Intraday market consists of the average price, a four-year price variation like in the PR and SR markets, a monthly price variation and a price variation dependent on the time of day.

To implement the monthly dependency, a sinusoidal function with an amplitude of 0.18, an offset of 1, and a period of one year is created ( $\underline{Appendix 6}$ ).

The hourly analysis shows peak prices in the morning and evening due to increased consumption (<u>Figure</u> 13). Low prices occur around midday due to increased PV production and at night due to low consumption.

To analyze time-of-day fluctuations, all prices within the analysis period are plotted against the time of day. The time of day is represented in 15-minute intervals to maintain original resolution. To ensure comparability across different months, all prices are adjusted using the curve fitting function from <u>Appendix 6</u>.

Three example days in April are analyzed at 00:15. The prices are  $12 \frac{ct}{kWh}$ ,  $9 \frac{ct}{kWh}$ , and  $10 \frac{ct}{kWh}$ . Since April exhibits prices that are 18 % lower than the annual average (<u>Appendix 6</u>), the example prices are increased by 18 % to  $14.16 \frac{ct}{kWh}$ ,  $10.62 \frac{ct}{kWh}$ , and  $11.8 \frac{ct}{kWh}$ .

From the comparable prices in the matrix of individual days across different times, the average price per time slot is determined (<u>Appendix 4</u>). For the example days, the mean price at 00:15 is calculated as  $12.19 \frac{ct}{kWh}$ . This procedure is repeated for each 15-minute time slot using all available values from the analysis period.

The mean price function is generated by multiplying the constant price of 8.6  $\frac{ct}{kWh}$  with the sinusoidal function of four-year price variations and the monthly price variation (<u>Appendix 6</u>). Subsequently, the values are corrected according to the time of day (<u>Appendix 4</u>).

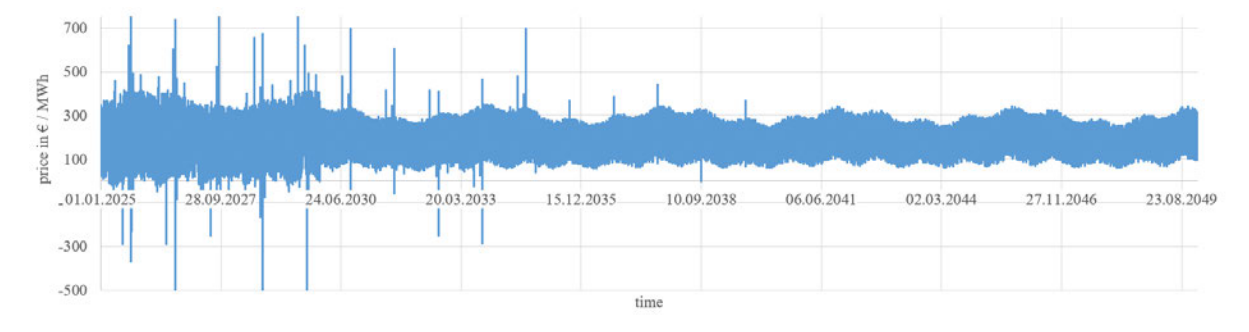
For volatility forecasting, the squared deviations of historical values from target mean values are calculated. The target mean values are determined by adjusting the time-dependent values from <u>Appendix 4</u> with the monthly variation from <u>Appendix 6</u>.

The objective is to determine how volatilities will evolve in the future. Volatilities are forecasted using the standard approach from chapter <u>3.4.1</u>, including a manual correction to account for the effects of increasing BESS market competition. The results are presented in <u>Appendix 28</u>.

A random function calculates forecast volatilities based on newly derived probabilities of volatility intervals. These probabilities change every five years until 2040.

The separate forecasts of the mean price function and volatilities are combined into price forecasts using Formula (18). <u>Appendix 45</u> shows the result. Monthly and four-year price variations, as well as a decline in extreme volatility, are observed.

## Appendix 45 Intraday Price Prognosis



The Intraday Price Prognosis is shown which is used for the simulation program. Monthly and four-year price variations, as well as a decline in extreme volatility, are observed (own Figure).

# Affidavit and declaration of publication



Hochschule für Angewandte Wissenschaften Hamburg

Hamburg University of Applied Sciences

#### Erklärung zur selbstständigen Bearbeitung einer Abschlussarbeit

Gemäß der Allgemeinen Prüfungs- und Studienordnung ist zusammen mit der Abschlussarbeit eine schriftliche Erklärung abzugeben, in der der Studierende bestätigt, dass die Abschlussarbeit "– bei einer Gruppenarbeit die entsprechend gekennzeichneten Teile der Arbeit [(§ 18 Abs. 1 APSO-TI-BM bzw. § 21 Abs. 1 APSO-INGI)] – ohne fremde Hilfe selbständig verfasst und nur die angegebenen Quellen und Hilfsmittel benutzt wurden. Wörtlich oder dem Sinn nach aus anderen Werken entnommene Stellen sind unter Angabe der Quellen kenntlich zu machen."

Quelle: § 16 Abs. 5 APSO-TI-BM bzw. § 15 Abs. 6 APSO-INGI

Dieses Blatt, mit der folgenden Erklärung, ist nach Fertigstellung der Abschlussarbeit durch den Studierenden auszufüllen und jeweils mit Originalunterschrift als <u>letztes Blatt</u> in das Prüfungsexemplar der Abschlussarbeit einzubinden.

Eine unrichtig abgegebene Erklärung kann -auch nachträglich- zur Ungültigkeit des Studienabschlusses führen.

Erklärung zur selbstständigen Bearbeitung der Arbeit						
Hiermit versichere ich,						
Name:	Tamschick					
Vorname:	Lukas					
dass ich die vorliegende Masterarbeit    bzw. bei einer Gruppenarbeit die entsprechend gekennzeichneten Teile der Arbeit – mit dem Thema:  Optimized Planning of Battery Storage Systems for Wind and Photovoltaic Power Plants in Germany by Development of a Simulation Program						
ohne fremde Hilfe selbständig verfasst und nur die angegebenen Quellen und Hilfsmittel benutzt habe. Wörtlich oder dem Sinn nach aus anderen Werken entnommene Stellen sind unter Angabe der Quellen kenntlich gemacht.						
- die folgende Aussage ist bei Gruppenarbeiten auszufüllen und entfällt bei Einzelarbeiten -						
Die Kennzeichnung der von mir erstellten und verantworteten Teile der -bitte auswählen- erfolgt durch:						
	Elmshorn	27.03.2025				
	Ort	Datum	Unterschrift im Original			